Biological Studies of Glaucoma Gene Myocilin

BY

HONGYU YING

BS Zhejiang University, 1991
MS Rush University, 2002
MEng University of Illinois at Chicago, 2011

THESIS

Submitted as partial fulfillment of the requirements
for the degree of Doctor of Philosophy in Bioengineering
in the Graduate College of the
University of Illinois at Chicago, 2013
Chicago, Illinois

Defense Committee:

Beatrice Y.J.T. Yue, Advisor
Michael Cho, Chair
Ali Djalilian, Ophthalmology and Visual Sciences
David Eddington
Deepak Shukla, Ophthalmologyand Visual Sciences, Microbiology and Immunology

ACKNOWLEDGMENTS

I would like to give special thanks to my PhD advisor Dr. Beatrice Yue. You guided me step by step in the past 7 years. You taught me how to write and criticize manuscripts, proposals; how to think and work independently which has become my priceless treasure. Most importantly, you boosted my self-esteem. I can't be here without your support and guidance.

I would also like to express my gratefulness to my committee members: Dr. Cho, Dr. Djalilian, Dr. Shukla and Dr. Eddington for serving on my committee and for their input and advice for my project.

Special thanks to lab colleagues: Sanja Turturro, Minghua Wang, Rajalekshmy Shyam and Xiang Shen. Thank you so much for your help and your encouragement all these years. I really enjoyed the time when we worked together.

Finally, I want to thank my dear husband, Xiang and two lovely kids, Joseph and Alice. Thank you for being understanding, and for your patience and encouragement.

TABLE OF CONTENTS

LIST OF TABLES

LIST OF FIGURES

LIST OF ABBREVIATIONS

3' UTR	The three prime untranslated region
3D	3-Dimensional
ACG	Angle-closure (acute) glaucoma
cAMP	Adenosine 3′,5′-cyclic monophosphate
CAV1/CAV2	Caveolin 1/caveolin 2
CDT6/ANGPTL7	Angiopoietin like-factor 7
CMV	Cytomegalovirus
ColI	Collagen type I
Ct	Cycle threshold
DAPI	4′,6′-diamidino-2-phenylindole dihydrochloride
DMEM	Dulbecco's modified Eagle's minimum essential medium
ECM	Extracellular matrix
EGFP	Enhanced green fluorescence protein
ELOVL5	Elongation of long-chain fatty acids family member 5
ER	Endoplasmic reticulum
FBS	Fetal bovine serum
Fn	Fibronectin
GAPDH	Glyceraldehyde 3-phosphate dehydrogenase
GDP	Guanosine diphosphate
GLuc	Gaussia luciferase
GSK-3β	Glycogen synthases kinase 3β
GST	Glutathione S-transferase
GTP	Guanosine triphosphate
GWAS	Genome-wide association study
HRP	Horseradish peroxidase
INS	5′-HS4 chicken β-globin insulator
IOP	Intraocular pressure
IPA	Interactive Pathway Analysis
iTRAQ	Isobaric tags for relative and absolute quantitation
JCT	Juxtacanalicular
kDa	Kilodalton
LC-MS	Liquid chromatography–mass spectrometry
Mdr	Multi drug resistant
MGP	Matrix GLA protein
miRNA	MicroRNA
miRNP	miRNA ribonucleoprotein complex
MYOC	Myocilin
ncRNA	Non-coding ribonucleic acid

Nid2	Nidogen 2
NES	N-linked glycosylation consensus
NTF4	Neurotrophin
nt	Nucleotide
NTG	Normal-tension (or pressure) glaucoma
OD	Optical density
OLF	Olfactomedin
OPTN	Optineurin
PEG	Polyethylene glycol
PKA	Protein kinase A
PSMB5	Proteasome subunit, beta 5
POAG	Primary open-angle glaucoma
PVA-PEG	Polyvinyl alcohol-polyethylene glycol
RISC	RNA induced silencing complex
RGC	Retinal ganglion cell
RGD	Arg-Gly-Asp
ROCK	Rho kinase
RT-qPCR	Reverse transcription quantitative polymerase chain reaction
SC	Schlemm's canal
SD	Standard deviation
SEAP	Secreted alkaline phosphatase
sFRP1	Secreted Frizzled-related protein 1
SILAC	Stable isotope labeling by/with amino acids in cell culture
SRBD1S1	RNA binding domain 1
Tcf/Lef	T-cell factor/lymphoid enhancing factor
TIGR	Trabecular meshwork-induced glucocorticoid response gene
TM	Trabecular meshwork
WDR36	WD-repeat domain 36

SUMMARY

Glaucoma is a major blinding disease. Myocilin is the first candidate gene identified for the most common form of glaucoma, primary open angle glaucoma (POAG). The human myocilin gene encodes for an acidic glycoprotein of 504 amino acids. Mutations of myocilin such as Pro370Leu (P370L) and Gln368Stop (Q368X) were found in 2-4% of POAG patients. Its structure, function and regulation are still largely unknown. We conducted new investigations on myocilin in five aspects (parts). Part I is to examine the involvement of Wnt pathway in myocilin mediated phenotypes such as loss of actin stress fibers and focal adhesions, elevated protein kinase A activity and downregulated RhoA activity. Wnt signaling is a key pathway involved in many important cellular processes. We showed that Wnt signaling is a player in the above mentioned myocilin phenotypes using Wnt specific inhibitor and activator. Blocking Wnt signaling pathway may have therapeutic potential for myocilin glaucoma. Part II is to establish 3 dimensional culture of human trabecular meshwork (TM) cells, a cell type that plays an important role in regulation of bulk flow of the aqueous humor. Several 3D platforms such as hydrogels and inserts were tested. Human TM cells were grown in multilayers when plated in QGel and Alvetex scaffold, formed cell-cell communication and showed a more *in vivo* like pattern of gene expression. The 3D system can be used for an effective *in vitro* model to help portray activities, characteristics, and stress responses of TM cells *in vivo*. Part III is to establish Tet-on inducible wild-type or mutated (P370L or Q368X) myocilin expressing neuronal RGC5 cell lines. The Tet-on inducible RGC5 cells provide a new tool for exploring the effects of myocilin up-regulation and mutations at cellular and molecular levels. Part IV is to detect alterations in protein expression profile and identify novel downstream pathways induced by

myocilin. Cutting-edge quantitative proteomics were used. RGC5 cell lines established in part III were induced to express wild-type or mutated myocilin-GFP. The global protein profiles of these cells were compared with non-induced controls. Differentially expressed protein profiles pinpointed molecular trafficking, cytoskeleton reorganization, autophagy, microtubule dynamics, organization of filaments, apoptosis, mitochondria dysfunction and several signaling pathways. The information obtained may provide clues as to the functions of myocilin and point to new directions for myocilin investigations. Finally, part V is to identify microRNAs (miRNAs) that regulate the expression of mouse myocilin gene. MiRNAs are short RNAs functioning as posttranslational regulators (mostly in translation silencing). MiRNA array was performed and the up- or down-regulated miRNAs in induced cells were identified. Along with miRNAs predicted by computer algorithms, miRNAs that target mouse myocilin were identified and validated. Since expression of mutated myocilin is likely to be under the same miRNA control as the wild-type myocilin, results from the proposed experiments may be applied to silence myocilin mutants to abrogate mutant phenotypes in myocilin glaucoma.

INTRODUCTION

Glaucoma:

Glaucoma is one of the leading causes of irreversible blindness worldwide, estimated to affect around 80 million peoples worldwide by 2020 (Quigley and Broman 2006). It is characterized by progressive loss of retinal ganglion cells and the accompanying axons, as well as cupping of the optic nerve head (Quigley 2011). In general, glaucoma in humans can be classified into four major types: open-angle (chronic) glaucoma (also called primary open-angle glaucoma, POAG), angle-closure (acute) glaucoma (ACG), congenital glaucoma and secondary glaucoma with POAG being the most common type.

In the anterior segment of the eye, the aqueous humor (transparent, gelatinous fluid similar to plasma, but containing low protein concentrations) constitutively produced by the ciliary body flows through the channel between the iris and lens and drains through the trabecular meshwork (TM) into Schlemm's canal (SC) and finally the aqueous veins (Grierson I 1995) (Figure 1). A pressure gradient, also called intraocular pressure (IOP, normally 10-20 mmHg), exists between the anterior chamber and the episcleral veins when the aqueous humor outflow is normal.

Although the final common tissue damages in all types of glaucoma are degeneration of retinal ganglion cells and axonal damage that manifests as optic nerve atrophy and progressive visual field defects leading eventually to blindness, each type of glaucoma may be caused by a different mechanism. In **ACG**, the channel between the iris and the lens is suddenly blocked. The aqueous humor cannot pass through and consequently leads to the elevation of IOP and visual loss progresses rapidly. Symptoms of ACG may include headaches, eye pain, nausea, rainbows around lights at night, and very blurred vision. Patients often seek medical attention due to the

discomfort before permanent damage occurs. **POAG**, on the contrary, is chronic and tends to progress slower. It happens when the eye's drainage canals (such as TM and SC) become clogged over time. It is painless and without symptoms. Patients may not notice until the disease has progressed significantly when their vision is lost.

The third type of glaucoma, **congenital glaucoma**, is seen in babies and often is inherited. It is caused by abnormal eye development. The symptoms may include: cloudiness of the front of the eye, enlargement of one or both eyes, red eye, and sensitivity to light and tearing. The symptoms can be noticed when the child is a few months old. Glaucoma caused by other factors is called **secondary glaucoma**. The causes could be drugs such as corticosteroids, eye diseases such as uveitis, systemic diseases and trauma (S.D.A.M. Medical Encyclopedia 2012, http://www.ncbi.nlm.nih.gov/pubmedhealth/PMH0002587/).

POAG accounts for approximately 90% of glaucoma cases in the United States. It is age-related. Elevated IOP is common in POAG and is a major risk factor for the disease (Kwon, Fingert et al. 2009). The relationship between the elevated IOP and retinal ganglion cell degeneration is not simple. Some individuals who have elevated IOP but without optic nerve damage, while some others with normal IOP but with optic nerve damage (such as in low-tension or normal-pressure glaucoma (NTG) which is recognized as a subtype of POAG (Kwon, Fingert et al. 2009; Jampel 2011). It is speculated that in NTG cases, retinal damage is resulted even with the so-called normal IOP and/or additional IOP-independent factors may play importance roles.

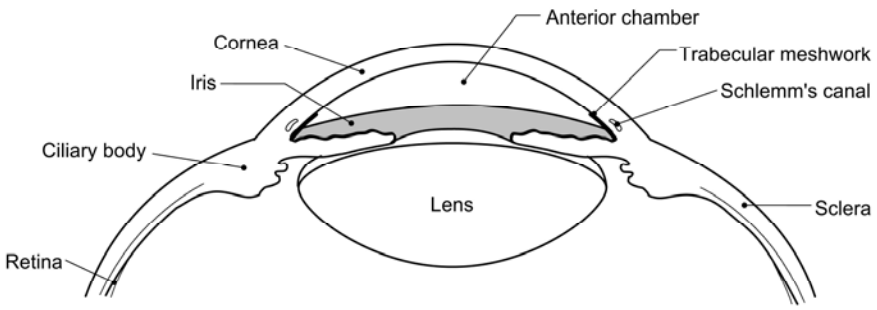

Figure 1. Cross-sectional representation of the anterior chamber of the eye. Reprinted from Yue, B. Y.J.T. 2008. Cellular Mechanisms in the Trabecular Meshwork Affecting the Aqueous Humor Outflow Pathway, Albert & Jakobiec's Principles and Practices of Ophthalmology, 3rd Edition, page 1, Chapter 192, with permission from Elsevier.

Trabecular Meshwork (TM):

The IOP is controlled by a balance between the production and outflow of the aqueous humor contained in the anterior chamber of the eye. TM, a specialized tissue located at the chamber angle next to the cornea, is believed to be the major site for regulation of the bulk flow of the aqueous humor (Bill 1975; Yue 1996). This tissue is divided into the uveal meshwork, corneoscleral meshwork, and juxtacanalicular (JCT) regions (Figure 2). In the uveal and corneoscleral meshworks, layers of trabecular beams made up of connective tissue or extracellular matrix (ECM) elements are lined by TM cells. In the JCT region, the TM cells reside relatively freely and embedded in the connective tissue. The outflow resistance is believed to locate largely in the JCT/SC area. The pressure gradients and resistance to aqueous outflow

are likely altered in the various types of glaucoma (Gardiner 1978; Gimelbrant, Ensminger et al. 2005).

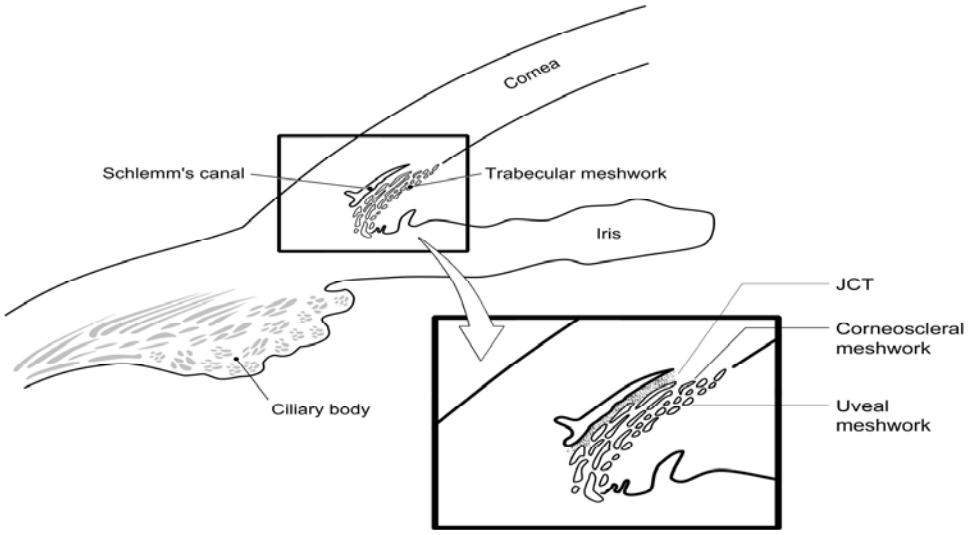

Figure 2. Schematic representation of the structures in the chamber angle and the circulation of aqueous humor. Three regions in the TM: the JCT area, corneoscleral meshwork, and uveal meshwork are indicated in the inset. Reprinted from Yue, B. Y.J.T. 2008. Cellular Mechanisms in the Trabecular Meshwork Affecting the Aqueous Humor Outflow Pathway, Albert & Jakobiec's Principles and Practices of Ophthalmology, 3rd Edition, Chapter 192, page 2, with permission from Elsevier.

TM cells that cover the beams display an endothelial cell-like morphology and lining property (Yue 1996). They are avid phagocytes (Zhou, Fukuchi et al. 1995), possess contractile and migratory apparatus (Stumpff and Wiederholt 2000), and have the capacity to produce ECM elements (Yue 1996; Keller, Aga et al. 2009). It is believed that changes in the TM cell activities, cytoskeletal structure, cell-matrix and cell-cell adhesion, and/or the quantity and composition of the ECM may all produce adverse effects on the outflow pathway, leading to IOP elevation and ultimately glaucoma (Keller, Aga et al. 2009; Tian, Gabelt et al. 2009; Stamer and Acott 2012).

The Genetics of Glaucoma:

Glaucoma is clinically and genetically heterogeneous (Wiggs 2012). Large pedigrees in which glaucoma was passed down from generation to generation in a Mendelian pattern (Tielsch, Katz et al. 1994; Kang, Willett et al. 2007; Wang, Harmon et al. 2010). Twin studies also showed a higher disease concordance in monozygotic twins than in dizygotic twins (Teikari 1990; Gottfredsdottir, Sverrisson et al. 1999). A substantial fraction of POAG has a genetic basis. More than 20 genetic loci have been reported for POAG (Wiggs 2007; Fan and Wiggs 2010; Fingert 2011). Genes associated with POAG with Mendelian inheritance or complex inheritance include: *MYOC* (myocilin, formerly: trabecular meshwork-induced glucocorticoid response gene or TIGR, GLC1A, OMIM #601652) (Fingert, Stone et al. 2002; Gong, Kosoko-Lasaki et al. 2004), *OPTN* (optineurin, GLC1E, OMIM #602432) (Sarfarazi, Child et al. 1998; Rezaie, Child et al. 2002), *WDR36* (WD-repeat domain 36, GLC1G, OMIM #609669) (Monemi, Spaeth et al. 2005) and *NTF4* (neurotrophin 4, GLC1O, OMIM #162662) (Pasutto, Matsumoto et al. 2009; Vithana, Nongpiur et al. 2010; Chen, Ng et al. 2012). There are also genetic susceptibility alleles which are frequently detected in patients with POAG but not in normal subjects. These alleles may promote the development of POAG when combined with other glaucoma risk alleles and/or with environmental risk factors. These alleles found by genome-wide association studies (GWAS) include *SRBD1* (S1 RNA binding domain1) (Meguro, Inoko et al. 2010), *ELOVL5* (elongation of long-chain fatty acids family member 5) (Meguro, Inoko et al. 2010), *CAV1*/*CAV2* (caveolin 1/caveolin 2) (Thorleifsson, Walters et al. 2010; Wiggs, Kang et al. 2011), and SNPs located near the TMCO1 and CDKN2BAS gene (Burdon, Macgregor et al. 2011).

Myocilin:

Myocilin is the first gene found to be associated with both juvenile- and adult-onset POAG (Stone, Fingert et al. 1997). It was initially referred as TIGR since it was originally identified as a 57−/55-kilodalton (kDa) protein secreted into the media of TM cultures after induction with glucocorticoids such as dexamethasone (Polansky, Kurtz et al. 1989; Polansky, Fauss et al. 1997; Nguyen, Chen et al. 1998). The myocilin mRNA and protein are found subsequently to be present not only in a variety of ocular tissues including the iris, ciliary body, TM and retina but also in nonocular tissues such as the heart, brain, skeletal muscle and testis (Tomarev, Tamm et al. 1998; Tamm 2002; Kwak and Kensler 2006).

Myocilin gene maps to the GLC1A locus at 1q24-25 (Fingert, Stone et al. 2002) and is composed of three exons (Figure 3, top panel) (Fingert, Ying et al. 1998). Exon 1 encodes the N-terminal myosin-like domain containing a signal peptide targeting myocilin for secretion, two coiled coils and one leucine zipper motif which is involved in myocilin self-aggregation. Exon 2 encodes the central linker domain which is cleaved by calpain II and exon 3 encodes the olfactomedin (OLF)-like globular domain (Kwak and Kensler 2006)(Figure 3).

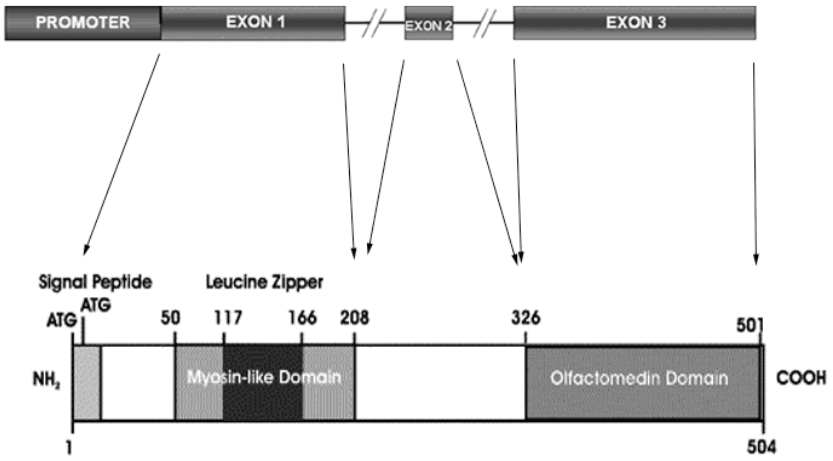

Figure 3. Structure of myocilin gene (top panel) and protein (bottom panel). Myocilin protein is a 504 amino acid long protein that contains a signal peptide at the N-terminus, a leucine zipper within the myosin-like domain and a C-terminal olfactomedin-like domain. Reproduced from Tamm, E. R. 2002. "Myocilin and glaucoma: facts and ideas." Prog Retin Eye Res **21**(4): 395-428 with modifications and permission from Elsevier.

Human myocilin is believed to be glycosylated (Caballero, Rowlette et al. 2000; Caballero and Borras 2001; Clark, Steely et al. 2001; Shepard, Jacobson et al. 2003). Human myocilin Asn57 was shown to be part of an N-linked glycosylation consensus (NES) and is the only residue on myocilin predicted to be N-glycosylated by both site-directed mutagenesis and deglycosylation (Shepard, Jacobson et al. 2003). It has also been reported that human wild-type myocilin was proteolytically cleaved between Arg226 and Ile227 in the aqueous humor and ocular tissues, resulting in a 35 kDa fragment containing the C-terminal OLF domain and a 20 kDa fragment containing the N-terminal leucine zipper domain (Tamm 2002).

More than 180 myocilin variants have been documented so far (Qi, Wickham et al. 2004). Approximately 36% of cases of the juvenile POAG and ~2-4% adult cases have a disease-causing myocilin mutation. Glaucoma patients with myocilin mutation tend to have high IOP.

Among the various myocilin mutations, Pro370Leu (P370L) mutation is responsible for one of the most severe glaucoma phenotypes and Gln368Stop (Q368X) is the most common mutation reported in POAG patients (Tamm 2002; Gong, Kosoko-Lasaki et al. 2004).

Neither the absence (Kim, Savinova et al. 2001) nor overexpression (Gould, Miceli-Libby et al. 2004) of wild-type myocilin in transgenic mice has been shown to be critical for the development of POAG. Many glaucoma-causing mutant myocilin especially mutations in the OLF domain have however been found to be misfolded and form detergent-resistant, secretion-incompetent aggregates (Zhou and Vollrath 1999; Jacobson, Andrews et al. 2001; Joe, Sohn et al. 2003; Liu and Vollrath 2004; Gobeil, Letartre et al. 2006). It has been hypothesized that toxic gain of function occurs as a result of myocilin mutant expression in TM cells. Myocilin mutations may lead to different levels of myocilin misfolding and aggregating in the endoplasmic reticulum (ER) of TM cells (Yam, Gaplovska-Kysela et al. 2007) which may contribute to the death of TM cells (Sohn, Hur et al. 2002; Joe, Sohn et al. 2003; Liu and Vollrath 2004), an increase in IOP, and onset of glaucoma.

Despite all the efforts made to unravel myocilin's biology, both normal function of this protein and the exact pathogenic mechanism of myocilin leading to glaucoma remain largely unknown. In the present study, we used cutting-edge tools to conduct studies to advance our knowledge such as the signaling events induced by myocilin and its regulation by microRNAs (miRNAs). The research effort can be divided into five parts. Specifically, in part I, the involvement of Wnt pathway in myocilin-induced phenotypes was investigated. In part II, 3 dimensional cultures of human TM cells were established as models that mimics more closely *in vivo* conditions to provide more relevant physiological insights. In part III, inducible wild-type and mutated (P370L and Q368X) myocilin expression stable cell lines were created to facilitate

studies of myocilin. In part IV, the inducible stable cell lines established in part III were used to evaluate the changes of protein profile when wild-type myocilin was up-regulated or mutated. Finally in part V, the miRNAs that regulate the expression of myocilin gene were identified. Efficiently knocking down the level of mutant myocilin might form a new therapeutic modality for myocilin glaucoma.

PART I: WNT ACTIVATION BY WILD-TYPE AND MUTANT MYOCILIN IN CULTURED HUMAN TRABECULAR MESHWORK CELLS

When upregulated, the wild-type myocilin may lead to pathology, as is observed in cases of corticosteroid glaucoma (Mao, Tovar-Vidales et al. 2011). Earlier studies from our laboratory and those from others (Peters, Herbert et al. 2005) showed that overexpressing wild-type myocilin intracellularly (Wentz-Hunter, Shen et al. 2004) by transfection or by protein transduction (Sakai, Park et al. 2006) in cultured human TM cells resulted in a loss of actin stress fibers and focal adhesions. Cell adhesion to fibronectin and cell spreading were also compromised (Wentz-Hunter, Shen et al. 2004). These myocilin-induced events were further shown to be mediated via Rho GTPase and adenosine 3′,5′-cyclic monophosphate (cAMP)/protein kinase A (PKA) signaling. The cAMP level and PKA activity were elevated, and the downstream the RhoA activity was reduced (Shen, Koga et al. 2008).

Recombinant myocilin protein has in addition been shown to interact with secreted inhibitors of Wnt signaling, secreted Frizzled-related protein 1 (sFRP1), sFRP3 and several other Frizzled receptors (Kwon, Lee et al. 2009). Wnts are a group of secreted, cysteine-rich glycoproteins (Jin, George Fantus et al. 2008; Cadigan and Peifer 2009; Mii and Taira 2011). The Wnt signaling can be divided into the β-catenin-dependent canonical and β-catenin-independent non-canonical pathways (Jin, George Fantus et al. 2008; Cadigan and Peifer 2009; Mii and Taira 2011). In the former, the Wnt pathway is activated when Wnts bind with a receptor complex consisting of Frizzled protein receptor and the low-density lipoprotein receptor-related proteins. Such activation induces breakdown of the destruction complex that consists of glycogen synthases kinase 3β (GSK-3β), whose major function is to phosphorylate β-catenin. In the absence of Wnt ligands, β-catenin is phosphorylated, and the phosphorylated β-

catenin is constantly degraded in the cytoplasm (Fig. 4a). Upon Wnt activation, GSK-3β activity is inhibited, β-catenin is thus not phosphorylated, leading to β-catenin stabilization and nuclear translocation. In the nucleus, β-catenin binds to T-cell factor/lymphoid enhancing factor (Tcf/Lef) and regulates expression of target genes (Fig. 4b) (Luo, Chen et al. 2007; Jin, George Fantus et al. 2008; Cadigan and Peifer 2009; Mii and Taira 2011). In contrast, all Wnt signaling activities that are apparently independent of β-catenin constitute different noncanonical Wnt signaling pathways. The non-canonical planar cell polarity pathway that activates small G proteins including Rac and Rho, and c-Jun N-terminal kinase (Veeman, Axelrod et al. 2003), is involved in regulation of cytoskeletal organization and cell polarity. The second non-canonical pathway, Wnt/Ca^{2+}, leads to release of intracellular Ca^{2+}, and is involved in activation of protein kinase C and Ca^{2+}/calmodulin-dependent protein kinase II. The Wnt/Ca^{2+} pathway has implications on cell proliferation and cell movement (Kuhl, Sheldahl et al. 2000).

Wnt signaling pathways have been shown to play a role in eye diseases including retinal degeneration, cataract and congenital ocular malfunctions (de Iongh, Abud et al. 2006). A possible involvement of Wnt signaling in the outflow system and glaucoma has also been reported (Wang, McNatt et al. 2008). While the underlying mechanism is still unclear, addition of exogenous sFRP1 to *ex vivo* perfusion cultured human eyes decreased outflow facility and increased the pressure, concomitant with reduced β-catenin levels. Expression of sFRP1 likewise induced IOP elevation in mice (Wang, McNatt et al. 2008).

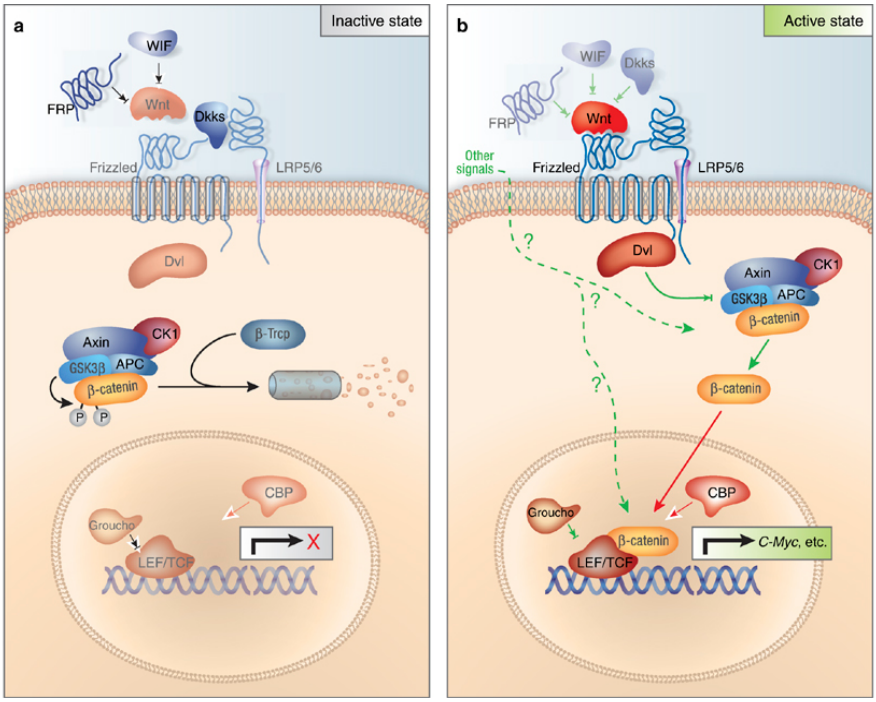

Figure 4. Schematic representation of the canonical Wnt/β-catenin signaling pathway. (**a**) In the absence of Wnt signal, GSK3β phosphorylate β-catenin leading to the proteosomal degradation of β-catenin. (**b**) Wnt binds to its Fz receptor and LRP5/6 co-receptor and activates Dvl, leading to the inhibition of APC/Axin/GSK3 β -mediated β-catenin degradation. Stabilized β-catenin translocates into nucleus and forms a transcriptional complex with LEF/Tcf and activates downstream targets. Reprinted from Luo, J., J. Chen, et al. 2007. "Wnt signaling and human diseases: what are the therapeutic implications?" Lab Invest **87**(2): 97-103 with permission from Nature Publishing Group.

In light of the possible myocilin connection with the Wnt signaling pathway, we undertook the study to determine whether Wnt signaling is a player in the myocilin-induced phenotypes. Results obtained indicated that Wnt was indeed activated upon myocilin overexpression. Interestingly, expression of P370L and Q368X mutant myocilins also induced phenotypes similar to those seen with the wild-type.

Materials and Methods

Cell Cultures

Normal human eyes were obtained from the Illinois Eye Bank (Chicago, IL). The TM tissues from donors 22, 27, 31, 39, 46, 52, and 55 years of age without any known ocular diseases were dissected and cultured as previously described (Shen, Koga et al. 2008) on Falcon Primaria flasks (BD Biosciences, Franklin Lakes, NJ) in complete media that contained Dulbecco's modified Eagle's minimum essential medium (DMEM), glutamine, 10% fetal bovine serum (FBS), 5% calf serum, and antibiotics. Second- or third-passaged cells were used for the study. In some experiments, normal human TM cells were treated overnight with 2 or 10 μM SB216763 (R&D Systems, Minneapolis, MN), a Wnt activator, in the absence of presence of 10 nM H89, a PKA inhibitor. To block the Wnt activation, cells after transfection were treated overnight with recombinant human sFRP-1 (50 nM, R&D Systems).

Caco2 cells obtained from American Type Cell Culture Collection (Manassas, VA) were cultured in complete media.

Plasmid Construction

Plasmids pTarget-wild-type myocilin (pTarget-myocilin$_{WT}$) was constructed as previously described (Shen, Koga et al. 2008). For pMyocilin$_{WT}$-EGFP, polymerase chain reaction (PCR) was performed to amplify myocilin$_{WT}$ and the *EcoRI/BamHI*-digested PCR product was cloned into pEGFP-N1 (BD Biosciences) at the corresponding sites. Sequencing was carried out to determine the proper orientation and confirm the construct sequences.

pMyocilin$_{P370L}$-EGFP was generated by QuikChange II Site-Directed Mutagenesis Kit (Stratagene, La Jolla, CA). Sense 5' -CCACGGACAGTTC*CTG*TATTCTTGGGGTGGC- 3'

(nucleotides for P370L change in italics) primer, and the antisense primer sequence was the reverse. pMyocilin$_{Q368X}$-EGFP was generated as follow: Myocilin$_{Q368X}$ was amplified by PCR using forward primer: TCGAATTCCCACCATGGCTATGAGGTTCTTCTGT (*EcoRI* site is underlined) and reverse primer: TTGGATCCCGTCCGTGGTAGCCAGCTCCAGG (*BamHI* site is underlined) using pMyocilin$_{WT}$-EGFP as template. PCR product was digested with *EcoRI* and *BamHI* and ligated in frame with same restriction enzymes digested pEGFP-N1 vector (Clontech) to generate plasmid pMyocilin$_{Q368X}$-EGFP. Positive clone was sequenced to verify the construct. pTarget-myocilin$_{P370L}$ and pTarget-myocilin$_{Q368X}$ were similarly prepared.

pTarget-myocilin$_{WT}$, pMyocilin$_{WT}$-EGFP, and myocilin mutant constructs were introduced into human TM cells using FuGENE 6 (Roche, Indianapolis, IN) or Lipofectamine LTX (Life Technologies, Grand Island, NY) transfection reagent. TM cells were plated at 60% confluence 18 h before transfection. The vector: transfection reagent mixture was added to the cells for 48 h. As mock control, TM cells were transfected in parallel with pTarget or pEGFP-N1 empty vector without the insert. The expression level of the transgene was examined by Western blotting (Shen, Koga et al. 2008) using a monoclonal (Ezzat, Howell et al. 2008) (a generous gift from Dr. M. Fautsch, Mayo Clinic) or a polyclonal (a generous gift from Dr. W.D. Stamer, Duke University) anti-myocilin antibody.

Immunofluorescence and Actin Staining

Transfected human TM cells were plated onto Lab-Tek CC2 glass chamber slides (Nalge Nunc International, Naperville, IL). Cells were fixed in either ice cold methanol or paraformaldehyde-lysine-phosphate buffer, without or with permeabilization in 0.2% Triton X-100. After treatment of 3% H_2O_2 and blocking, the slides were incubated for 1 h with monoclonal anti-vinculin (Millipore, Billerica, MA) or anti-β-catenin (Santa Cruz Biotech.,

Santa Cruz, CA). Normal mouse IgG was used as a negative control. The cells were further incubated with Cy3-goat anti-mouse IgG. Slides were mounted in Vectashield (Vector Laboratories, Burlingame, CA) with DAPI (4′,6′-diamidino-2-phenylindole dihydrochloride). The staining was examined under a Leica confocal or a Zeiss 100 M microscope.

The actin structure in nontransfected, mock transfected and myocilin construct-transfected cells was examined using rhodamine-phalloidin (Life Technologies). The actin structure in normal human TM cells after treatment of SB216763 was stained with Oregon Green 488-phalloidin (Life Technologies).

Trypsin Sensitivity

Trypsin sensitivity was examined using a Zeiss live cell imaging system (Carl Zeiss MicroImaging, Thornwood, NY). Cells were transfected with pEGFP-N1, pMyocilin$_{WT}$-EGFP, pMyocilin$_{P370L}$-EGFP, or pMyocilin$_{Q368X}$-EGFP for 48 h. The cells were washed with Versene and observed under the Zeiss system using a 20× objective. Images were captured every 15 s after the addition of 0.25% trypsin solution to the culture. Cell changes were monitored and the time (mean ± SD) needed for the cells to shrink, round up and break away from the culture plate was determined (Shen, Koga et al. 2008).

Active RhoA

Active RhoA was measured with pull down assay (Shen, Koga et al. 2008) or with G-LISA assays for RhoA (G-LISA kit, Cytoskeleton Inc., Denver, CO) in the colorimetric detection format. Normal human TM cells were untreated or treated overnight with 2 or 10 μM SB216763. Another set of cells was also co-treated with 10 nM H89. The cells were lysed in lysis buffer (G-LISA kit, Cytoskeleton Inc.) containing protease inhibitors (Roche). The proteins

in the lysate were quantified by Bradford protein assay using bovine serum albumin as a standard. Pull down assays (Rho activation kit, Cytoskeleton Inc.) were performed as previously described (Shen, Koga et al. 2008). pTarget mock- and pTarget-myocilin$_{WT}$-, pTarget-myocilin$_{P370L}$- or pTarget-myocilin$_{Q368XT}$-transfected cells that had been serum starved for 18 h were lysed. Lysates from transfected cells were mixed at 4°C with GST-Rhotekin bound to Sepharose beads for 1 h. The proteins bound to the beads were resolved by 12% SDS-PAGE and immunoblotted with anti-RhoA. Cell lysates preincubated with GTPγ S and GDP served as positive and negative controls respectively. Prior to incubation with the beads, aliquots were removed from samples for total RhoA. Amounts of active GTP-RhoA bound to GST-Rhotekin were normalized against amounts of total RhoA in the cell lysates and the myocilin transfectant data were compared to controls.

G-LISA was performed as per manufacturer's instructions. Briefly, the active GTP-bound form of Rho present in the cell lysate (25 µg of total protein) was allowed to bind to the 96-well plate coated with Rhotekin RBD domain of Rho-family effector proteins. Following incubation with mouse monoclonal anti-RhoA antibody (Cytoskeleton Inc.) and horseradish peroxidase (HRP)-conjugated secondary antibody as well as detection by the HRP detection reagent, the amounts of active RhoA in samples were measured by the absorbance at 490 nm using a Tecan microplate reader. The Rho control protein and lysis buffer served as positive and negative controls respectively**.** Amounts of active GTP-RhoA in myocilin transfectants were compared to mock-transfected controls.

PKA Assay

The PKA activity in equal protein aliquots of lysates from mock- and myocilin-transfected cells was assessed by the incorporation of phosphate in Leu-Arg-Arg-Ser-Leu-Gly

peptide using the non-radioactive Peptag system (Promega, Madison, WI). Negative and positive controls were included and the PKA activity was determined by densitometric analyses (Shen, Koga et al. 2008).

TOP/FOP-Flash Assays

Normal human TM and Caco-2 cells were co-transfected with TOP-Flash or FOP-Flash reporter plasmid (Millipore, Temecula, CA), pTarget-myocilin$_{WT}$, pTarget-myocilin$_{P370L}$, pTarget-myocilin$_{Q368X}$, or pTarget, as well as pEGFP-N1 (1:1:0.5 ratio) for 48 h. The cells were harvested and lysed in Promega luciferase assay lysis buffer. Using the Promega luciferase assay kit, the luminescence from the TOP- or FOP-Flash was read on a luminometer (OPTOCOMP II, MGM instruments). GFP florescence was monitored using a Tecan microplate reader (excitation wavelength, 485 nm; emission wavelength, 535 nm). The TOP/FOP-Flash readings were normalized to the GFP reading. Experiments were performed in triplicates. At least 3 experiments were performed.

Results

Aversion of the Actin and Focal Adhesion Phenotypes by Treatment of sFRP1

The myocilin construct pTarget-myocilin$_{WT}$ or pMyocilin$_{WT}$-EGFP was introduced into human TM cells. After transfection, the levels of myocilin protein, as judged by Western blotting, were approximately 10–20 fold higher than those in mock controls (data not shown). In agreement with findings from our previous studies (Wentz-Hunter, Shen et al. 2004; Shen, Koga et al. 2008), the pMyocilin$_{WT}$-EGFP-transfected green cells, compared to pEGFP-N1-transfected

mock controls, showed an apparent loss of both actin stress fibers (Fig. 5A) and vinculin-positive focal adhesions (Fig. 5B).

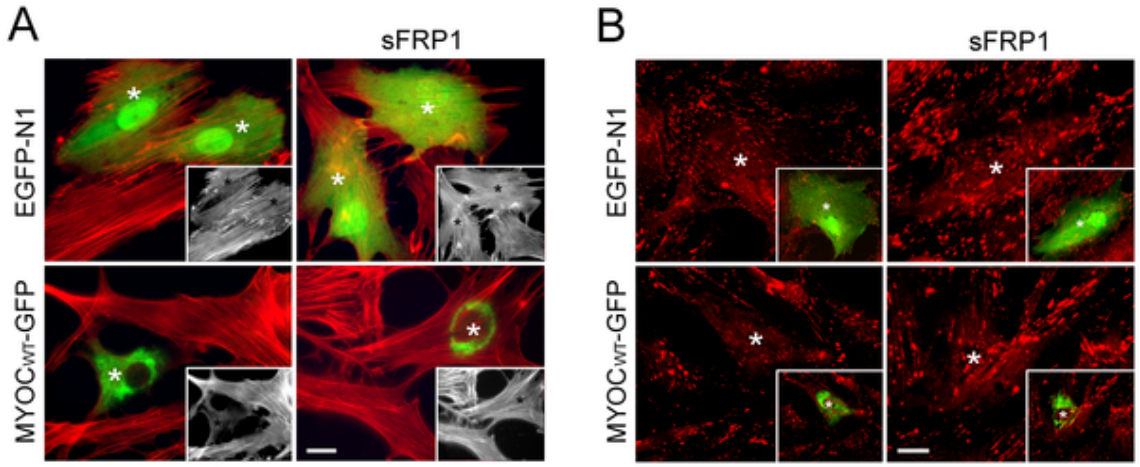

Figure 5. Treatment of sFRP1 averts the myocilin actin and focal adhesion phenotypes. TM cells were transfected with pEGFP-N1 (EGFP-N1, mock control) or pMyocilin$_{WT}$-EGFP (MYOC$_{WT}$-GFP) for 48 h, treated overnight with 50 nM sFRP1 and stained for actin (in red, **A**) or vinculin (in red, **B**). The transfected cells were marked by green fluorescence and/or white asterisks. Myocilin overexpression induced a loss of actin stress fibers (**A**) and vinculin-positive focal adhesions (**B**). The loss was averted by treatment of sFRP1. The staining was visualized using a Zeiss 100 M microscope. Insets in **A** show the actin stress fibers in same fields in black and white. The same transfected cells are indicated by black asterisks. Insets in **B** show the green transfected cells (white asterisks). Scale bar, 10 μm.

To test whether Wnt signaling is involved in the myocilin phenotype, TM cells after myocilin transfection were treated with sFRP1, a Wnt signaling pathway inhibitor (Mii and Taira 2011). Results indicated that inhibition of Wnt pathway in pMyocilin$_{WT}$-EGFP-transfected cells prevented, at least partially, the stress fiber dissolution and the focal adhesion reduction (Fig. 5A and 5B), suggesting that Wnt signaling might mediate the myocilin-induced actin alteration.

Effects of SB216763 on Human TM Cells

To support the notion that the myocilin phenotype was mediated via Wnt signaling, the effects of SB216763, a selective, cell permeable GSK-3 inhibitor, on normal human TM cells were investigated. This GSK-3 inhibitor has been commonly used to mimic the action of Wnt molecules to activate β-catenin (Braeuning and Buchmann 2009). As shown in Fig. 6, treatment with 2 and 10 μM of SB216763 triggered dissolution of actin stress fibers and loss of vinculin-positive focal adhesions (Fig. 6A). An enhanced nuclear staining of β-catenin was seen as expected in treated cells (Fig. 6A). SB216763 in addition caused an approximately 1.8-fold increase in the activity of PKA (Fig. 6B), a classical intracellular effector of the cAMP signaling. The level of active RhoA as measured by both pull down (Fig. 6C) and G-LISA (Fig. 6D) assays, on the other hand, was diminished. All these changes were reminiscent of those observed with myocilin overexpression. Furthermore, co-treatment of both SB216763 and H89, a PKA inhibitor, brought the RhoA activity back to normal (Figs. 6C and 6D), in keeping with our previous finding that cAMP/PKA activation was upstream of Rho inactivation (Shen, Koga et al. 2008).

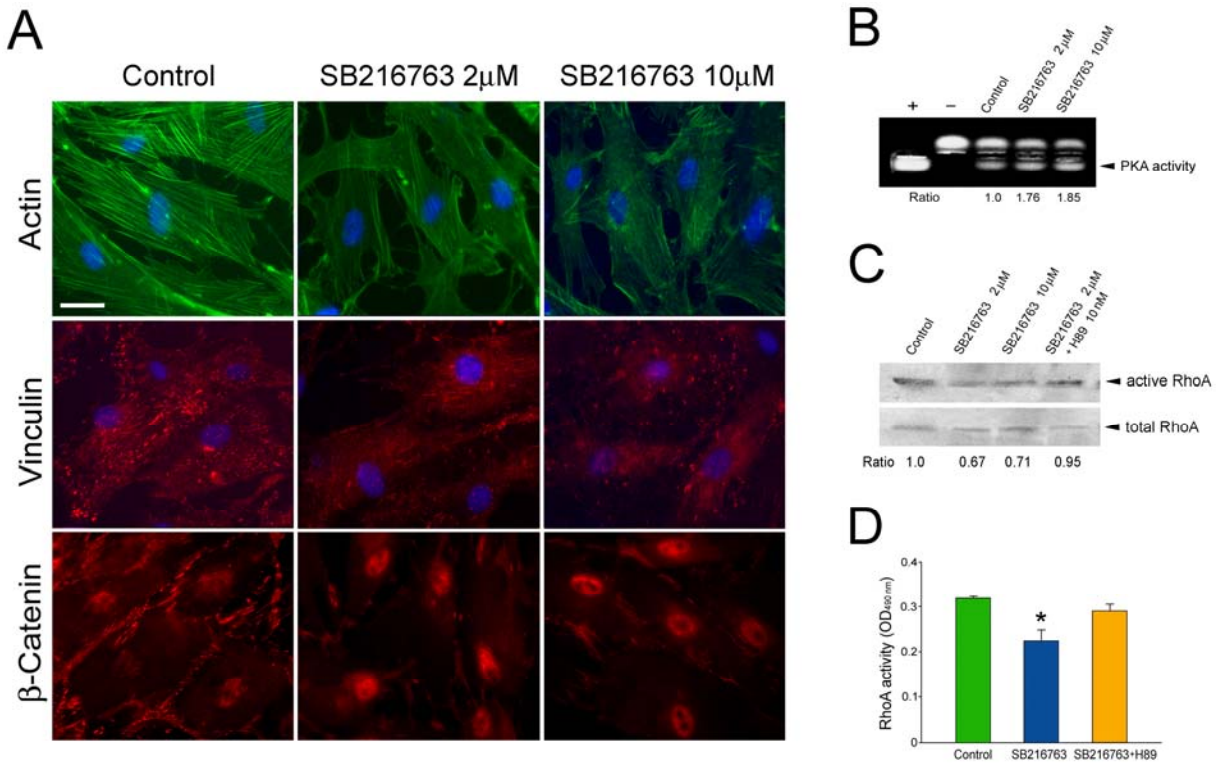

Figure 6. A. Actin (green), vinculin (red), and β-catenin (red) staining in normal human TM cells without (control) or with overnight treatment with 2 and 10 μM SB216763.Bar, 20 μm. **B.** PKA activity in TM cells without (control) or with treatment with SB216763. Equal amounts of protein lysates were subjected to PKA assays. Positive (+) and negative (-) controls were included. The non-phosphorylated (upper band) and the phosphorylated (lower band, arrowhead) substrates were resolved on agarose gels. The PKA activity, judged by the level of the phosphorylated substrate, in 2 (1.76±0.14, mean ± SD, n = 3) and 10 (1.85±0.15, n = 3) μM SB216763 treated cells ($P<0.006$ compared to control) was determined by densitometric analyses and normalized to that in untreated controls. **C**. RhoA activity in TM cells treated with 2 and 10 μM SB216763 or 2 μM SB216763 plus 10 nM H89, a PKA inhibitor. Cells untreated served as control. Active RhoA, measured by pull down assays, was normalized to total RhoA. The level of active RhoA was reduced by approximately 30% by treatment of SB216763. Its level however returned to normal when H89 was included in the treatment. **D**. RhoA activity as measured by G-LISA. The activity was lower in TM cells treated with 10 μM SB216763 (0.227±0.022 vs. 0.318±0.004 in control, mean ± SEM, n = 3). H89 treatment elevated the RhoA back to the control range (0.293±0.016, n = 3). *, $P<0.001$ compared to untreated control.

Wnt Activation upon Myocilin Transfection

For the analysis of β-catenin/Tcf/Lef signal activation, TOP-Flash/FOP-Flash luciferase assay has been the most commonly used (Osada, Chen et al. 2011). The TOP-Flash construct contains two repeats of three optimal copies of the Tcf/Lef binding sites upstream of a thymidine kinase minimal promoter that directs transcription of a luciferase reporter gene. The FOP-flash, containing mutated Tcf/Lef binding sites, is used as a negative control.

Normal human TM cells were transfected with TOP-Flash or FOP-Flash plasmid. The cells in each well were co-transfected with pTarget-myocilin$_{WT}$ or pTarget (control) to determine the myocilin effect, and also with pEGFP-N1 to control for variation in transfection efficiency. Results obtained revealed that in TM cells, the TOP-Flash response or the β-catenin/Tcf/Lef transactivation with or without myocilin transfection was marginal. The TOP-Flash/FOP-flash ratio was close to 1, contrasting to that seen in SW480 and Caco-2 human colorectal adenocarcinoma cell lines where the ratio was typically higher than 20 (Kuroda, Rabkin et al. 2006). It is possible that similar to cell lines such as A549 and HeLa cells (Kuroda, Rabkin et al. 2006), TM cells are simply a cell type in which the constitutive Wnt signaling is less than modest. Furthermore, the thymidine kinase minimal promoter used in the TOP−/FOP-Flash constructs to drive luciferase expression is a relatively weak promoter. The low promoter activity plus the poor transfection efficiency (10–15%) in primary human TM cells might also explain for the low TOP-Flash readouts observed in the TM experiments.

Caco-2 cells, as mentioned above, have been used in the literature for TOP-Flash reporter assays (Logan and Nusse 2004; Wang, Liu et al. 2011). Experiments were thus repeated using Caco-2 cells as surrogates to determine the Wnt activation upon myocilin transfection. An approximately 2.7 fold, significant ($P<0.001$ compared to pTarget control, $n = 3$) increase in the

Lef/Tcf/Wnt activation following co-transfection of myocilin construct was found in Caco-2 cells (Fig. 7A). The TOP-Flash to FOP-Flash ratios were 55.3 ± 3.4 and 20.0 ± 2.9, respectively, in pTarget-myocilin$_{WT}$- and pTarget-co-transfected samples. In agreement with the Wnt activation, the nuclear β-catenin staining was enhanced in myocilin-overexpressing TM cells compared to GFP mock transfected and non-transfected controls (Fig. 7B).

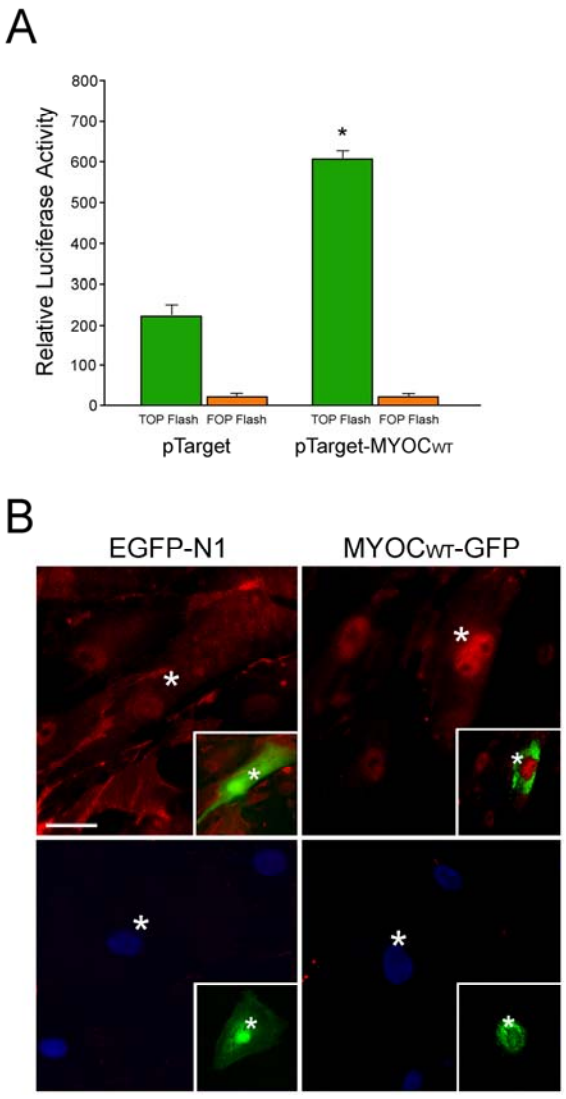

Figure 7. A. Myocilin expression activates Tcf/Lef-dependent transcription in Caco-2 cells. Caco-2 cells were co-transfected with TOP- or FOP-Flash reporter construct, and pTarget-myocilin$_{WT}$ (pTarget-MYOC$_{WT}$) or pTarget plasmid for 48 h. A pEGFP-N1 vector was also co-transfected for standardization. Luciferase activity measured was normalized to the GFP reading. Three experiments were performed in triplicate. Results (mean ± SEM) from a representative experiment are shown. *, P<0.001 compared to pTarget control. **B**. β-catenin (red) staining (top panel) in human TM cells after transfection with pEGFP-N1 (EGFP-N1, mock control) or pMyocilin$_{WT}$-EGFP (MYOC$_{WT}$-GFP). Minimal staining was observed when normal mouse IgG was used in place of primary anti-β-catenin (bottom panel) in the procedure. Insets highlight the green transfected cells (white asterisks) in the same fields. Nuclei were stained by DAPI in blue. Scale bar, 20 μm.

Mutants Display Phenotypes Similar to the Wild-type Myocilin

Transfection of normal human TM cells with pMyocilin$_{P370L}$-EGFP and pMyocilin$_{Q368X}$-EGFP, similar to that observed with the wild-type, resulted in a loss of actin stress fibers (Fig. 8A). To examine the cell-matrix cohesiveness, TM cells were subjected to trypsin sensitivity tests as previously described (Shen, Koga et al. 2008). It was found that the cells, upon myocilin mutant transfection, became more sensitive to trypsinization. The trypsinization time (Fig. 8B) needed for cells to round up was significantly ($P<0.0001$) shorter for P370L (88.9 ± 1.5 s, n = 30) and Q368X (85.3 ± 3.7 s, n = 30) myocilin mutant transfectants than that for mock controls (106.0 ± 3.1 s, n = 30).

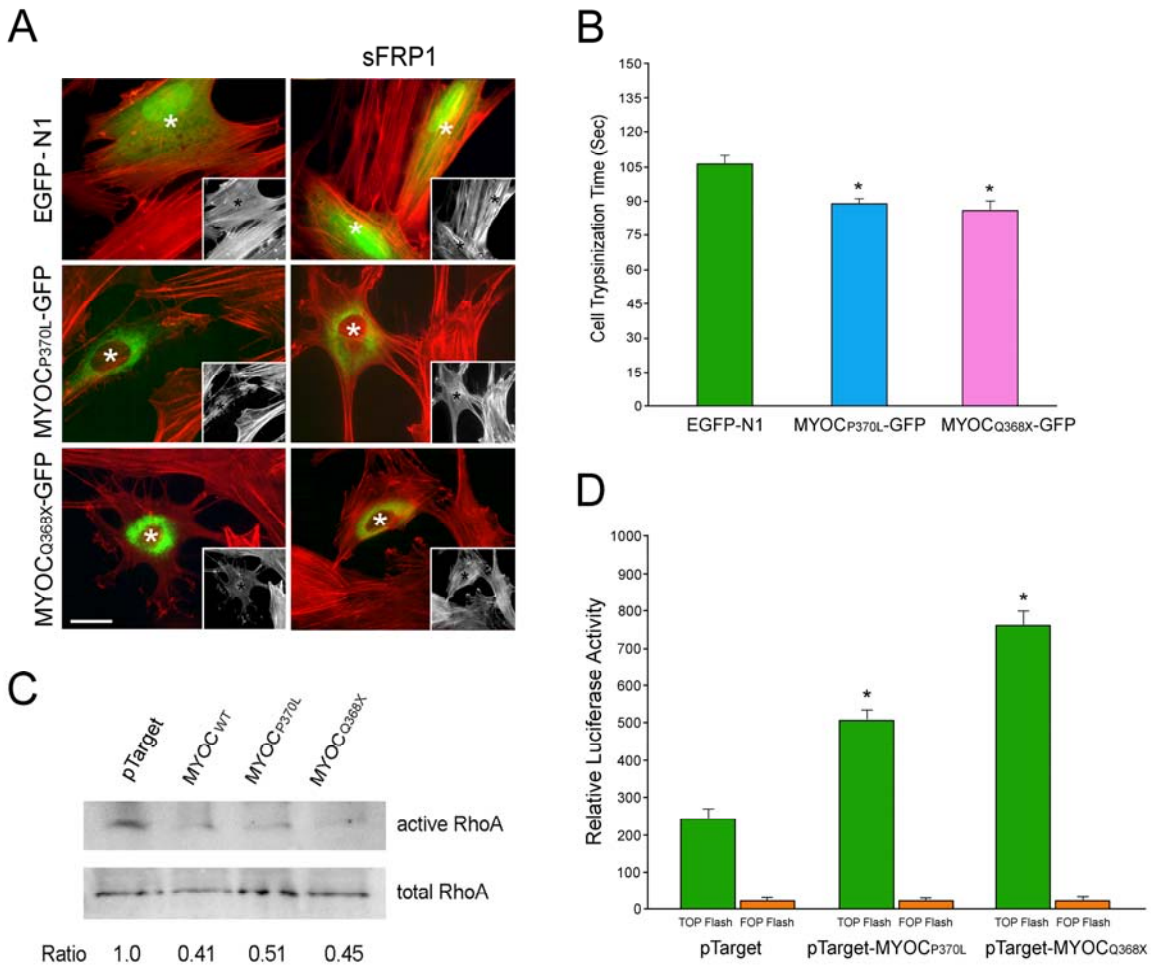

Figure 8. A. Actin (red) staining in pEGFP-N1 (EGFP-N1)-, pMyocilin$_{P370L}$-EGFP (MYOC$_{P370L}$-GFP)-, and pMyocilin$_{Q368X}$-EGFP (MYOC$_{Q368X}$-GFP)-transfected TM cells without or with subsequent overnight treatment of sFRP1. Insets show the same field in black and white. Transfected cells are marked by green fluorescence, or white or black (in insets) asterisks. Scale bar, 20 μm. **B**. The trypsinization time (mean ± SEM) needed for pEGFP-N1 (EGFP-N1)-, pMyocilin$_{P370L}$-EGFP (MYOC$_{P370L}$-GFP)-, and pMyocilin$_{Q368X}$-EGFP (MYOC$_{Q368X}$-GFP)-transfected TM cells to become refractile. Asterisk indicates that the trypsinization time for myocilin mutant transfectants was significantly ($P<0.0001$, $n = 30$) lower than that of GFP controls. **C**. GTP-bound active RhoA in pTarget-, pTarget-myocilin$_{WT}$ (MYOC$_{WT}$)-, pTarget-myocilin$_{P370L}$ (MYOC$_{P370L}$)- and pTarget-myocilin$_{Q368X}$ (MYOC$_{Q368X}$)-transfected TM cells. Pull down assays were performed in duplicates to determine the RhoA activity. The amount of the active or GTP-bound RhoA was normalized against the total amount in cell lysates and expressed as mean ± SD relative to that in pTarget control. The RhoA activity upon myocilin wild-type (0.41 ± 0.04, $n = 2$) and mutant transfection (0.51 ± 0.03 for P370L; 0.45 ± 0.04 for Q368X, $n = 2$) was found to be significantly reduced ($P < 0.0001$) compared to controls. Experiments were repeated two times with similar results. **D.** Top−/Fop-Flash assays. Caco-2 cells were co-transfected with TOP- or FOP-Flash reporter construct, pTarget-myocilin$_{P370L}$, pTarget-myocilin$_{Q368X}$, or pTarget, as well as pEGFP-N1. Luciferase activity (mean ± SEM, $n = 8$) was measured post transfection and was normalized to the GFP level. *, $P < 0.001$ compared to the pTarget control.

Pull down assays were carried out to measure the amounts of active RhoA in mock-, pTarget-myocilin$_{P370L}$ -, and pTarget-myocilin$_{Q368X}$-transfected cells. The level of GTP-bound or active RhoA in myocilin mutant transfectants was lower (Fig. 8C) than that in controls. Quantitation by densitometry and normalization to the total RhoA revealed that the RhoA activity upon P370L and Q368X transfection was significantly ($P < 0.0001$) reduced compared to the mock control.

Both P370L and Q368X mutants activated Wnt signaling in Caco-2 cells (Fig. 8D), as indicated by the higher TOP-Flash to FOP-Flash ratios in pTarget-myocilin$_{P370L}$ (45.8 ± 7.5, $n = 8$)- and pTarget-myocilin$_{Q368X}$ (67.3 ± 9.2, $n = 8$)-co-transfected samples compared to the pTarget (19.9 ± 3.3, $n = 8$) controls. The ratios were significantly ($P < 0.0001$) different.

PKA Activity

To determine whether Wnt signaling is up- or down-stream that of cAMP/PKA, human TM cells transfected with pTarget-myocilin$_{WT}$ were treated with sFRP1. PKA assays showed that the enzyme activity (Fig. 9A) was elevated by approximately 40% ($P < 0.016$), as seen previously (Shen, Koga et al. 2008) by forced expression of wild-type myocilin (1.40 ± 0.13, mean ± SD, $n = 3$) but the activity was reduced back to normal when Wnt activation was inhibited (1.10 ± 0.12, $n = 3$, $P > 0.05$ compared to pTarget control). Furthermore, PKA assays revealed that the kinase activity (Fig. 9B) was significantly ($P < 0.05$) increased in myocilin P370L (1.35 ± 0.15, $n = 3$) and Q368X (1.38 ± 0.21, $n = 3$) mutant-expressing TM cells. Similar to that observed with the wild-type, the PKA elevation in the mutant transfectants (1.15 ± 0.12 and 0.85 ± 0.10 respectively, $P > 0.05$) was obviated by treatment of sFRP1, signifying again that Wnt pathway was upstream of PKA signaling.

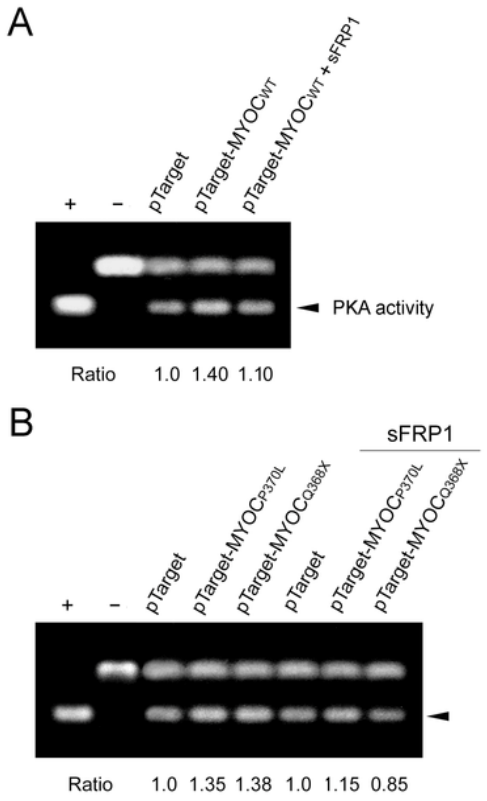

Figure 9. Effects of sFRP1 on PKA activity in TM cells. **A.** Cells were transfected with pTarget and pTarget-myocilin$_{WT}$ (pTarget-MYOC$_{WT}$) for 48 h. One set of samples was treated overnight with sFRP1 and the other was untreated. Lysates collected were subjected to PKA assay as described in Fig. 2B. **B**. Cells transfected with pTarget, pTarget-myocilin$_{P370L}$ (pTarget-MYOC$_{P370L}$) and pTarget-myocilin$_{Q368X}$ (pTarget-MYOC$_{Q368X}$) were untreated or treated overnight with sFRP1. Lysates were subjected to PKA assays. The PKA activity (arrowhead) was determined by densitometric analyses. Results were expressed as ratios relative to the pTarget control. Experiments were repeated 3 times. Data from one representative experiment are presented.

Discussion

The study demonstrated that wild-type myocilin, when overexpressed at a moderate level, activated the Wnt signaling pathway, which in turn mediated downstream events such as loss of actin stress fibers and elevation of the PKA activity. The notion of Wnt mediation is supported by observations that a Wnt inhibitor, sFRP1, was able to avert the myocilin-induced alterations (5 & 8). Moreover, treatment of SB216763, a Wnt-enhancing agent, led to myocilin phenotypes including loss of actin stress fibers and focal adhesions, increase of PKA activity, as well as inhibition of RhoA activity (Fig. 6). The Wnt activation by myocilin expression, as evidenced by TOP−/FOP-Flash luciferase assays (Fig. 7) in the current study, is in agreement with an earlier

observation that the β-catenin immunostaining was enhanced, compared to control littermates, in the angle tissues (including TM) of transgenic mice produced using bacterial artificial chromosome DNA containing full length human myocilin gene (Kwon, Lee et al. 2009).

The Wnt signaling is a major intracellular pathway that plays important roles in diverse biological processes including cell proliferation, differentiation, development, and inflammation (Jin, George Fantus et al. 2008; Cadigan and Peifer 2009; Dejana 2010; Rao and Kuhl 2010). Extensive studies of the Wnt pathway have been documented in the areas of cancer, stem cells and neural development (Logan and Nusse 2004; Luo, Chen et al. 2007; Jin, George Fantus et al. 2008; Cadigan and Peifer 2009). The Wnt genes can signal through a β-catenin/Tcf/Lef-dependent canonical pathway as well as two β-catenin-independent, non-canonical pathways. In the case of myocilin, it seems that the canonical pathway was a player since sFRP1 has been indicated in the literature to be an inhibitor to the Wnt canonical pathway (Yang, Liu et al. 2009). Moreover, transactivation of Tcf/Lef transcription factors in the canonical pathway by myocilin was demonstrated by TOP/FOP-Flash assays (Fig. 7). sFRP1 and other sFRPs however have also been shown to exert their effects via both canonical and non-canonical signaling (Yang, Liu et al. 2009; Mii and Taira 2011). There have been many examples more recently noting that individual modulators of Wnt signaling can be involved in several interwoven branches (Rao and Kuhl 2010). The additional involvement of non-canonical pathways in the myocilin-induced event is hence a distinct possibility.

The Wnt activation depends on Wnt ligands and specific sets of receptors. The aspects of Wnt network activated may depend on the cell type, conditions and the cellular context such as local concentrations of Wnt individual elements (Rao and Kuhl 2010). Wnt/β-catenin signaling can additionally be activated via Wnt-independent mechanisms including G proteins (Luo, Chen

et al. 2007). The mechanism by which myocilin regulates the Wnt signaling is unclear. Myocilin has been shown to interact with sFRP1, sFRP3 and other Frizzled receptors (Kwon, Lee et al. 2009). Such direct interactions, along with other factors/events, may be involved in the Wnt activation upon myocilin overexpression.

The Wnt signaling is known to cross talk with other signaling mechanisms (Kikuchi, Yamamoto et al. 2011) including Notch, NF-κB, mTOR, protein kinase C (Luo, Chen et al. 2007) and PKA (Fang, Yu et al. 2000; Moon, Kohn et al. 2004; Chen, Ginty et al. 2005; Taurin, Sandbo et al. 2006). Among them, PKA has been shown in a number of investigations to act upstream of Wnt signaling, resulting in β-catenin stabilization either via phosphorylation on Ser 9 of GSK-3ß inhibiting thereby its activity (Fang, Yu et al. 2000), or by direct phosphorylation of ß-catenin on Ser 675 to inhibit ß-catenin degradation or promote its binding to CREB-binding protein (Taurin, Sandbo et al. 2006). PKA has also been noted in a few reports to act downstream of Wnt signaling. For instance, Wnt proteins such as Wnt1 and Wnt7a were found to activate adenyl cyclase, cAMP and PKA to induce myogenesis during embryogenesis (Chen, Ginty et al. 2005). Adding to this list, the present study also concluded that PKA was downstream of Wnt signaling since the heightened PKA activity in myocilin-expressing cells declined back to the normal level (Fig. 9) following treatment of Wnt inhibitor sFPR1.

Based on the current findings, a previously proposed schematic model can be modified as in Fig. 10. We surmise that moderately up-regulated wild-type myocilin activates Wnt signaling pathway, which leads to cAMP elevation, PKA activation and RhoA inactivation, and in turn triggers the loss of actin stress fibers and focal adhesions in TM cells, rendering them in a de-adhesive state. Through these steps and/or other pathways, the de-adhesion process on a long term chronic basis may leave the cells vulnerable to develop pathology upon additional stress.

The involvement of the Wnt signaling demonstrated herein suggests an intervention possibility in rescuing the myocilin phenotypes.

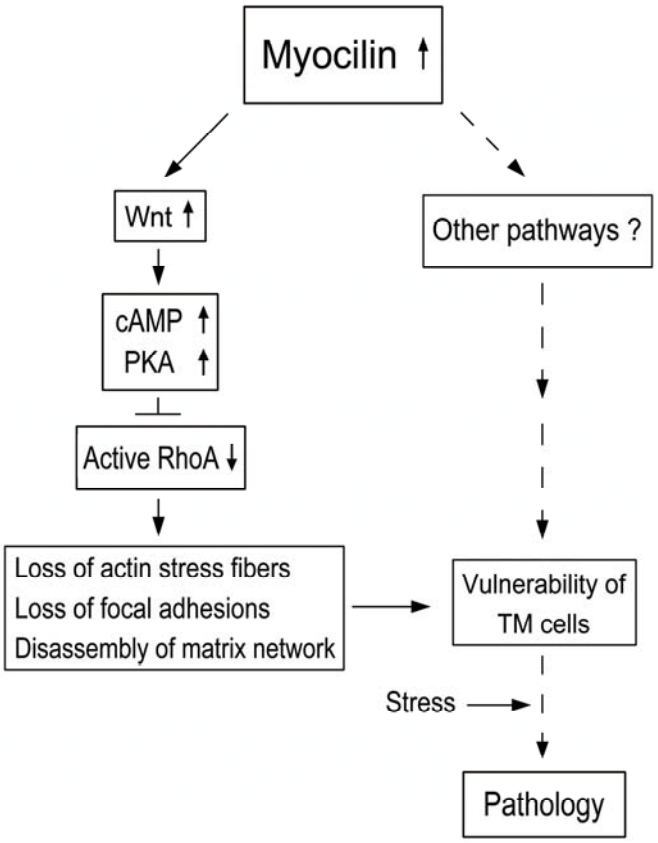

Figure 10. A schematic model of possible events in human TM cells triggered by up-regulation of myocilin.Myocilin, when moderately up-regulated, induces Wnt activation, and the downstream cAMP/PKA activation and RhoA inactivation, resulting in a loss of actin stress fibers and focal adhesions and disassembly of matrix network. These changes or other pathways may affect the integrity of TM cells, rendering them more susceptible to additional stress or challenge on a chronic, long-term basis, leading to pathologic consequences. Other intermediate mediators or pathways are yet to be identified. Dotted lines indicate steps that have not been investigated in the present work or our previous investigation (Wentz-Hunter, Shen et al. 2004; Sakai, Park et al. 2006; Shen, Koga et al. 2008).

In the *in vivo* TM system, the actin cytoskeleton system has been linked to regulation of the aqueous humor outflow (Tian, Gabelt et al. 2009; Stamer and Acott 2012). Experiments in living monkeys or perfusion organ cultures have shown that agents including cytochalasins and H-7, which perturb the actin structure increase the outflow facility. The increased flow is believed to result from the separation of cells from their neighboring cells and the ECM and the change in the overall TM geometry through cellular relaxation and contraction. A decrease in actin stress fibers and focal adhesions has also been found to occur upon treatment with Rho

kinase (ROCK) inhibitor Y-27632 (Honjo, Tanihara et al. 2001), and gene transfer of dominant negative RhoA (Vittitow, Garg et al. 2002) or C3 transferase (Liu, Hu et al. 2005) in TM cells. ROCK inhibitors have in addition been shown to decrease myosin light chain phosphorylation, which leads to relaxation of TM and SC cells (Zhang, Maddala et al. 2008). Currently, selective ROCK inhibitors such as AR-12286 are in clinical trials (Chen, Runyan et al. 2011; Kopczynski, Novack et al. 2013).

It is of note that experiments with monkey and perfusion organ culture were all short term, from a few hours to up to 7 days (Tian, Gabelt et al. 2009; Stamer and Acott 2012). A phase IIb, 28-day, safety and efficacy trial of topical AR-12286 has been completed (Chen, Runyan et al. 2011) although its long term tolerability profile is still unknown. Glaucoma is a chronic, age-related disease. On a long term and persistent basis and especially because the TM cells *in situ* are continually subjected to stress from the aqueous flow and IOP fluctuations, it is conceivable that the altered actin cytoskeleton and impaired cell-matrix adhesiveness observed with overexpressed wild-type myocilin would ultimately weaken the TM cells and destabilize the system. Cell loss and pathologic consequences may then ensue. The vulnerability of myocilin-transfected TM cells has been implicated by their susceptibility to apoptotic challenge (Wentz-Hunter, Shen et al. 2004). Evidence was presented that anti-Fas treatment triggered a significantly higher level of apoptosis in myocilin transfectants than the mock controls (Wentz-Hunter, Shen et al. 2004).

The activation of Wnt is also detected in cells expressing P370L and Q368X myocilin mutants (Fig. 8). These cells display all the wild-type phenotypes: loss of actin stress fibers and focal adhesions, impairment in TM cell-matrix cohesiveness, activation of PKA, and reduction in the active RhoA level (Fig. 8). Since the 1–368 myocilin sequence is intact in both mutants, one

may conclude that such a sequence is responsible for the myocilin phenotypes. On the other hand, the phenotypes may also be related to the retention of wild-type, endogenous myocilin in the cells. P370L and Q368X mutants have been well documented to be secretion incompetent (Caballero, Rowlette et al. 2000; Jacobson, Andrews et al. 2001). They not only cannot be secreted themselves, but can also additionally block or suppress secretion of the endogenous myocilin. The net result would thus be intracellular accumulation of both mutant and wild-type myocilins (Caballero, Rowlette et al. 2000; Jacobson, Andrews et al. 2001), displaying the ensuing phenotypes.

Myocilin mutants including P370L and Q368X are detergent resistant (Liu and Vollrath 2004). Not being secreted, they accumulate intracellularly and have been shown to induce ER stress (Joe, Sohn et al. 2003; Yam, Gaplovska-Kysela et al. 2007; Zode, Kuehn et al. 2011). As a stress response, the cells activate the unfolded protein response, upregulating ER chaperones with the subsequent activation of caspases 12 and 3 and the expression of ER stress–initiated apoptotic transcriptional factor CHOP, leading to apoptosis (Joe, Sohn et al. 2003; Yam, Gaplovska-Kysela et al. 2007; Zode, Kuehn et al. 2011). Furthermore, P370L mutant has been reported to cause dysregulation of calcium channels and mitochondrial membrane depolarization (He, Leung et al. 2009). Our demonstration of the myocilin phenotypes offers an additional mechanism as to how P370L and Q368X mutants may lead to cell vulnerability, increased cell susceptibility to stress, cell death, and ultimately pathology.

PART II: 3-DIMENSIONAL (3D) CULTURE OF HUMAN TRABECULAR MESHWORK CELLS

TM cells are essential for maintenance of the normal aqueous humor outflow system. Understanding the physiology of TM cell is of vital importance for illustration of disease mechanism(s) for glaucoma.

In vivo, TM cells have limited proliferative activity. TM cells however have been isolated, propagated, and maintained *in vitro* from bovine, calf, porcine, murine, monkey, and human eyes. The *in vitro* models used so far to investigate TM cells include 2-dimensional (2D) cell culture and organ cultures (Gasiorowski and Russell 2009). Areas of research including cell behavior, ECM production/turnover, signal transduction, gene expression, protein expression, mechanical and other stress effects are mostly performed using 2D monolayer cultures (McKee, Wood et al. 2011; Wood, McKee et al. 2011; Polansky, Weinreb et al. 1979; Zhou, Zhang et al. 1996; Zhao, Ramsey et al. 2004; Fautsch, Howell et al. 2005; Borras, Xue et al. 2006).

2D culture bears the benefits of relative ease and economy due to the fact that sufficient number of cells/materials can be made available for more in-depth exploration. In the 2D culture system, cells are grown on flat, rigid substrates such as glass or plastic, confined to a monolayer environment. It is now well recognized that the 2D cell culture may be a suitable *in vitro* model only in limited situations for particular types of investigations. It does not allow understanding of the complex morphologies, such as cell-to-cell and cell-to-matrix interactions, that are observed *in vivo* (Matsuda, Kawamoto et al. 1253; Tibbitt and Anseth 2009). It also does not provide the architecture, proper transport or diffusion mechanisms, or essential biophysical cues to represent the environment of cells exposed *in vivo* (Wood, McKee et al. 2011; Fautsch, Howell et al. 2005; Kim 2005; Gasiorowski and Russell 2009). By contrast, a 3-dimensional (3D) system provides

an additional dimension for external mechanical inputs and cell adhesion (Griffith and Swartz 2006) and could offer assessments of cell mechanics, cell interactions and cell characteristics in an *in vivo*-like environment (Kim 2005). The 3D culture system has not yet to be applied to human TM cells. In this part of the study, we set our goal to establish an effective *in vitro* 3D culture model to help portray activities, characteristics, and stress responses of TM cells *in vivo.*

Two major 3D platforms in the market are hydrogels and inserts. We carried out initial experiments, testing several products from each that included commercially available hydrogels such as 3DLife (Cellendes), Puramatrix (BD BioSciences), QGel (Qgelbio), Extracel (Glysan Biosystems) and inserts such as 3D Insert (3D Biotek), Preset VECELL (Nacalai USA), and Alvetex (Reinnervate). Puramatrix and Extracel caused cell death due to the low pH buffer used in the procedure. The 3D Insert couldn't hold cells because of the large pore size (300 μm) and Preset VECELL, in which the 50 - 70 μm thick membrane are composed of 2 - 10 μm diameter fibril networks, on the contrary, did not let cells grow inside of the scaffold (pore size was unknown). Human TM cells did survive in QGel, 3DLife and Alvetex. QGel™ MT 3D Matrix is a synthetic PEG (polyethylene glycol)-based hydrogel. It contains structural component PEG and cell adhesion-promoting components such as covalently-bond RGD peptide and degradation component (enzymatically degradable matrix crosslinker). QGel™ degradation is exclusively mediated by the cells themselves via protease secretion and activation depending on how they migrate. 3DLife is a synthetic PVA-PEG (polyvinyl alcohol-polyethylene glycol) hydrogel. The Alvetex®Scaffold is a highly porous, cross-linked polystyrene scaffold, which has been engineered into 200 μm thick membranes. These systems were further examined and characterized. Genes that differentially expressed in human TM cells in 2D cultures vs. *in vivo* such as myocilin (MYOC), matrix GLA protein (MGP), angiopoietin like-factor 7

(CDT6/ANGPTL7), fibronectin, and collagen type I were studied. Overall, human TM cells grown in QGel and Alvetex scaffold showed more *in vivo* like pattern of gene expression. Human TM cells grown in the Alvetex scaffold was additionally optimized as to the coating conditions, scaffold pore sizes, and the seeding density of cells.

Materials and Methods

Cell Culture

Normal human eyes were obtained from the Illinois Eye Bank (Chicago, IL). The TM tissues from donors 10 and 31 years of age without any known ocular diseases were dissected and cultured as previously described. These monolayer cells cultured on a flask are referred as a 2D culture system. 3rd or 4th passage of human TM cells from 2D cultures was used in the 3D culture system.

Synthetic Peptide Hydrogel (QGel)

Human TM cells were seeded in the REF 1001 QGEL™ MT 3D Matrix (MMP-Degradable, with RGD-peptide) (Qgel bio, Switzerland) following manufacturer's protocol. Briefly, QGel^{TM} MT 3D Matrix powder was resuspended in the QGel^{TM} buffer A and vortexed for 10 s. TM cells were then mixed with QGel matrix and vortexed quickly for homogenization. After mixing, the solution was pipetted out and drops were quickly applied onto the sterilized QGelTM 3D Disc Caster. The disc caster was closed carefully and the system was incubated in a cell culture incubator (37°C) for 30-45 min to polymerize the gel. Each gel disc was then carefully transferred into a 24-well plate containing 1 ml pre-warmed culture medium. The medium was subsequently replaced after a 2 h-incubation and changed every two days for longer term culture.

3-D Life PVA-PEG Hydrogel (Cellendes)

3-D Life PVA-PEG hydrogel was acquired from Cellendes GmbH (Reutlingen, Germany). Hydrogel was formed following manufacturer's protocol. In brief, water, 10x CB (concentrated buffer) (pH 5.5) and Mal-Polymer were combined in an eppendorf tube. Human TM cells were added and mixed into the tube. Crosslinker (PEG-Link, 4.5 µl) was placed on the surface of a 12 well culture plate. The cell mixture (25.5 µl) from the tube was quickly mixed with 4.5 µl of PEG-Link in the plate by pipetting up and down 3 times, avoiding the formation of air bubbles. The mixture was left on the surface of culture dish in a 37^{o}C incubator. The gel was formed in approximately 3 min. After 1 h, complete culture medium was added. The medium was replaced every 2-3 days thereafter.

Alvetex Scaffold System

Avetex scaffold was acquired from Reinnervate (Rurham, United Kingdom). The scaffold membrane located at the bottom of each well in Avertex 24 well plates was first treated with 70% alcohol to render it hydrophilic. The scaffolds were subsequently washed with serum free DMEM medium (Sigma) 3 times to remove trace of alcohol. In some experiments, the scaffolds were coated with fibronectin (Sigma), collagen type I (BD Biosciences, San Jose, CA) or left uncoated. Human TM cells at 3rd -4th passage were seeded in scaffold at 200,000 cells/40 µl per well. The 24-well plate was incubated at 37°C for 1 h to allow the cells attach. Fresh complete medium was added to each well subsequently. The cells on Alvetex scaffolds were cultured up to 14 days, with medium changed every two days.

MTT Assay

To study cell attachment on coated or uncoated Alvetex scaffold, 200,000 cells were seeded in each well of Alvetex 24-well plates (fibronectin or collagen type I coated or uncoated). After 24 h, the culture medium was replaced with 0.5 mg/ml of thiazolyl blue tetrazolium bromide (MTT, Sigma) in serum free DMEM medium. After incubation at 37°C for 2 h, MTT containing medium was discarded and the purple crystals formed by the cells were dissolved in acidified isopropanol. The plate was covered by alumni foil and shaked for 5 min on an orbital shaker. The purple solution was transferred into 96 well plates and the optical density at 562 nm (OD_{562}) (reference wavelength 650 nm) was measured.

To study human TM cell proliferation on Alvetex, 200,000 cells were seeded in each well of Alvetex scaffold (uncoated, 24 well plate format). For parallel comparison, 200,000 cells were seeded in each well of 2D 24-well tissue culture plates. The culture medium was replaced every two days. At days 1, 3, 7, 10 and 14, cells from 3D Alvetex plate as well as 2D tissue culture plate were stained with MTT as described above. OD_{562} (reference wavelength 650 nm) was measured. Experiments were repeated three times.

Analysis of Cell Morphology, Actin and Immunofluorescence staining

Human TM cells grown on Alvetex (20 or 40 μm pore size) for 2 weeks were fixed with 4% paraformaldehyde in PBS and embedded in paraffin. Ten-μm-thick sections were cut, deparaffined and mounted by VECTASHIELD mounting medium with DAPI to visualize the cell location in the scaffold. To compare the expression level of fibronectin, myocilin and type I collagen in 3D vs. 2D culture, sections were also immunostained with mouse anti-human fibronectin (BD Transduction Laboratories, Lexington, KY), myocilin (kindly provided by Dr. Michael Fautsch at the Mayo Clinic, Rochester, MN) and collagen type I (EMD Millipore) antibodies. To examine the activation of β catenin, human TM cells grown on Alvetex for two

weeks were transfected with pMYOC-GFP for 48 h. The entire Alvetex scaffold was fixed and incubated with anti-β catenin antibody as in part I of this thesis. Actin was examined using rhodamine-phalloidin as described in part I of this thesis. Human TM cells grown in 2D chamber slides for identical time period were similarly examined for comparisons.

RT-qPCR

Total RNA was extracted from QGel, and Alvetex systems using RNeasy®kit (Qiagen, Valencia, CA). Total RNA (100 ng) was reverse transcripted into cDNA using first strand cDNA synthesis kit (Fermentas, Glen Burnie, MD). mRNA levels of human myocilin (MYOC), matrix GLA protein (MGP), angiopoietin-related protein 7 (CDT6/ANGPTL7), fibronectin (Fn) and collagen type I (ColIA1) were measured by Taqman gene expression assay (Life technology, Carlsbad, CA). Human glyceraldehyde 3-phosphate dehydrogenase(GAPDH) level was measured also by Taqman gene expression assay (Life technology) as an internal control. qPCR was performed on ViiA™ 7 real-time PCR system using program: 50°C, 2 min, 95°C, 10 min, 95°C, 15 sec; 60°C, 1 min; 40 cycles. The cycle threshold (Ct) of target genes such as human myocilin was normalized against that of GAPDH from the same sample. The ratio of differential expressed was calculated as following:

Ratio target gene expression (experimental/control) =

$$\frac{\text{fold change in target gene expression (expt/control)}}{\text{fold change in reference housekeeping gene expression (expt/control)}}$$

Results

Human TM cells Cultured in Hydrogel Systems

HTM cells seeded in two commercially available hydrogel systems (QGel and Cellendes) were tested. QGel is synthetic PEG hydrogel ECM mimics and Cellendes is PVA -PEG hydrogel. Gel polymerization occurs at neutral pH for QGel but pH 5.5 for Cellendes. Both gels were formed quickly. Observation by inverted phase contrast microscopy was very easy since both gels were transparent.

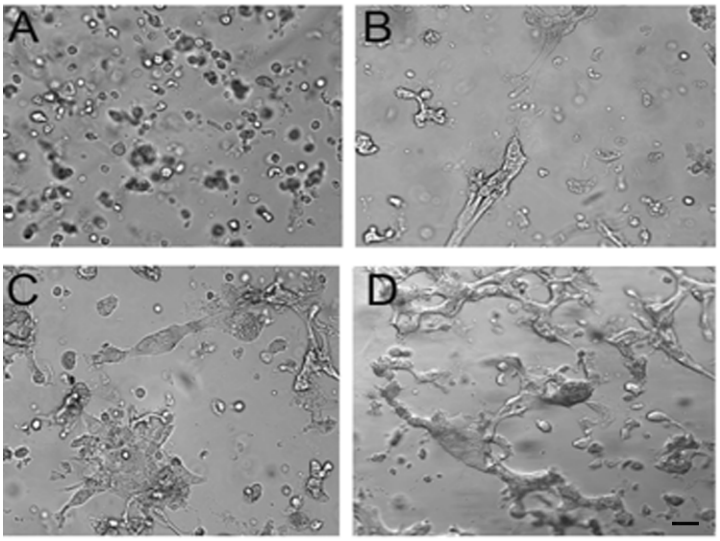

Figure 11. Morphologic changes of human TM cells in QGel hydrogel system. **A**. The cells were separated as single cell suspension when initially seeded in QGel. **B**. Some cells became elongated 24 h after seeding. Cell to cell connection commenced. **C**. Large cell clumps formed 3 days after seeding. **D**. Cell-cell connection network formed 1 week after seeding. (resembling tube formation by endothelial cells (Sacharidou, Stratman et al. 2012)). Scale bar, 20 μm.

In the QGel system, human TM cells stayed as single, round cells upon seeding (Fig. 11 A). They started to migrate and became elongated after 2 day. Cell to cell extension was seen (Fig. 11B). By 3 days, cell clusters were observed (Fig. 11C) and in one week, tubular networks that resembled those formed by endothelial cells in 3D systems were formed (Yang, Cao et al. 2004; Sacharidou, Stratman et al. 2012) (Fig. 11D).

3-D Life PVA-PEG hydrogel from Cellendes was also tested. The major components in the hydrogel are maleimide-functionalized polyvinyl alcohol (Maleimide-PVA) and thiol-functionalized polyethylene glycol (PEG-Link). Both components can be mixed under

physiological conditions (pH 7.2) or acidic condition (pH 5.5) in the presence of cells; thiol groups form stable thioether bonds with maleimide groups, which results in the formation of a gel. The gel formation reaction proceeds very fast at neutral pH, while the lower pH slows down gel formation (manufacture's user guide). We used pH 5.5 for cell seeding. Human TM cells survived but failed to migrate. They remained to be single cells even after 1 week in culture (data not shown) maybe because the PEG-link is non-biodegradable.

Alvetex Supported TM Cell Growth

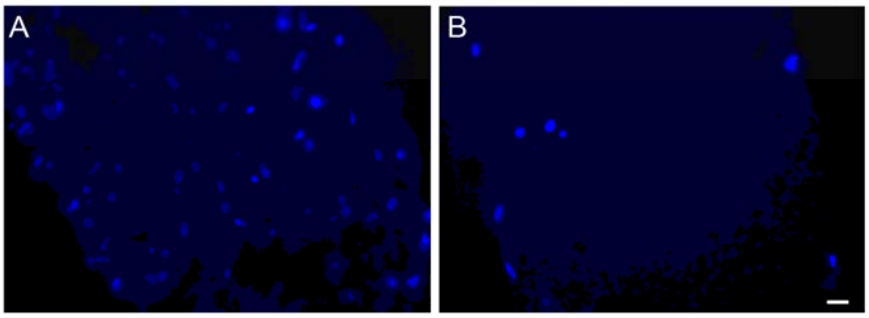

Figure 12. Human TM cells grow on Alvetex 40 µm (**A**) or 20 µm (**B**) scalffold. Nuclei were stained with DAPI to indicate the position in the scaffold. Scale bar, 20 µm.

Alvetex scaffold is a 200 µm thick inert porous polystyrene insert. It came with two pore sizes (40 and 20 µm). When grown in the scaffold with 40µm pore size, human TM cells were present in multilayers, covering the entire thickness of the scaffold after two weeks in culture (Fig. 12A). On the other hand, with the 20 µm-pore-size scaffold, the cells were seen only at the surfaces (Fig. 12B). They either failed to attach or grow. It is possible that the pore size was too small for the cells to pass through to inner layers and survive.

Gene Expression Pattern in 3D Culture Systems vs. in 2D

The 3D *in vitro* systems were further assessed by gene and protein expression to determine whether or which system(s) most accurately replicate that observed *in vivo* status. Human MYOC, MGP, CDT6/ANGPTL7, Fn1 and ColIA1 mRNA levels were examined on samples from 2D and 3D cultures (QGel or Alvetex) utilizing the Taqman gene expression kit (Life Technology). After normalization using human GAPDH Taqman gene expression kit, MYOC and MGP message levels from all the Alvetex and QGel 3D samples were found higher than those from 2D culture samples while CDT6/ANGPTL7, Fn1, ColIA1 results were the opposite, their levels in 3D were lower than those of 2D (Fig. 13). This indicates that cells grown in 3D were quite different from 2D cultures. The pattern of gene expression in 3D resembled more closely to that of *in vivo* which normally shows higher levels of MYOC and MGP but lower levels of ANGPL7 and ColI (Liu, Munro et al. ; Stamer, Peppel et al. 2001; Borras 2003; Tomarev, Wistow et al. 2003; Liton, Luna et al. 2006; Xue, Wallin et al. 2006; Comes, Buie et al. 2011).

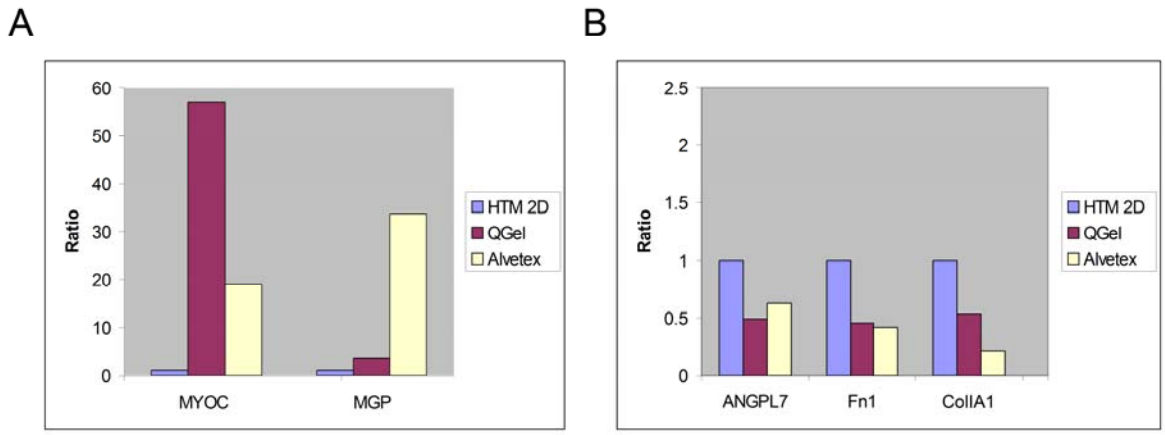

Figure 13. Comparison of gene expression level of human TM cells grown in 3D vs. 2D culture. RT-qPCR showed that human MYOC and MGP mRNA were at higher level (up-regulated in **A**) while ANGPL7, Fn1 and ColIA1 and were at a lower level (down-regulated in **B**) in 3D (QGel and Alvetex) compared with 2D human TM cultures.

Immunostaining further confirmed human TM cells grown in Alvetex expressed a higher level of myocilin protein, but a lower level of fibronectin and collagen I than those grown in 2 D culture (Fig. 14).

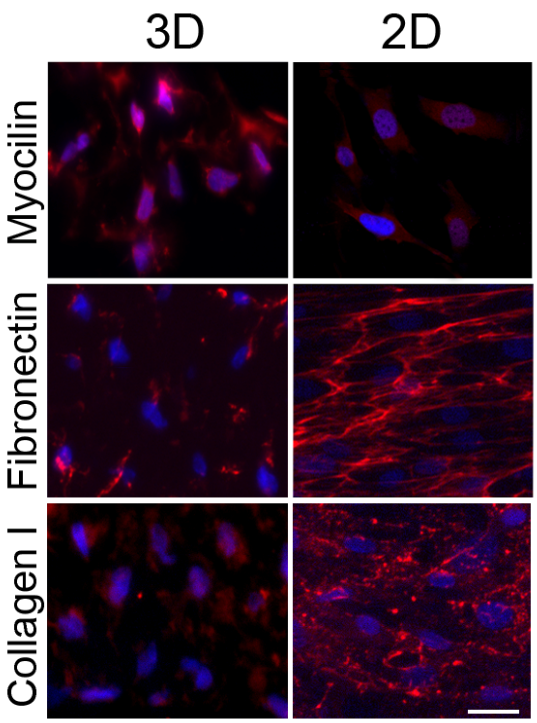

Figure 14. Immunostaining of myocilin (top panel), fibronectin (middle panel) and collagen type I (lower panel) in human TM cells grown in Alvetex scaffold (3D, left panel), or 2D chamber slides (right panel). Cells were generally smaller when grown in Alvetex scaffold, but showed stronger myocilin staining (red) compared to 2D culture. Fibronectin (red, middle panel) and collagen type I (red, lower panel) deposite on 2D culture was much stronger than the Alvetex by the human TM cells. Nuclei were stained with DAPI in blue. Scale bar, 20 μm

Coating Made No Difference for Cell Attachment:

The Alvetex scaffold system was further studied for the pretreatment such as scaffold coating with fibronectin, collagen type I, or uncoated. The MTT assay performed after culturing for 1 day indicated that there was no difference in terms of cell attachment among the three groups (Fig. 15).

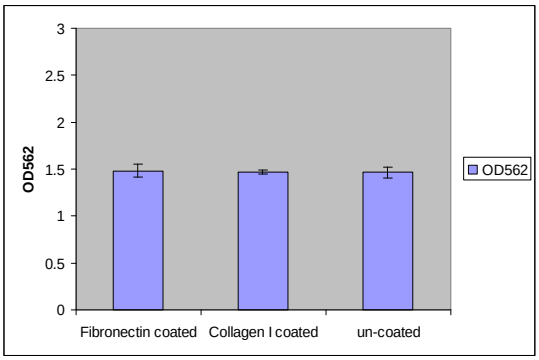

Figure 15. Pretreatment of Alvetex scaffold did not increase cell adhesion. Alvetex scaffold was either pretreated with fibronectin, collagen type I or remained uncoated (control). 200,000 human TM cells were seeded on the scaffold and MTT assay was carried out 1 day later.

Cell Proliferation in 2D vs. 3D Alvetex Scaffold:

Cell proliferation on 2D or 3D Alvetex scaffold was compared. Human TM cells from 2D cultures (3rdor 4thpassages) were seeded at 200,000 cells/well in uncoated Alvetex scaffold in the 24 well plate platform. In parallel, 200,000 cells/well were also seeded on 2D 24 well plates. Since Alvetex scaffold is not transparent, observation of the cell morphology by regular microscopy was a challenge. However, it was relatively easy to measure cell proliferation by MTT assay on Alvetex scaffold and the results were highly reproducible. After seeding on day 1, the number of cells in 2D cultures increased steadily throughout the time course of the study (up to 14 days). In 3D Alvetex system, the cells grew initially. However, by day 7, the cell number dropped and it was leveled off thereafter (Fig. 16). It seemed that the cells cultured in Alvetex scaffold quickly lost proliferative ability and showed perhaps a more differentiated phenotype.

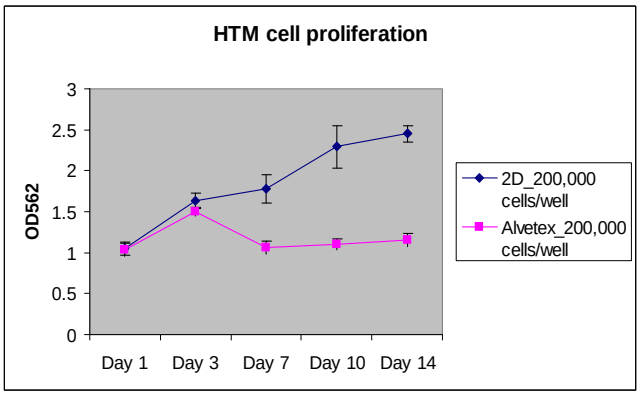

Figure 16. Human TM cell proliferation in 2D vs. Alvetex scaffold by MTT method. 200,000 (dark blue diamond) cells per well seeding in 2D 24-well plates showed continuous proliferation during the two-week growth period. Cells plated on Alvetex (pink square) initially proliferated during the first three days. The cell number however dropped subsequently and was not increased for the remaining incubation period.

Wnt Pathway Was Activated When Wild-type Myocilin Was Expressed in Human TM Cells Grown in Alvetex Scaffold:

HTM cells grown in 2D culture showed Wnt signaling pathway activation when transfected with wild-type myocilin (in part I of this thesis). To check whether this phenomenon can be replicated in 3D scaffold, human TM cells grown in Alvetex scaffold (40 μm) for two weeks were transfected with pMyocilin$_{WT}$-GFP for 48 h, fixed and the scaffold was stained with anti-β catenin antibody. Immunofluoresence was observed by Zeiss 710 confocal microscope. As shown in Figure 17, the β-catenin staining was observed in the nuclei of myocilin transfected human TM cells, indicating that the Wnt pathway was activated upon myocilin transfection in 3D, similar to that seen in 2D cultures (Fig. 17).

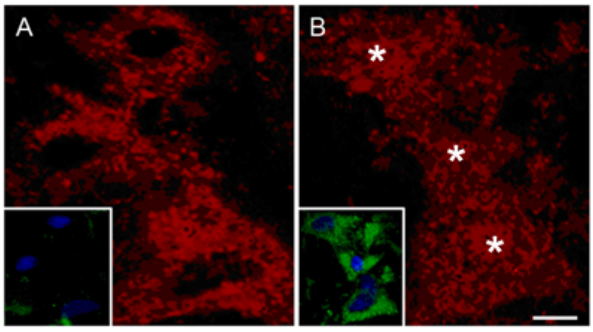

Figure 17. β-catenin staining in human TM cells grown in Alvetex scaffold. (**A**) β-catenin staining (red) was seen in the cytoplasm of non-trasnfected cells. (**B**). Nuclear (red *) staining of β-catenin was observed in myocilin-GFP-transfected green cells in dicating that Wnt signaling was activated. Insert, green fluorescence to show transfected cells. Scale bar, 10 μm.

Discussion

Human TM cells in the traditional 2D cultures have been reported to exhibit polygonal endothelial morphologic features with a growth pattern distinct from that of fibroblastic and corneal endothelial cultures. They lay down prominent basement membranes and deposit ECM materials, including fibronectin, laminin, and collagen type I. TM cells are also actively phagocytic in culture (Yue 2007). More recently, biophysical cues related to substrate topography and stiffness have been demonstrated to impact TM cellular behavior (Russell,

Gasiorowski et al. 2008) including cell alignment, migration, as well as gene and protein expression patterns. In 2D cultures, the substrate is flat and stiff and biophysical cues are minimal. 3D cell culture models may overcome these 2D disadvantages and resemble more closely the *in vivo* environment for cells.

In the present study, we established 3D *in vitro* systems for human TM cells to provide effective models that mimic *in vivo* situations. Cells grown on two popular 3D platforms, namely, hydrogels and inert scaffold inserts, were compared. QGel has elastic modulus (also called Young's modulus) in the range of 2.4-3 kPa, similar to that of normal human TM tissue which has Young's modulus ranging from 1.7 to 8.8 kPa with an average of 4 kPa (Last, Pan et al. 2011). Human TM cells in QGel displayed an elongated morphology, migration inside the hydrogel and formation of cell-cell interaction network, mimicking the cell phenotypes seen in the tissue (Figure 11).

The 3-D Life PVA-PEG hydrogel from Cellendes was in addition tested. However, the cells showed no proliferation, no migration, and no connection in this hydrogel even after one week of culturing. We suspected that the cell vitality was compromised by the low pH (pH 5.5) of buffer used during the gel polymerization procedure. The PEG-link used in the system is non-degradable by the cell which may also be a contributing factor. PuraMatrix Peptide Hydrogel from BD Biosceinces that consists of standard amino acids (1% w/v) and 99% water was also tested. Under physiological conditions, the peptide component self-assembles into a 3D hydrogel and exhibits a nanometer scale fibrous structure (with average pore size of 50-200 nm) (manufacture's user manual). However, due to the low pH of the material (pH = 2-4) during the gel formation, human TM cells did not survive (data not shown).

The Alvetex scaffold is a highly porous, cross-linked polystyrene scaffold, which has been engineered into 200 μm thick membranes. It has been successfully used to culture rat primary hepatocytes (Maaike Schutte October 2011), adipose tissue-derived stem cells (Neofytou, Chang et al. 2011), HepG2 liver cells (Bokhari, Carnachan et al. 2007) and human neuron (Hayman, Smith et al. 2004). Human TM cells attached nicely on uncoated Alvetex scaffold and were multilayered in the scaffold (Fig. 12).

The expression levels of MGP, MYOC, ANGPTL7, Fn1 and ColIA1 in 3D cultures were assessed. These genes have been documented to have different expression patterns in 2D TM cultures from what were found *in vivo* (Liu, Munro et al. ; Stamer, Peppel et al. 2001; Borras 2003; Tomarev, Wistow et al. 2003; Liton, Luna et al. 2006; Xue, Wallin et al. 2006; Comes, Buie et al. 2011). MGP functions in inhibition of soft-tissue calcification (Luo, Ducy et al. 1997; Yagami, Suh et al. 1999). It is one of the most expressed genes in the human TM tissue (Gonzalez, Epstein et al. 2000; Borrás 2008) and its expression is affected by insults associated with glaucoma such as elevated pressure (Vittitow and Borras 2004) and mechanical stretch (Vittal, Rose et al. 2005). MGP is considered to be one of the common markers of TM that should be expressed in 3D systems. MYOC is highly expressed in human TM cells in tissue and yet its expression is down-regulated in 2D systems. On the other hand, Fn1, Col I and ANGPTL7 (whose function is cell signaling) are highly expressed in the 2D system but not *in vivo* (Borras 2003; Fautsch, Howell et al. 2005). Our results proved that MGP1 and MYOC were up-regulated in both QGel and Alvetex systems than in the 2D cultures while Fn1, ColIA1 and ANGPTL7 were down-regulated in 3D culture compared with 2D cultures (Fig. 13). Immunofluorescent staining further confirmed similar trends of protein pattern variations between 3D and 2D

systems. These indicate that TM cells in the 3D cultures we established adopted more of the *in vivo* characteristics.

The Wnt signaling pathway has been shown to be activated in human TM cells upon overexpression of wild-type and mutated (P370L or Q368X) myocilin (Part I of this thesis). We also replicated and validated this result in the Alvetex scaffold culture system.

Overall, human TM cells grown in both the QGel hydrogel and the Alvetex scaffold systems resemble more closely their *in vivo* status. We believe that the Alvetex system may be superior to the QGel. Alvetex has the following advantages: no special need for coating; good reproducibility; and easiness for transfection, RNA, DNA, and protein extractions. The drawback is that this scaffold is not transparent, difficult therefore to observe the cells in real time. QGel hydrogel by contrast is itself transparent, ready for direct morphological observations. However, the gel is thick with some depth, and is not ideal for manipulations such as transfection and RNA extraction. Overall, Alvetex and QGel hydrogel both can be used to grow and maintain TM cells in 3D environment. Investigators may choose either the Alvetex or the QGel system that best fit their needs or use both systems to complement each other. The 3D system can be used for an effective *in vitro* model to help portray activities, characteristics, and stress responses of TM cells *in vivo*.

PART III: ESTABLISHMENT OF INDUCIBLE WILD-TYPE AND MUTANT MYOCILIN-GFP-EXPRESSING RGC5 CELL LINES

Myocilin is a gene linked to POAG. It is expressed in the TM, iris, ciliary body, and retina in the eye. Most of the myocilin studies used TM cells, which are responsible for outflow of the aqueous humor and regulation of the IOP. The primary human TM cells however are notoriously difficult for transfection when studying the myocilin mutant in the cells. To facilitate studies of myocilin and its mutants, we established tetracycline-inducible (Tet-on) RGC5 stable cell lines that would express, upon induction, GFP-tagged wild-type and mutant (Q368X and P370L) myocilin. These cell models allowed studies that require confluent myocilin-expressing cell cultures such as migration and barrier functions. Our results disclosed that when the expression of wild-type or mutant myocilin was induced, the actin stress fibers were lost, RhoA activity was reduced and cell migration was blocked. In addition, the trypsinization sensitivity was heightened.

Materials and Methods

Plasmids

A plasmid vector pTRE-MYOC-EGFP-INS-rtTA-IRES-hyg-pcDNA3.1z which contains both tetracycline regulatory and responsive components based on the Clontech's Tet-on advance system (Clontech, Mountain View, CA) was constructed (Fig. 18). The procedure of preparing construct pTRE-MYOC-EGFP-INS-rtTA-IRES-hyg-pcDNA3.1z was similar to that of pTRE-OPTN-EGFP-INS-rtTA-IRES-hyg-pcDNA3.1z described and reported earlier (Ying, Shen et al. 2010). Briefly, to produce pTRE-MYOC-EGFP construct, MYOC-EGFP fusion gene was digested from pMYOC-EGFP and cloned into *EcoR I* and *BamH I* linearized pTRE-tight vector

(Clontech). TRE-MYOC-EGFP was then shuttled to pBluescriptII-SK(+) vector and the insulator (INS) fragment was inserted to generate pBS-TRE-OPTN-EGFP-INS. Finally, rtTA-IRES-hygromycin fragment was digested from construct rtTA-IRES-hyg-pcDNA3.1z and ligated into pBS-TRE-OPTN-EGFP-INS (Ying, Shen et al. 2010). Two other plasmid vectors containing mutation Q368X or P370L were similarly prepared.

Antibodies

Rabbit anti-GFP and anti-RhoA antibodies were from Santa Cruz Biotechnology. Horseradish peroxidase (HRP)- or Cy3-conjugated goat anti-rabbit and goat anti-mouse secondary antibodies were from Jackson ImmunoResearch (West Grove, PA). Anti-GAPDH antibody was obtained from Trevigen (Gaithersburg, MD). Monoclonal anti-myocilin antibody was from Dr. Michael Fautsch at the Mayo Clinic.

Cell Cultures

Rat retinal ganglion RGC5 cells were obtained from the departmental core facility, deposited by Dr. Paul Knepper (Choi, Miller et al. 2005) generously provided and originally established (Krishnamoorthy, Agarwal et al. 2001) by Dr. Neeraj Agarwal (North Texas Health Science Center, Fort Worth, TX). RGC5 cells were grown in DMEM supplemented with 10% FBS and antibiotics.

Establishment of Tet-on Inducible Myocilin-GFP-expressing RGC5 Stable Cell Lines

RGC5 cells transfected with above-mentioned plasmid vectors were selected in hygromycin (100 μg/ml)-containing medium for approximately 2 weeks until colonies grew out. The cells were then trypsinized and induced with 1 μg/ml of Dox for 48 h. GFP positive cells

that were sorted using DakoCytomation MoFlo into 96 well plates (1 cell/well) were incubated with maintenance medium (containing 50 µg/ml of hygromycin but without Dox) for another 2 weeks. Cells were screened for low, moderate, or high myocilin-GFP expressers after Dox induction by fluorescence microscopy. These expresser clones were allowed to multiply and were banked in liquid nitrogen.

In vitro Scratch Assay

RGC5 inducible cells from moderate clones were plated in 6 well plates and induced for 48 h. Cells were serum starved for 2 h and treated with 5 µg/ml of mitomycin C for 2 h (Lee and Kay 2009). Each well in confluence was scratched gently using a disposable 10 µl pipette tip to generate a confined scratch area (Wentz-Hunter, Shen et al. 2004; Lee and Kay 2009). The cells were incubated in serum-free media in the presence of mitomycin C (to block cell proliferation). The ability of cells to migrate into the scratched areas was monitored 11 h later by differential interference contrast and fluorescence microscopy (Zeiss Axiovert100M inverted microscope, Thornwood, NY) and documented by photography. The total area of the scratch and the area covered by the cells within the scratch in each 10× field were measured with Image J software. A total of 8 fields were analyzed and the percentage of areas covered by migratory cells in each sample was calculated. Experiments were repeated 3 times and the statistical significance of the data was determined by Student's t tests.

Actin Stress Fibers, Trypsin Sensitivity, and RhoA Activities

The actin stress fibers of induced or non-induced control RGC5 cells was examined using rhodamine-phalloidin. Trypsin sensitivity and RhoA activities were examined as Part I of this thesis.

Results

Establishment of Tetracycline Inducible (Tet-on) Wild-type and Mutant Myocilin-GFP RGC5 Stable Cell Lines

The inducible Tet-on wild-type myocilin-GFP ($myocilin_{WT}$-GFP or $MYOC_{WT}$-GFP) expressing RGC5 stable cell lines were established using a single plasmid vector pTRE-MYOC-EGFP-INS-rtTA-IRES-hyg-pcDNA3.1z, which contains both tetracycline regulatory and responsive components based on Clontech's Tet-on advance system (Fig. 18). When transfected into RGC5 cells, $myocilin_{WT}$-GFP was expressed following doxycycline (Dox) induction.

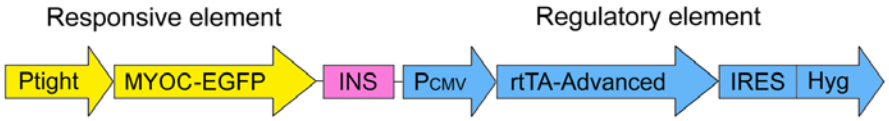

Figure 18. Single plasmid construct with two expression cassettes. The two cassettes (responsive element, in yellow, and regulatory element, in blue) are separated by 5′-HS4 chicken β-globin insulator (INS, in pink).

After several rounds of selection, clones with different expression levels of wild-type myocilin-GFP were obtained. When non-induced with no Dox present, only background fluorescence was detected in the cells (Fig. 19A). After Dox induction, the low expresser exhibited faint (Fig. 19B), while the moderate (Fig. 19C) and the high (Fig.18D) expressers showed stronger green fluorescence in the cytoplasm. Microscopic examination indicated that $myocilin_{WT}$-GFP in the low expresser had a more spread out, cytoplasmic distribution pattern similar to that of the endogenous myocilin. Cytoplasmic granules or aggregates, in varying

extents, were observed in the moderate and high expressers. Western blotting using both anti-GFP (Fig. 19E) and anti-myocilin (Fig. 19F) antibodies confirmed that the induced level of myocilin$_{WT}$-GFP was low in the low expresser but moderate or high in the others. As a secreted protein (Polansky, Fauss et al. 1997; Fingert, Ying et al. 1998; Rao, Allingham et al. 2000; Jacobson, Andrews et al. 2001), myocilin$_{WT}$-GFP was detected in medium samples from induced cultures (Fig. 19F) as anticipated.

Inducible cell lines that expressed two mutant myocilin (myocilin$_{Q368X}$ or myocilin$_{P370L}$)-GFP were additionally prepared using a similar strategy. Clones with different expression levels (low, moderate, and high) were also obtained and banked in liquid nitrogen. Myocilin$_{Q368X}$-GFP in the low expressers displayed a diffuse cytoplasmic distribution pattern (Fig. 20B). In the moderate and high expressers, aggregates in the cytosol of the cells were evident (Fig. 20C, D). Likewise, cytoplasmic aggregation was observed in moderate and high expressers of myocilin$_{P370L}$-GFP (Figs. 21B–D). Again, in non-induced clones, the fluorescence signal was minimal (Figs. 20A and 21A). The fusion protein expression level in various clones was verified by Western blotting probed with both anti-GFP (Figs. 20E and 21E) and anti-myocilin (Figs. 20F and 21F) antibodies. No mutant fusion protein was detected in the media collected from the various cultures, consistent with the notion that Q368X and P370L mutants were secretion incompetent (Jacobson, Andrews et al. 2001; Liu and Vollrath 2004).

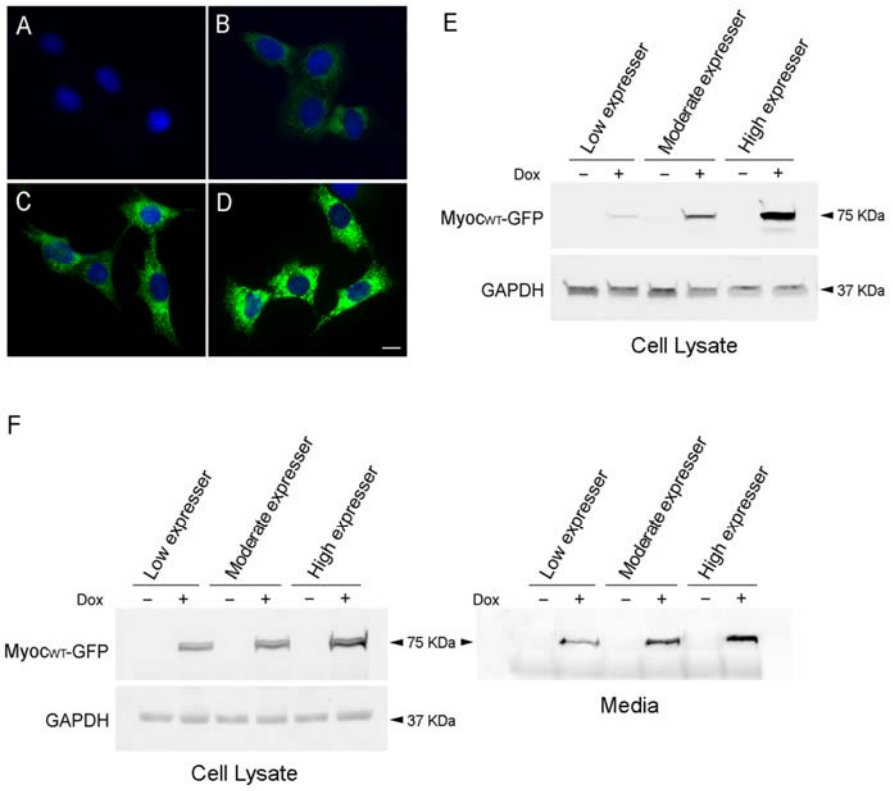

Figure 19. Tet-on inducible RGC5 cell lines that express wild-type myocilin-GFP upon Dox induction. Clones with different expression levels of myocilin-GFP ($MYOC_{WT}$-GFP) fusion protein are presented. Without Dox induction, the green fluorescence in the cells, indicative of $MYOC_{WT}$-GFP expression, was minimal at a background level (**A**). After Dox treatment, low (**B**), moderate (**C**) and high (**D**) levels of $MYOC_{WT}$-GFP were seen in, respectively, low, moderate, and high expresser clones. $MYOC_{WT}$-GFP had a more spread out, cytoplasmic distribution pattern similar to that of the endogenous myocilin in the low expresser. Accumulation of $MYOC_{WT}$-GFP was seen in high expresser clones. Scale bar, 10 μm. **E.** Western blot analyses of cell lysates using polyclonal anti-GFP and anti-GAPDH antibodies. **F**. Western blotting of cell lysates (left panel) and media samples (right panel) using monoclonal anti-myocilin antibody. Results in **E** and **F** confirmed that the level of $MYOC_{WT}$-GFP relative to that of GAPDH in total cell lysates was low, moderate, and high from the various expresser clones. $MYOC_{WT}$-GFP fusion protein was also detected in the culture media (**F**, right panel) with anti-myocilin antibody. −, Non-induced control; +, Induced cells.

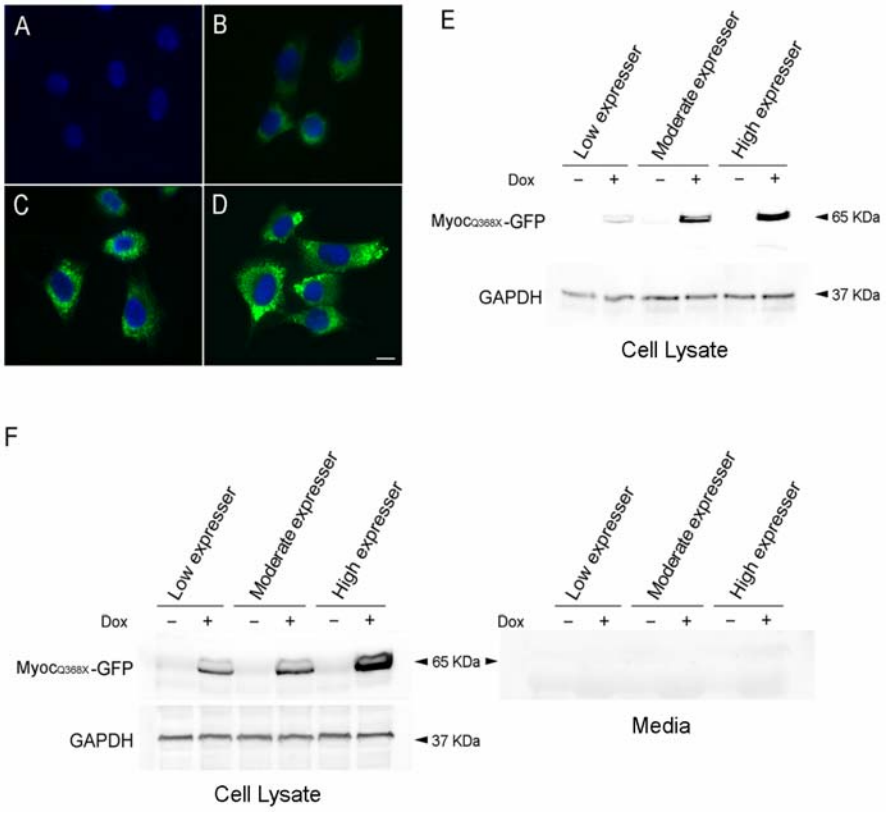

Figure 20. Tet-on inducible RGC5 cell lines that express mutant Q368X myocilin-GFP upon Dox induction. Clones with different expression levels of Q368X myocilin-GFP ($MYOC_{Q368X}$-GFP) fusion protein are presented. Without Dox induction, the green fluorescence in the cells was minimal (**A**). After Dox treatment, low (**B**), moderate (**C**) and high (**D**) levels of $MYOC_{Q368X}$-GFP were seen in respectively, low, moderate, and high expresser clones. Cytoplasmic aggregates were visible in moderate and high expressers. Scale bar, 10 μm. **E.** Western blot analyses using anti-GFP and anti-GAPDH polyclonal antibodies. **F**. Western blot analyses of cell lysate (left panel) and medium (right panel) samples using anti-myocilin monoclonal antibody. The blots confirmed that the level of $MYOC_{Q368X}$-GFP relative to that of GAPDH in total cell lysates was low, moderate, and high from the various expresser clones. No $MYOC_{Q368X}$-GFP protein band was observed in medium samples. −, Non-induced control; +, Induced cells.

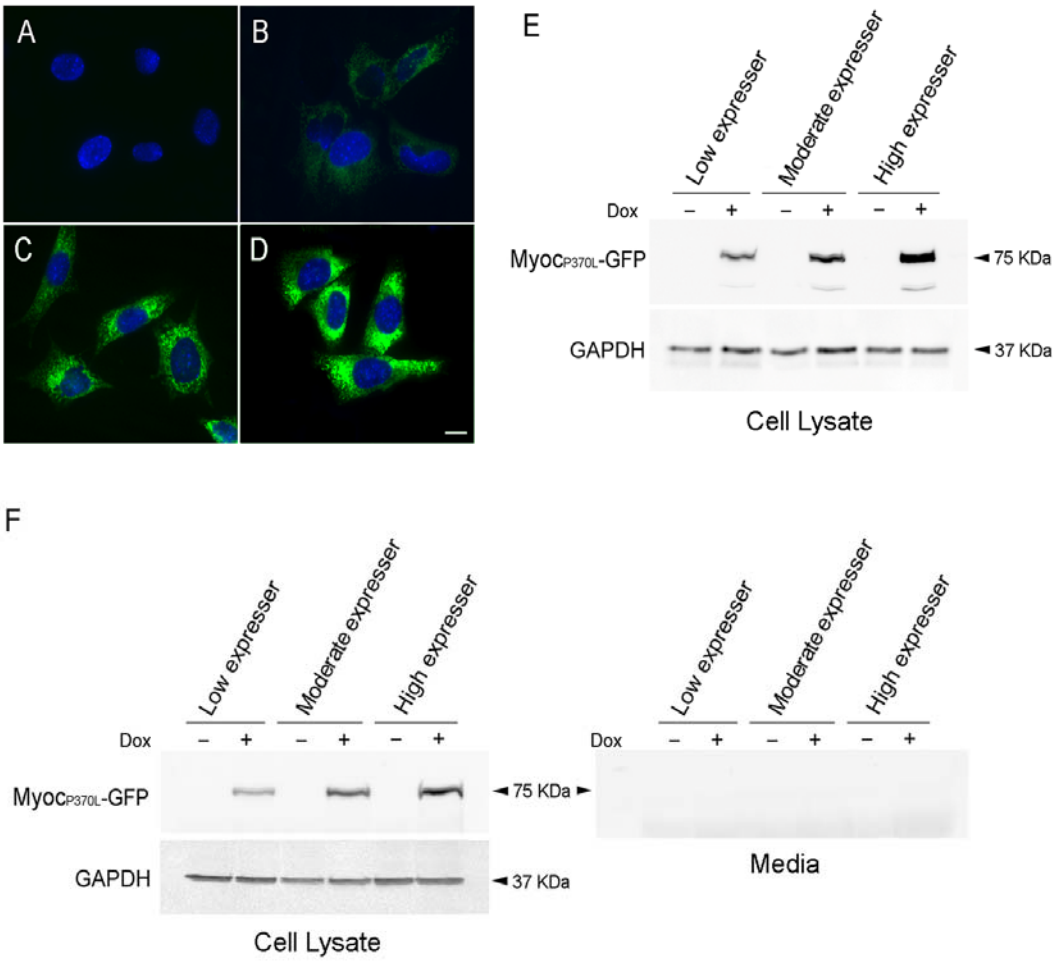

Figure 21. Tet-on inducible RGC5 cell lines express mutant P370L myocilin-GFP upon Dox induction.Clones with different expression levels of P370L myocilin-GFP (MYOC$_{P370L}$-GFP) fusion protein are presented. Without Dox induction, the green fluorescence in the cells was minimal (**A**). After Dox treatment, low (**B**), moderate (**C**) and high (**D**) levels of MYOC$_{P370L}$-GFP were seen in, respectively, low, moderate, and high expresser clones. Cytoplasmic aggregates were visible in both moderate and high expressers. Scale bar, 10 µm. **E.** Western blot analyses of cell lysates using anti-GFP and anti-GAPDH polyclonal antibodies. **F**. Western blot analyses of lysate (left panel) and media samples (right panel) using anti-myocilin monoclonal antibody. The blots confirmed that the level of MYOC$_{P370L}$-GFP relative to that of GAPDH in total cell lysates was low, moderate, and high from the various expresser clones. No MYOC$_{P370L}$-GFP protein band was seen in medium samples. −, Non-induced control; +, Induced cells.

Inhibition of Cell Migration upon Wild-type and Mutant Myocilin-GFP Expression

Cell migration was examined using an *in vitro* scratch assay. RGC5 cells were serum starved, treated with 5 μg/ml of mitomycin C for 2 h (Lee and Kay 2009) and subjected to scratch assay in the presence of mitomycin C to block cell proliferation. It was found that compared to non-induced controls (Fig. 22A, upper panel), moderately induced expression of myocilin$_{WT}$-, myocilin$_{Q368X}$ -, or myocilin$_{P370L}$-GFP caused a marked decrease in the ability of RGC5 cells to migrate (Fig. 22A, lower panel). At the 11 h post scratch time point, the percent of scratched area covered by migratory cells was reduced by 2 - 3 fold in the induced cultures (Fig. 22B, values for the wild-type myocilin, non-induced [N]: 70.1 ± 6.2%, induced [I]: 23.0 ± 4.0%; for Q368X myocilin, N: 72.3 ± 7.7%, I: 27.1 ± 7.6%; for P370L myocilin, N: 64.6 ± 8.3%, I: 25.3 ± 7.5%; n = 8). The differences between non-induced and induced samples were statistically significant ($P < 0.0001$).

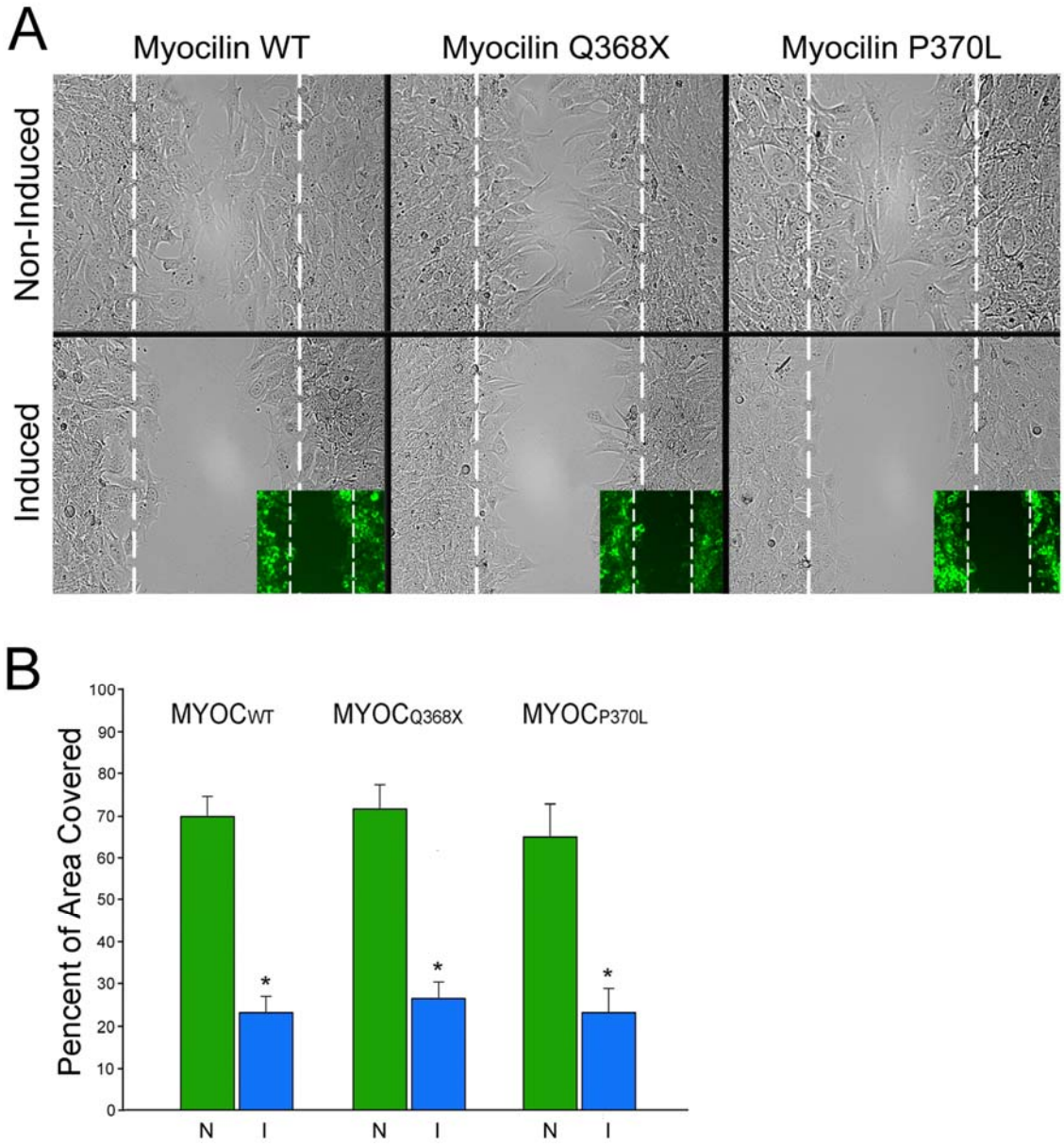

Figure 22. A. *In vitro* scratch assays. Cell migration was inhibited when moderate expressers were induced to express myocilin wild-type (WT), Q368X, or P370L-GFP (lower panel) compared with non-induced controls (top panel). Inset shows the same view under a fluorescence microscope. The induced cells are in green. Scale bar, 50 µm. **B.** Bar graph to show the percent area (mean ± SD) covered by myocilin $(MYOC)_{WT}$-, $MYOC_{Q368X}$-, or $MYOC_{P370L}$-GFP-expressing cells that were migrated into the scratched area. N, Non-induced control; I, Induced cells. *, P<0.0001 compared to non-induced control.

Loss of Actin Stress Fibers, Increased Trypsin Sensitivity, and Lowered RhoA Activities

By phalloidin staining, a loss of actin stress fibers was observed when RGC5 cells were induced to express wild-type myocilin at low, moderate or high levels (Fig. 23A). This result was in agreement with our previous study, in which myocilin transfection was shown to result in reduction of actin stress fibers and focal adhesions in human TM cells (Wentz-Hunter, Shen et al. 2004; Sakai, Park et al. 2006). The loss of actin stress fibers was dose-dependent (Fig. 23A). When low expresser was mix-cultured with moderate or high expresser and induced together, the actin loss was more dramatically observed in cells that displayed stronger green fluorescence with higher levels of myocilin-GFP expression (Fig. 23B). A loss of actin stress fibers was also seen when RGC5 cells were induced to express Q368X and P370L mutant myocilins (Fig. 23C). The actin loss phenotype was not related to the Dox treatment as such treatment did not trigger any changes in the actin structure in parental RGC5 cells (Fig. 23D).

To further examine the cell-matrix adhesiveness, RGC5 inducible cells were subjected to trypsin sensitivity tests. The time needed for cells to round up was recorded using a confocal live cell imaging system and analyzed. It was found that RGC5 cells became more sensitive to trypsinization when induced (Fig. 24A). The trypsinization time for cells to round up was significantly ($P<0.001$) shorter for myocilin$_{WT}$-, myocilin$_{Q368X}$- and myocilin$_{P370L}$-GFP-expressing cells than their respective non-induced counterparts (for wild-type myocilin, non-induced [N]: 97 ± 17 s; induced [I]: 78 ± 15 s; for Q368X myocilin, N: 104 ± 19 s, I: 81 ± 18 s; for P370L myocilin, N: 116 ± 29 s, I: 88 ± 21 s, n = 20), indicating increased trypsin sensitivity or reduced cell-matrix adhesiveness.

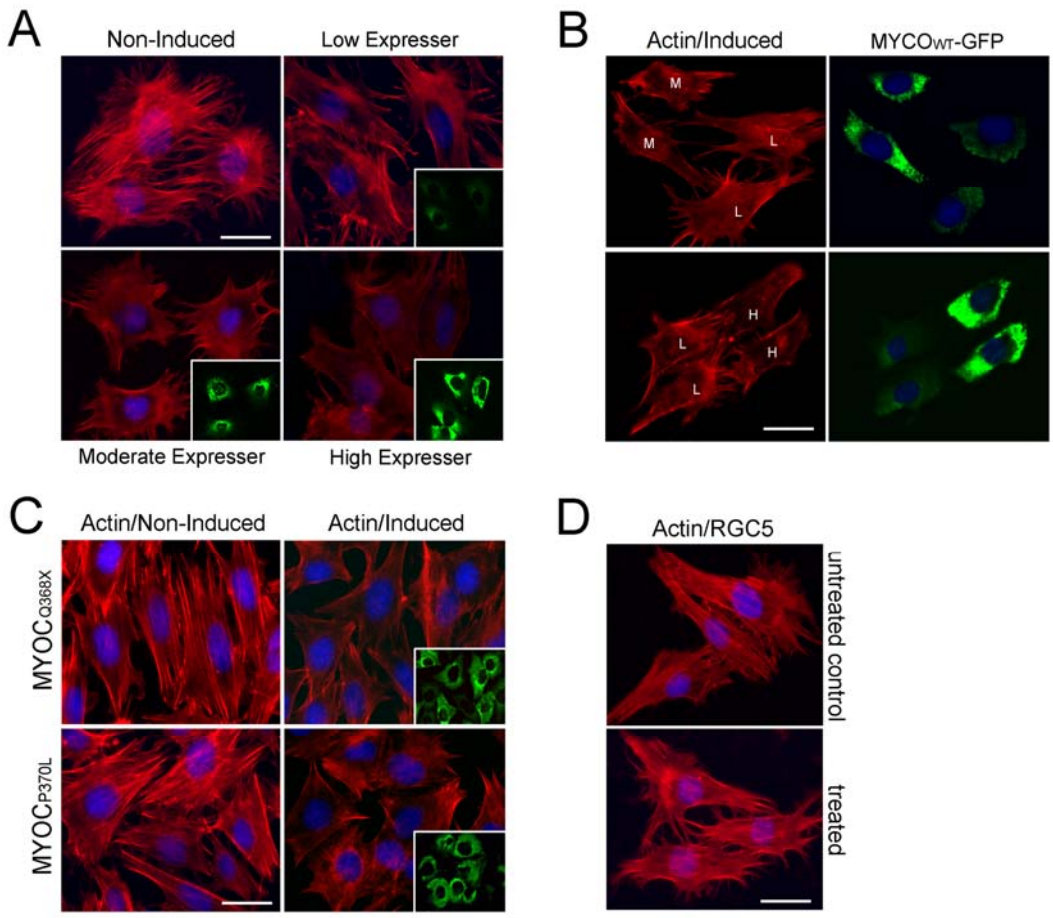

Figure 23. Actin staining in inducible RGC5 cells. **A**. Non-induced control cells, as well as low, moderate and high expressers of $MYOC_{WT}$-GFP were stained with rhodamine-phalloidin for actin stress fibers. Compared to non-induced cells, the actin staining (red) was much reduced in Dox-induced ones. Insets show the same view of induced cells under FITC filter (green for myocilin-GFP expression). Scale bar, 10 μm. The loss of actin stress fibers, most dramatically observed in high expresser, was dose-dependent. **B**. Actin staining (red, left column) in mix cultures of low (L) and moderate (M) (top panel) or low (L) and high (H) (bottom panel) expressers was performed. The right column shows the same view with FITC filter to depict the green fluorescent transgene level. The stronger the green fluorescence, the more dramatic was the loss of actin fibers. **C**. Compared to non-induced controls (left column), Q368X- and P370L-GFP expression in induced cells (moderate expressers, right column) also caused a loss of actin stress fibers (red). Insets show the same view of induced cells under FITC filter. **D**. Robust actin stress fibers (red) were observed in parental RGC5 cells without (untreated control, top panel) or with Dox (1 μg/ml, bottom panel) treatment. Scale bar, 20 μm.

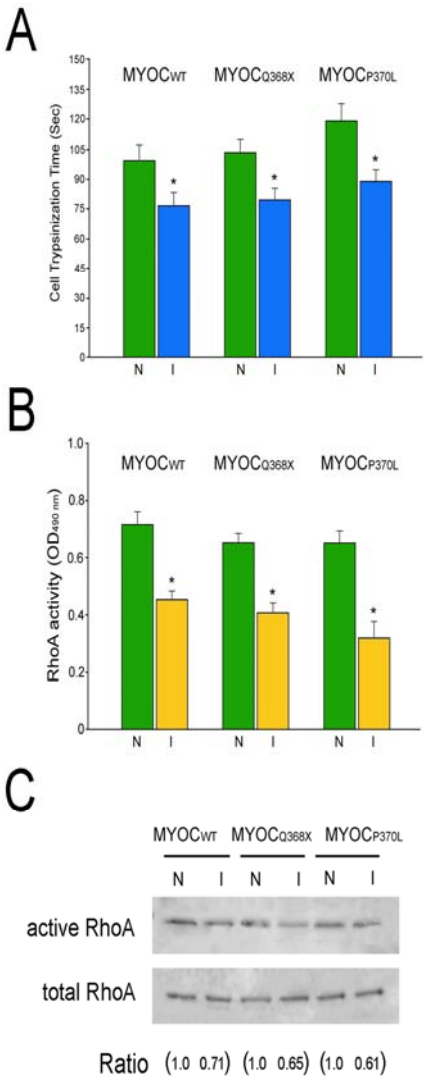

Figure 24. Trypsin sensitivity and active RhoA levels. **A**. Compared to non-induced (N) controls, the trypsinization time needed to round up the cells was reduced in induced (I) cells when moderate level of wild-type ($MYOC_{WT}$) or mutant ($MYOC_{Q368X}$ and $MYOC_{P370L}$) myocilin was expressed. **B**. Compared to non-induced (N) controls, active RhoA activity, measured by G-LISA RhoA assays, was lowered when wild-type ($MYOC_{WT}$) or mutant ($MYOC_{Q368X}$ and $MYOC_{P370L}$) myocilin was induced (I) to express in RGC5 cells. Results (mean ± SD) were analyzed by Student's t tests. *, $P<0.001$ compared to non-induced controls. **C**. Pull down assay showed a similar trend of active RhoA reduction as seen by G-LISA assay in B. Total RhoA was comparable between induced and non-induced samples. Ratios between active and total RhoA that were normalized to the respective non-induced controls are presented.

G-LISA RhoA activation assays were carried out to measure the amounts of active RhoA in the cells. The level of GTP-bound or active RhoA in wild-type or mutant myocilin-GFP-expressing RGC5 cells was approximately 35–50% lower (Fig. 24B, $P < 0.01$) than that in non-induced controls (for wild-type myocilin, non-induced [N]: 0.72 ± 0.05, induced [I]: 0.46 ± 0.03; for Q368X myocilin, N: 0.62 ± 0.03, I: 0.41 ± 0.03; for P370L myocilin, N: 0.64 ± 0.05, I: 0.32 ± 0.06, n = 2). Pull down assays for active and total RhoA were also performed (Fig. 24C). The

active RhoA, relative to total RhoA level, was reduced by 30–40% in induced cells (Fig. 24C), corroborating the G-LISA results (Fig. 24B).

Discussion

Myocilin mutations are typically associated with high IOP cases (Tamm 2002). This suggests that myocilin may have more of an impact on the cells in the aqueous outflow pathway such as the TM than those in the optic nerve head and the retina such as RGCs. Myocilin is also found expressed in adult eyes in the RGCs, optic nerve axons and photoreceptors (Takahashi, Noda et al. 1998; Karali, Russell et al. 2000; Swiderski, Ross et al. 2000; Clark, Kawase et al. 2001; Jurynec, Riley et al. 2003). Its expression has been noted to increase in reactive astrocytes in the glial scar (Jurynec, Riley et al. 2003). Wild-type and mutant myocilins have also been shown to inhibit neurite outgrowth in RGC5 and PC12 cells (Koga, Shen et al. 2010). Despite these observations however, it is still not clear whether myocilin has a functional role in RGCs. Neither the absence of myocilin in knockout mice (Kim, Savinova et al. 2001) nor elevated levels of wild-type mouse myocilin in the eye drainage structures of transgenic mice (Gould, Miceli-Libby et al. 2004) led to IOP elevation or morphological changes in the retina. In transgenic mice expressing the Tyr437His mutant of human myocilin protein, the IOP was increased (Senatorov, Malyukova et al. 2006; Zhou, Grinchuk et al. 2008). RGC loss and axonal degeneration (Senatorov, Malyukova et al. 2006; Zhang, Maddala et al. 2008) were also observed.

Our laboratory has performed studies on myocilin using cultured cells derived from normal human TM tissues (Wentz-Hunter, Shen et al. 2004; Park, Tibudan et al. 2007; Sakai, Shen et al. 2007; Shen, Koga et al. 2008). Several technical issues were encountered. First of all, fresh eyes from human donors are of limited availability. The TM tissue dissected from donor

eyes is minute, containing limited number of cells and often resulting in poor yield of primary cultures. The proliferation potential of TM cells also diminishes generally with increasing post mortem time and age of the donors. Furthermore, the transfection efficiency of primary TM cells is very low (<10–15%), making it exceedingly challenging to conduct cellular and molecular biology investigations.

Progressive loss of RGCs and their exons is one of the hallmarks in POAG. In light of the potential impact of myocilin mutations on neuronal cells, and also due to the difficulties associated with cultured human TM cells, we undertook the current study, establishing inducible cell lines and extending our efforts to examine the consequences of myocilin and Q368X and P370L mutants on neuronal cells. RGC5, an immortalized RGC cell line used widely for various biological investigations (Harvey and Chintala 2007; Yang, Lafleur et al. 2009), was established by transforming postnatal day 1 rat retinal cells with E1A adenovirus (Krishnamoorthy, Agarwal et al. 2001). It was however recently re-characterized as mouse, not rat origin by both mitochondrial and nuclear DNA analysis (Van Bergen, Wood et al. 2009). The cells were not positive for known markers of ganglion cells such as neurofilaments or Thy1.2. Nevertheless, they did stain positively for neuronal markers β-tubulin and PGP9.5, as well as for the microtubule-associated protein tau, and were able to differentiate with neurite extensions after treatment of staurosporine (Frassetto, Schlieve et al. 2006; Harvey and Chintala 2007), or trichostatin A (Schwechter, Millet et al. 2007), suggesting that these cells, while no longer a good model of RGCs, still represent neuronal precursor cells. They may still be suitable for molecular and cellular mechanistic studies of myocilin and be useful for future neuroprotection type of investigations.

Tet-on stable RGC5 cell lines were created to express wild-type and mutant myocilin-GFP upon Dox induction. Three clones each with low, moderate, and high expression levels were obtained. Microscopic observation of low expresser of wild-type myocilin-GFP revealed that it mimics the normal scenario with myocilin expression at the endogenous level while the high expressers represent overexpression situations displaying myocilin granules/aggregates in the cytosol of the cells (Fig. 19). The moderate and high expressers of myocilin$_{Q368X}$- and myocilin$_{P370L}$-GFP also showed prominent cytoplasmic aggregates (Figs. 20 and 21).

The endogenous, wild-type myocilin in human TM cells is a secreted protein (Polansky, Fauss et al. 1997; Nguyen, Chen et al. 1998; Tamm 2002). It undergoes an intracellular endoproteolytic processing in the central linker region by calpain II, producing two stable protein fragments, 35 and 20 kDa (Aroca-Aguilar, Sanchez-Sanchez et al. 2005; Sanchez-Sanchez, Martinez-Redondo et al. 2007). This cleavage is speculated to regulate extracellular interactions of myocilin with proteins such as structural protein of lipid rafts, flotillin-1 (Joe, Sohn et al. 2005), fibronectin (Filla, Liu et al. 2002; Ueda, Wentz-Hunter et al. 2002; Fautsch, Vrabel et al. 2006), laminin (Ueda, Wentz-Hunter et al. 2002; Fautsch, Vrabel et al. 2006), collagens (Ueda, Wentz-Hunter et al. 2002), fibrillin-1 (Ueda, Wentz-Hunter et al. 2002), optimedin (Torrado, Trivedi et al. 2002), hevin (Li, Aroca-Aguilar et al. 2006) and SPARC (Aroca-Aguilar, Sanchez-Sanchez et al. 2011), contributing thereby to the IOP control. Most of the myocilin mutations are located in the C-terminal olfactomedin-like domain (326–501 aa). These mutants, unlike the wild-type protein, are not secreted and tend to aggregate inside the cells (Caballero, Rowlette et al. 2000; Jacobson, Andrews et al. 2001; Tamm 2002; Yam, Gaplovska-Kysela et al. 2007). Such secretion patterns were verified in our Tet-on inducible RGC5 cell lines. Upon Dox induction, myocilin$_{WT}$-GFP was detected in both the culture medium (Fig. 19F) and the cell lysate while

myocilin$_{P370L}$- and myocilin$_{Q368X}$ –GFP were only detected in the cell lysates, not in the culture media (Figs. 20F and 21F).

The function of wild-type myocilin is still unclear. Data in the literature suggested that myocilin may play a role in cell-matrix interactions (Filla, Liu et al. 2002; Gobeil, Letartre et al. 2006; Goldwich, Scholz et al. 2009) and may inhibit neurite outgrowth (Jurynec, Riley et al. 2003; Koga, Shen et al. 2010). Using conditional medium containing myocilin, its proteolytic fragments or purified myocilin, Kwon et al. (Kwon, Lee et al. 2009) noted that extracellular myocilin modulates Wnt signaling, affecting actin cytoskeleton organization that is essential for TM contractility and regulation of the IOP. When myocilin construct was transfected into human TM cells, however, the forced expressed protein within the cells provoked phenotypes that include elevation of the cAMP level, protein kinase A (PKA) activation, RhoA inactivation, and the ensuing loss of actin stress fibers, focal adhesions, matrix deposition, and cell-matrix adhesiveness (Shen, Koga et al. 2008).

With inducible RGC5 cell lines, it became feasible to determine whether myocilin phenotypes observed in TM cells were also replicated in neuronal cells. Contrasting the transfection situation, nearly 100% of the inducible cells are expressing the transgene upon induction, affording investigations of cell migration by scratch assays. Another advantage is the avoidance of myocilin overexpression by transfection using strong promoters that often lead to high amounts of forced expressed protein. Our Tet-on RGC5 inducible cells in addition offer useful model systems, since low, moderate as well as high expressers for both wild-type and mutant myocilins are available. These clones would allow comparisons of pathologic phenotypes caused by transgene expression ranging from the endogenous to transfection/overexpression levels.

Similar to that found in TM cells in transfection studies (Shen, Koga et al. 2008), myocilin$_{WT}$-GFP expression led to a loss of actin stress fibers (Fig. 23), a reduction of the cell-matrix adhesiveness as evidenced by trypsin sensitivity assay (Fig. 24A), and a decrease in the RhoA activity (Figs. 24B and 24C). Such alterations are similarly observed with myocilin$_{P370L}$- and myocilin$_{Q368X}$ -GFP mutants. The migratory activity was found to be impaired (Fig. 22), consistent with the demonstrated cytoskeletal alterations in both wild-type and mutant myocilin-GFP-expressing RGC5 cells (Fig. 23).

With mutations in the olfactomedin-like domain of the myocilin sequence, Q368X and P370L mutants have been shown previously not to be secreted and exhibit gain-of-function effects (Liu and Vollrath 2004; Yam, Gaplovska-Kysela et al. 2007). In the current study, these mutants were discovered to also produce nearly identical actin/cell adhesion/migration phenotypes as the wild-type myocilin. Such findings suggest that the N-terminal sequence, rather than the C-terminal olfactomedin-like domain, is the key contributor to the myocilin phenotypes. Future sequence deletion experiments may help pinpoint the exact site(s) or motif(s) required.

In summary, the Tet-on inducible RGC5 cells provide a new tool for exploring the effects of myocilin upregulation and mutations at cellular and molecular levels. Since the percentage of cells on the plate that would express the transgene upon induction approaches 100, studies including genomics, proteomics, and signal transduction are made possible. The consequences of a combination of myocilin mutation and stress such as hypoxia can also be examined utilizing the inducible cells.

PART IV: ALTERATIONS IN PROTEIN EXPRESSION PROFILE AND IDENTIFICATION OF NOVEL DOWNSTREAM PATHWAYS INDUCED BY MYOCILIN

The Wnt signaling has been shown to be a player in the myocilin-induced phenotypes (part I of this thesis). To identify other potential downstream pathways induced by mycoilin, we performed quantitative proteomics and compared the global proteins differentially expressed in RGC5 cells that express wild-type myocilin or mutated P370L and Q368X myocilin.

Quantitative proteomics is a powerful tandem mass spectrometry (MS/MS)-based tool for the global measurement of proteins. Different biological samples are normally isotope labeled in quantitative proteomics, pooled and run on MS/MS. Data are analyzed and the relative quantitative information of proteins in different samples can be acquired (Cox and Mann 2011). The introduction of an isotope label results in a predictable mass difference between a labeled peptide and the unlabeled counterpart, allowing the mass analyzer to discriminate between the two forms (Filiou, Martins-de-Souza et al. 2012). There are two main types of labeling: metabolic labeling such as SILAC (Stable Isotope Labeling by/with Amino Acids in Cell Culture) and chemical labeling such as iTRAQ (Isobaric Tags for Relative and Absolute Quantitation). In SILAC, arginine or lysine is provided in light or heavy forms to the two cell populations and is incorporated into each protein after a few cell doublings (Fig. 25A). SILAC labeling is capable of nearly 100% label incorporation into proteins of living cells but the disadvantage is that it normally only allows two samples to be labeled (one light and one heavy) and compared. On the contrary, iTRAQ, based on the *in vitro* covalent labeling of the N-terminus and side chain amines of peptides from protein digestions with tags of varying mass (Fig. 25B), allows multiple

labeling of samples and comparisons. The disadvantage for iTRAQ is that it's hard to achieve 100% labeling for each peptide.

In the present study, we used quantitative proteomics to detect changes in protein profiles induced by myocilin (wild-type or mutants) and identify the downstream biological pathways. In part III of this dissertation, we have established Tet-on inducible RGC5 cell lines which can be induced to express wild-type and mutated myocilin-GFP. We used both SILAC (two biological samples: non-induced and wild-type myocilin) and iTRAQ labeling (four biological samples: non-induced, wild-type myocilin, P370L myocilin and Q368X myocilin) in the experiments and compared the results with each other. Database search engines Mascot and SEQUEST were used to search protein hits, proteomic software Scaffold 3.0 Q+ was used to extract protein quantitative information between different samples or groups. Software Interactive Pathway Analysis (IPA) and MetaCore systems were used for protein classification, protein-protein interaction and pathway analysis. Validation of regulated proteins found in quantitative proteomics was performed by RT-qPCR for mRNA levels (Boylan, Andersen et al. 2010; Munday, Surtees et al. 2012) and immunostaining for the protein level.

Our results indicated that a number of proteins involved in molecular transportations, cytoskeleton remodeling, oxidative stress, ECM, nuclear factor NF-κB signaling pathway, Golgi transportation, PKA signaling pathway, proteasome function, autophagy, mitochondrial dysfunction, and ER stress were differentially expressed in wild-type or mutated (P370L, Q368X) myocilin-GFP induced RGC5 cells compared to non-induced controls.

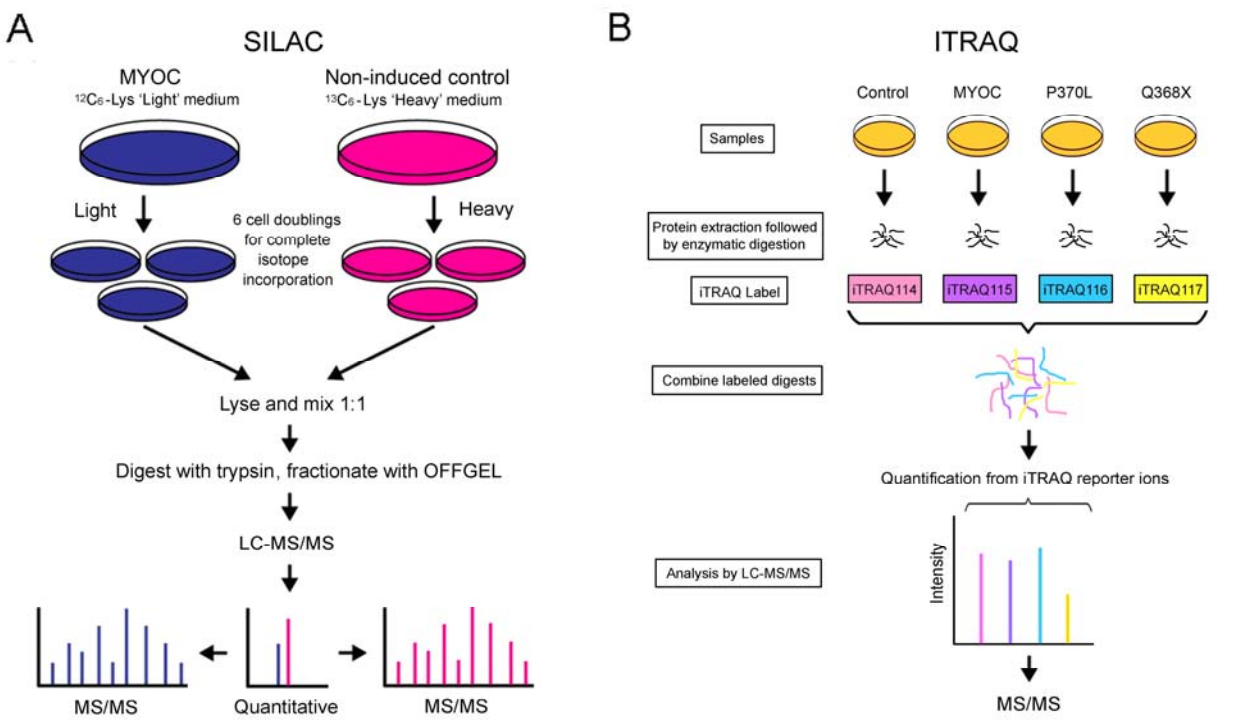

Figure 25. Workflow of quantitative proteomics using SILAC (**A**) and iTRAQ (**B**) isotope labeling.

Materials and Methods

SILAC Labeling, OFFGEL Fractionation and LC-MS/MS

Tet-on inducible RGC5 cells were grown for six passages in SILAC DMEM containing 0.1 mg/ml light $^{12}C_6$L-lysine-2HCl and then induced to express wild-type myocilin-GFP by adding Dox (1 µg/ml) in the light medium for 48 h. Non-induced control cells were grown in similar DMEM medium but containing 0.1 mg/ml heavy $^{13}C_6$ L-lysine-2HCl supplemented with 10% dialyzed FBS. Cells were washed with PBS and pelleted by centrifuge at 1,000 rpm for 10 min. Cells were lysed and the proteins were reduced, alkylated and digested overnight at 37ºC

with trypsin (1:20 w/w; enzyme:substrate). Peptides were desalted and heavy and light samples were combined at 1:1 ratio (v/v). Peptides were fractionated by OFFGEL isoelectric focusing apparatus (Agilent Technologies, Santa Clara, CA). Twelve fractions were analyzed by LC-MS/MS (liquid chromatography–mass spectrometry) with data-dependent acquisition on *Orbitrap* Velos pro mass spectrometer (Thermo Fisher Scientific, West Palm Beach, FL). There were three sets of samples in SILAC experiment (biological replicates) and MS/MS were repeated three times (three technical repeats) on each set of biological samples.

iTRAQ Labeling, OFFGEL Fractionation and LC-MS/MS

Tet-on RGC5 inducible cells were treated for 48 h with 1 μg/ml of Dox to induce the expression of wild-type or mutated (P370L or Q368X) myocilin-GFP. Non-induced cells were used as controls. Cells were washed with PBS and pelleted. Cell pellets were lysed and the proteins were reduced, alkylated and digested with trypsin. Peptides (100 μg) were desalted and labeled with iTRAQ labeling kit from Thermo scientific (non-induced control was labeled with iTRAQ-114, wild-type myocilin labeled with iTRAQ-115, P370L labeled with iTRAQ-116, and Q368X labeled with iTRAQ-117) per manufacturer's protocol. The labeling reactions were quenched and equal amounts of peptide samples from each iTRAQ labeling were pooled in a ratio of 1:1 (v/v), cleaned-up by cation-exchange chromatography and fractionated by OFFGEL. Twelve fractions were analyzed by LC-MS/MS. There were two sets of samples (biological duplicates) in iTRAQ experiment and MS/MS were repeated three times (three technical repeats) on each set of biological samples.

Data Analysis

MS/MS query information was extracted from raw data files (data conversion from .RAW file to MGF or mzXML files). Database search using two most commonly used database search engines was performed: Mascot and SEQUEST. For Mascot, database search was conducted using SILAC or iTRAQ labels as fixed modification. Tolerance was set to 5 ppm, trypsin +/- 2 missing cleavages was selected and multiple variable modifications such as oxidized methionine, deamidation and carbamidomethyl cysteine were selected. For SEQUEST, mass tolerance was set to 5 ppm, IPI mouse database was chosen and oxidized methionine, deamidation and carbamidomethyl cysteine was selected as posttranslational or purification-related modifications. Mascot or SEQUEST search results were imported into proteome software Scaffold Q+ (version Scaffold_3.4.3, Proteome Software Inc., Portland, OR) to extract relative quantitation information for valid protein hits. Peptide identifications were accepted if they could be established at greater than 80.0% probability as specified by the Peptide Prophet Algorithm (Keller, Nesvizhskii et al. 2002). Protein identifications were accepted if they could be established at greater than 95.0% probability and contained at least 2 identified peptides. Protein probabilities were assigned by the Protein Prophet Algorithm (Nesvizhskii, Keller et al. 2003). Proteins that contained similar peptides and could not be differentiated based on MS/MS analysis alone were grouped to satisfy the principles of parsimony. Channels were corrected by the matrix [0,0.01000,0.925,0.0630,0.00200]; [0,0.0200,0.919,0.0600,0.001000]; [0,0.0300,0.920,0.0490,0.001000]; [0.001000,0.0400,0.920,0.0380,0.001000] in all samples according to the algorithm described in i-Tracker (Shadforth, Dunkley et al. 2005). The acquired intensities in the experiment were globally normalized across all acquisition runs. Individual quantitative samples were normalized within each acquisition run. The intensity for each peptide identificated was normalized within the assigned protein. The reference channels were

normalized to produce a 1:1 fold change. All normalization calculations were performed using medians to multiplicatively normalize data. The threshold set for significance was 0.05 and fold difference was set to 1.5 (Bollinger, Crabb et al. 2011).

Biological Process, Pathway or Molecular Functions Analysis

The protein IDs that were found either up- or down- regulated were input into IPA (Ingenuity system, Redwood City, CA) and MetaCore (Thomson Reuters, New York, NY) for the biological process, pathway or molecular functions analyses.

RT-qPCR

To validate quantitative proteomics data, RT-qPCR was performed. The forward and reverse primers targeting the potential up- or down-regulated genes were listed in Table 1. Total RNAs were extracted from non-induced RGC5 cells (control) and those induced to express myocilin. 1 μg of total RNAs were reverse transcribed into cDNAs (First Strand cDNA Synthesis kit, Thermo Fisher Scientific, Waltham, MA). qPCR was performed using SYBR green master mixture (Applied Biosystems). GAPDH was used for normalization. Ratio calculation was the same as that in part II of this thesis.

Immunostaining

RGC5 cells induced to express wild-type or mutated (P370L or Q368X) myocilins or un-induced as control were immunostained with rabbit anti-MDR (Santa Cruz biotechnology, Santa Cruz, CA), anti-Nid2 (Santa Cruz), anti-PSMB5 (Abcam, Cambridge, MA) polyclonal antibodies and mouse anti-Fn monoclonal antibody (BD Transduction Laboratories, Lexington, KY) using protocol described in part I of this thesis.

Table 1. List of forward and reverse primers used for RT-qPCR to validate proteomic results.

Gene Name	GenBank accession number	Sequence Name	Sequence
Abcc1	NM_008576.3	Forward	TAC TCC ATG GCT GTG TCC AT
		Reverse	CGG TTC ACT AGG TTC CCA CT
Arhgap11a	NM_181416.3	Forward	GGT CCC ACT GCT CCA CTT AT
		Reverse	GGA TCC GGA TGT CTC TTC AT
Nid2	NM_008695.2	Forward	ACA CCG AGC AGT CTG TGA AG
		Reverse	GAA GGG TCA CCT CCA ACT GT
Nfkb2	NM_019408.3	Forward	ATC TCC CGA ATG GAC AAG AC
		Reverse	TTG CCA TCC ATT CTC ATC AT
Anxa1	NM_010730.2	Forward	GAA GCT GTA CGA AGC CAT GA
		Reverse	GCT TGG CAA AGA GAG ATT CC
Sec23b	NM_019787.4	Forward	GTT TGG TGC TAC GTT GGA TG
		Reverse	TTC ACA TTC AGA GAC ACG CA
Atxn2l	NM_183020.1	Forward	GCC ACA CCC TAT TCC TCC TA
		Reverse	TGT GAA GGG TAG TGT GCC AT
AHNAK	NM_009643.1	Forward	AGG GTC CCA AGT TCA AGA TG
		Reverse	AGG ACC CTT CAA TTC TCC CT
Arpc5	NM_026369.2	Forward	CTT TGA GAG CCC ATC TGA CA
		Reverse	ACT TCT GTG AAC GGT GTC CA
Itgb1	NM_010578.2	Forward	ATT CAC ATG CAG GTT TGG AA
		Reverse	GTG ACC TCA GCT GAC AAG GA
Capn2	NM_009794.3	Forward	TGG ACA TGC TGG ATG AAG AT
		Reverse	GGA ATT CAT GGT TCC AGA CC
map1a	NM_032393.2	Forward	ATG ACT GGA CAG AGG GTT CC
		Reverse	TTA GGT ACC CAT GGT GGG AT
Hyou1	NM_021395.4	Forward	ACA GAG CCT CAG TCC CAC TT
		Reverse	AGG AAA GGA CAG AAG AGC CA
Actn1	NM_134156.2	Forward	ACC AAG ATG GAG GAG ATT GG
		Reverse	AGC TGG TCA ATC TTT GGC TT
Casp3	NM_009810.2	Forward	AAG GAG CAG CTT TGT GTG TG
		Reverse	GAA GAG TTT CGG CTT TCC AG
PSMB5	NM_011186.1	Forward	GAT CAA CCC GTA CCT TCT GG
		Reverse	GAC CGA GAT GCG TTC CTT AT

Results

SILAC

SILAC labeling only allows two biological samples (one heavy and one light) to be labeled in each experiment. Therefore only wild-type myocilin (light) and non-induced control (heavy) were labeled and examined in the SILAC study. Over 2300 protein hits were identified. 293 proteins showed differentially expression (ratio of wild-type myocilin vs. non-induced control) for more than 1.5 fold (Supplemental Table 1). Among them, 42 were up-regulated and 251 were down-regulated. The molecular and cellular functions of these differentially expressed proteins included: molecular transport, cell death and survival, cell morphology, cellular assembly and organization, as well as cellular function and maintenance (Fig. 26). The canonical pathways that may be involved included: TNFR1 signaling, interferon induction and antiviral response, actin cytoskeleton signaling, ephrin B signaling and GNRH signaling.

Functions and Diseases	p-value	# Molecules
Molecular Transport	4.07E-07 - 1.69E-02	41
export	4.07E-07 - 7.07E-03	11
export of molecule	4.07E-07	11
↑ABCC1, ↑ANXA6, ↑DDX25, ↑EGR2, ↑NME2, ↑NPC1, ↑NUP133, ↑PHAX, ↑STRADA, ↑THOC5, ↑XPOT		
export of cholesterol	3.10E-03	2
↑ANXA6, ↑NPC1		
export of protein	7.07E-03	3
↑EGR2, ↑NME2, ↑STRADA		
nuclear export	4.13E-05 - 1.69E-02	7
nuclear export of molecule	4.13E-05	7
↑DDX25, ↑EGR2, ↑NUP133, ↑PHAX, ↑STRADA, ↑THOC5, ↑XPOT		
nuclear export of RNA	4.01E-04	5
↑DDX25, ↑NUP133, ↑PHAX, ↑THOC5, ↑XPOT		
nuclear export of snRNA	1.47E-02	1
↑PHAX		
nuclear export of mRNA	1.69E-02	3
↑DDX25, ↑NUP133, ↑THOC5		
transport	1.81E-04 - 1.47E-02	33
transport of protein	1.81E-04	14
↑AP3D1, ↑CFL1, ↑COG2, ↑DYNLT1, ↑EGR2, ↑ERP29, ↑IPO9, ↑JUP, ↑MAPK14, ↑NME2, ↑RANGAP1, ↑SPTBN1, ↑STRADA, ↑YWHAH		
transport of glutathione	4.30E-03	2
↑ABCC1, ↑SLC25A11		
transport of molecule	1.01E-02	33
↑ABCC1, ↑ANXA6, ↑AP3D1, ↑ATOX1, ↑CFL1, ↑CLIC1, ↑COG2, ↑DDX25, ↑DYNLT1, ↑EGR2, ↑ERP29, ↑IKBKB, ↑IPO9, ↑JUP, ↑MAPK14, ↑MCU, ↑NME2, ↑NPC1, ↑NUP133, ↑PCYOX1, ↑PHAX, ↑PLIN3, ↑PRKACA, ↑RANGAP1, ↑SLC25A11, ↑SLC25A12, ↑SLC27A5, ↑SPTBN1, ↑STRADA, ↑THOC5, ↑VDAC2, ↑XPOT, ↑YWHAI		
Cell Death and Survival	1.54E-06 - 1.66E-02	88
cell death	1.54E-06 - 1.66E-02	88
cell death of fibroblast cell lines	1.54E-06	23
↑ABCC1, ↑APAF1, ↑ARID1A, ↑CASP3, ↑COX5A, ↑EGR2, ↑EIF2B5, ↑EIF2S1, ↑EIF3H, ↑FN1, ↑GLO1, ↑GSTP1, ↑IKBKB, ↑ITSN1, ↑MAPK14, ↑NFKB2, ↑PAK1, ↑PAK2, ↑PPP2R1B, ↑RAI14, ↑SUN2, ↑TOP2A, ↑YWHAZ		
cell death	3.19E-05	88
↑ABCC1, ↑ADA, ↑ADNP, ↑AHCTF1, ↑AKAP12, ↑ANXA1, ↑ANXA2, ↑ANXA4, ↑ANXA5, ↑APAF1, ↑ARID1A, ↑BCL2L13, ↑CAPRIN1, ↑CASP3, ↑CCT2, ↑CFL1, ↑COMT, ↑COX5A, ↑CSK, ↑CUL5, ↑CYB5R3, ↑DCTN2, ↑DDX25, ↑DECR1, ↑DKC1, ↑DNM1L, ↑ECE1, ↑EGR2, ↑EIF2B5, ↑EIF2S1, ↑EIF3H, ↑EPHA4, ↑FN1, ↑GLO1, ↑GNAI3, ↑GSTP1, ↑HK1, ↑HPRT1, ↑IKBKB, ↑ILF3, ↑ISG15, ↑ITSN1, ↑JUP, ↑KANK2, ↑LAMA5, ↑LIG3, ↑LRRK2, ↑MAPK14, ↑MDC1, ↑MDH1, ↑MPRIP, ↑MSN, ↑MTCH1, ↑MVK, ↑MYO18A, ↑NAE1, ↑NFKB2, ↑NME2, ↑NPC1, ↑NT5C1B, ↑PAK1, ↑PAK2, ↑PAK3, ↑PLIN3, ↑PPP2R1B, ↑PRDX2*, ↑PRDX4, ↑PRKACA, ↑PSMB1, ↑PSMC4, ↑RAI14, ↑RFC1, ↑SARM1, ↑SIRT2*, ↑SLC4A7, ↑SMPD4, ↑SP1, ↑SPR, ↑SPTBN1, ↑SUN2, ↑TK1, ↑TOP2A, ↑TRAP1, ↑UBA3, ↑UBR4, ↑VAV3, ↑VDAC2, ↑YWHAZ		
neuronal cell death	1.66E-02	19
↑ADA, ↑ADNP, ↑APAF1, ↑CAPRIN1, ↑CASP3, ↑FN1, ↑HPRT1, ↑IKBKB, ↑ITSN1, ↑LRRK2, ↑MAPK14, ↑NAE1, ↑NPC1, ↑PAK1, ↑PAK3, ↑PRDX2*, ↑PRKACA, ↑SP1, ↑UBA3		
apoptosis	1.11E-05 - 1.43E-02	76
apoptosis	1.11E-05	76
↑ABCC1, ↑ADA, ↑ADNP, ↑AHCTF1, ↑AKAP12, ↑ANXA1, ↑ANXA2, ↑ANXA4, ↑ANXA5, ↑APAF1, ↑BCL2L13, ↑CAPRIN1, ↑CASP3, ↑CCT2, ↑CFL1, ↑COX5A, ↑CSK, ↑CUL5, ↑DDX25, ↑DECR1, ↑DKC1, ↑DNM1L, ↑ECE1, ↑EGR2, ↑EIF2B5, ↑EIF2S1, ↑EIF3H, ↑EPHA4, ↑FN1, ↑GLO1, ↑GSTP1, ↑HK1, ↑IKBKB, ↑ILF3, ↑ITSN1, ↑JUP, ↑KANK2, ↑LAMA5, ↑LRRK2, ↑MAPK14, ↑MDC1, ↑MDH1, ↑MPRIP, ↑MSN, ↑MTCH1, ↑MVK, ↑MYO18A, ↑NAE1, ↑NFKB2, ↑NME2, ↑NPC1, ↑PAK1, ↑PAK2, ↑PAK3, ↑PPP2R1B, ↑PRDX2*, ↑PRDX4, ↑PRKACA, ↑PSMB1, ↑RAI14, ↑RFC1, ↑SARM1, ↑SIRT2*, ↑SLC4A7, ↑SMPD4, ↑SP1, ↑SPTBN1, ↑SUN2, ↑TK1, ↑TOP2A, ↑TRAP1, ↑UBA3, ↑UBR4, ↑VAV3, ↑VDAC2, ↑YWHAZ		
Cell Morphology	1.30E-05 - 1.59E-02	55
reorganization	1.30E-05 - 9.59E-03	12
reorganization of cytoskeleton	1.30E-05	12
↑ADNP, ↑AKAP12, ↑CFL1, ↑CRKL, ↑EPHA4, ↑FN1, ↑JUP, ↑LCP1, ↑MAPK14, ↑MSN, ↑PAK1, ↑PLXNB2		
reorganization of filaments	1.85E-03	4
↑ADNP, ↑JUP, ↑LCP1, ↑MAPK14		
reorganization of actin filaments	9.50E-03	3
↑JUP, ↑LCP1, ↑MAPK14		
reorganization of actin cytoskeleton	9.59E-03	5
↑AKAP12, ↑CFL1, ↑EPHA4, ↑FN1, ↑PAK1		
microtubule dynamics	1.00E-03	12
↑ABCC1, ↑ADNP, ↑AKAP12, ↑CFL1, ↑Clip1, ↑COMT, ↑CRKL, ↑DNM1L, ↑DOCK7, ↑DYNC1LI2, ↑DYNLT1, ↑EPHA4, ↑EPHB3, ↑FN1, ↑HPRT1, ↑IKBKB, ↑ITSN1, ↑KTN, ↑LAMA5, ↑LCP1, ↑MAGI2, ↑MPRIP, ↑MSN, ↑NPC1, ↑PAK1, ↑PAK3, ↑PLXNB2, ↑PRKACA, ↑SP1, ↑SPTBN1, ↑VAV3, ↑YWHAH		
organization of actin stress fibers	2.97E-03	3
↑CSK, ↑FN1, ↑LCP1		
depolarization of mitochondria	1.67E-03	4
↑APAF1, ↑DNM1L, ↑PAK1, ↑PLIN3		
autophagy	3.43E-03 - 1.47E-02	10
autophagy of colon cancer cell lines	3.43E-03	3
↑GNAI3, ↑IKBKB, ↑MAPK14		
autophagy of cells	4.60E-03	9
↑APAF1, ↑COX5A, ↑DNM1L, ↑EIF2B1, ↑EIF2S1, ↑GNAI3, ↑IKBKB, ↑MAPK14, ↑NPC1		
autophagy	1.04E-02	10
↑APAF1, ↑COX5A, ↑DNM1L, ↑EIF2B1, ↑EIF2S1, ↑GNAI3, ↑IKBKB, ↑LRRK2, ↑MAPK14, ↑NPC1		
transmembrane potential	1.59E-02 - 1.59E-02	8
transmembrane potential of mitochondria	1.59E-02	8
↑APAF1, ↑ARID1A, ↑CASP3, ↑CLIC1, ↑GPD2, ↑IKBKB, ↑ITSN1, ↑MAPK14		

Figure 26. Data analysis by IPA using the list of genes that were up- or down-regulated for more than 1.5 fold in wild-type myocilin-GFP expressing RGC5 cells in SILAC proteomic experiment.

iTRAQ

iTRAQ allows labeling of multiple biological sample differently. The samples can then be mixed and run together in mass spectrometry. We compared protein profiles of wild-type or mutated (P370L, Q368X) myocilin-GFP expression RGC5 cells vs. non-induced control cells. Over 2800 protein hits were identified. 127 proteins were found to be differentially expressed. Supplemental Table 2 showed combined results from two sets of data (human protein IDs and redundancy were removed). Among 127 proteins that were differentially expressed, 60 were up-regulated (ratio of wild-type myocilin, P370L or Q368X vs. non-induced control) and 67 were down-regulated for more than 1.5 fold. Data analyzed by IPA gave very similar results to wild-type myocilin, P370L and Q368X mutants. The cellular compromises predicted by IPA include: endoplasmic reticulum stress response, loss of actin stress fibers, and disruption of actin cytoskeleton (Table 2).

Table 2. Cellular compromises predicted by IPA when wild-type or mutated (P370L, Q368X) myocilin was expressed in RGC5 cells.

Category	Functions Annotation	p-Value	Predicted Activati	Activation z-score	Molecules		# Molecules
Cellular Compromise	endoplasmic reticulum stress response of cervical cancer cell line	3.95E-05			↑CALR, ↑HSP90B1, ↑HSPA5	all 3	3
Cellular Compromise	loss of actin stress fibers	9.26E-05			↑MYOC, ↑PDLIM1, RALB	all 3	3
Cellular Compromise	endoplasmic reticulum stress response of leukemia cell lines	1.47E-04			↑HSP90B1, ↑HSPA5	all 2	2
Cellular Compromise	endoplasmic reticulum stress response	1.47E-04		-1.982	↑AARS, ↑CALR, ↑ERO1L, ↑HSP90B1, ↑HSPA5, ↑HYOU1	all 6	6
Cellular Compromise	endoplasmic reticulum stress response of hepatoma cell lines	7.25E-04			↑HSP90B1, ↑HSPA5	all 2	2
Cellular Compromise	degeneration of Sertoli cells	7.05E-03			↓HMGB2	all 1	1
Cellular Compromise	disruption of actin cytoskeleton	8.61E-03			↑CSPG4, ↑ITGB1	all 2	2
Cellular Compromise	injury of ventricular myocytes	1.40E-02			PDCD4	all 1	1

Validation of Proteomics Data

To further validate the proteomic results, RT-qPCR was performed. Genes such as Abcc1, Actn1, AHNAK, Anxa1, Arpc5, Arhgap, Atxn2l, Casp3, Capn2, Hyou1, Itgb1, Map1a, Nfkb2,

Nid2, PSMB5, and Sec23 were chosen because they were either most differentially expressed or associated with some interesting signaling pathways. The qPCR results for most of the genes examined corroborated those of the proteomics (Fig. 27A). Abcc1 (also called MDR, multi drug resistant protein) and Nid2, two up-regulated genes were tested by immunostaining. Fig. 27B (top panel) showed that compared to non-induced control, MDR and Nid2 were up-regulated in the wild-type or mutated (P370L and Q368X) myocilin-GFP expressing RGC5 cells. The staining of fibronectin and PMSB5 (proteasome subunit, beta 5), were reduced validating these two genes were down-regulated in induced RGC5 (Fig. 27B lower panel). The ubiquitin-proteasome pathway (UPP) is one of the major routes for protein clearance in eukaryotic cells (Pagan, Seto et al. 2013). Proteasomes predominantly degrade, in a specific manner, short lived nuclear and cytosolic proteins. Down-regulation of PMSB5 may indicate that cell's capability of clearing protein was damaged or decreased (Kwak and Kensler 2006) when wild-type or mutated myocilin is overexpressed in the cells.

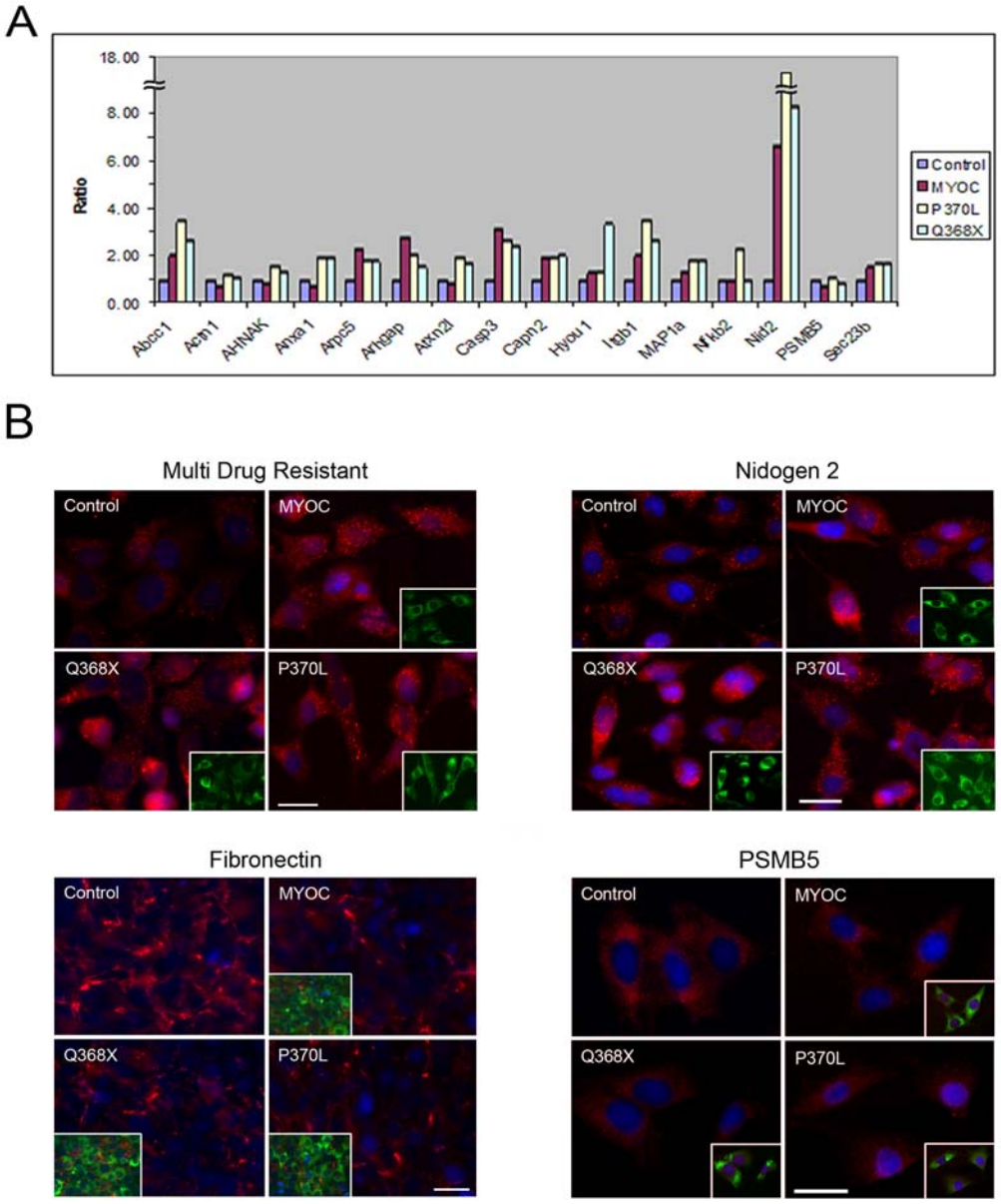

Figure 27. Validation of gene expression levels by RT-qPCR (**A**) and immunostaining (**B**). **A**. Most genes showed corroboration with proteomics at mRNA level. **B**. Immunostaining of multi drug resistant protein (MDR, red) and nidogen 2 (Nid2, red) showed up-regulation in the wild-type and mutated (P370L and Q368X) myocilin-GFP expressing RGC5 cells (top two panels) in comparison with non-induced control. On the contrary, fibronectin (Fn, red) and PMSB5 (red) showed down-regulation in the wild-type and mutated (P370L and Q368X) myocilin-GFP expressing RGC5 cells in comparison with non-induced control (lower two panels). Green channel was shown in the insets. Scale bar, 20 μm.

Discussion

To better understand the cellular changes induced by expression of wild-type myocilin and mutated myocilins, we quantified proteomic changes in Tet-on inducible RGC5 cells by LC--MS/MS iTRAQ technology. The cells were either induced to express wild-type myocilin-GFP, myocilin$_{P370L}$-GFP, and myocilin$_{Q368X}$-GFP, or non-induced. Over 2800 protein hits were identified in this experiment and most of them (95.5%) were present in similar amounts in four different groups. Wild-type or mutated myocilin overexpression significantly altered the abundance of 127 proteins; and the up-or down-regulation of 16 of them was verified independently by RT-qPCR. Bioinformatic analyses suggested that the major biological processes associated with the altered proteins included cellular movement (cell movement, migration of cells), cellular compromise (ER stress, loss of actin stress fibers, destruction of actin cytoskeleton), cellular function and maintenance (organization of actin cytoskeleton, linkage of actin cytoskeleton, formation of focal adhesions), and cellular development.

SILAC is another labeling technology which has been widely used in quantitative proteomics. It incorporates a label into proteins *in vivo* with the advantage of capable of nearly 100% label incorporation into proteins of living cells. When comparing with LC-MS/MS iTRAQ technology, it can actually be used as a good technical replication (for the pair of non-induced and wild-type myocilin) and these two methods can compensate the disadvantages of each other. Again, non-induced RGC5 cells were used as a control in the SILAC experiments. 293 proteins were found to be differentially expressed (the ratio of induced vs. non-induced control was > 1.5). These proteins were noted to associate with molecular transportation, cell death, apoptosis, cytoskeleton reorganization, depolarization of the cell, autophagy formation, permeabilization of

mitochondria, microtubule dynamics, organization of filaments, and organization of mitotic spindles.

Over 30 proteins found significantly decreased in SILAC were associated with molecular trafficking, suggesting that overexpression of wild-type myocilin impacted small molecule transport (such as ferric ion transport, transferrin transport, glucose transport, hexose transport) and protein trafficking (MetaCore analysis).

More than 70 proteins identified in SILAC experiment were associated with apoptosis. Myocilin mutants have been shown to lead to different levels of ER stress and increased apoptosis after treatment of cells with hydrogen peroxide (Joe and Tomarev 2010). Overexpression of wild-type myocilin in the Drosophila eye also activates the unfolded protein response and apoptosis (Carbone, Ayroles et al. 2009). Twelve proteins were also found to be associated with mitochondria dysfunction and lowered mitochondria membrane potential. Previous study in our lab has demonstrated that transfection of myocilin in TM cells caused a reduction of the mitochondrial potential. Myocilin was imported into the mitochondria and might have a proapoptotic role in TM cells (Sakai, Shen et al. 2007). Our proteomic data corroborated this finding and confirmed that apoptosis is a consequence of the myocilin overexpression.

Myocilin has also been shown to reduce actin stress fiber, diminish focal adhesion formation, and compromise cell migration in the cells (part III of this thesis). In the proteomic data, over 30 proteins were found to be associated with organization of the cytoskeleton. Of note is that those proteins were also implicated in microtubule dynamics. The new role of myocilin in the microtubule dynamics and its contribution to myocilin glaucoma will merit further investigations.

A few proteins were co-identified in both SILAC and iTRAQ systems. The multiple drug resistance-associated protein (Abcc1 and Abcb1b) family was one of them. This protein family is also called superfamily of ATP-binding cassette (ABC) transporters which is involved in many cellular process such as defense against toxic compounds and serves as the major high-affinity transporter of leukotriene C4 (Payen, Gao et al. 2005). The encoded protein may also play an essential role in steroid hormone homeostasis as a transporter for steroid hormones and their metabolites (Sivils, Gonzalez et al. 2010). Interestingly, the expression level of ABC transporter was found to be highly up-regulated in circulating leukocytes in patients with glaucoma, implicating that it might be a potential molecular marker for the diagnostics of glaucoma (Yeghiazaryan, Flammer et al. 2005). Actual role of this superfamily in myocilin phenotype needs to be further studied.

Another gene which was co-identified in both SILAC and iTRAQ experiments is Nid2. This gene encodes a member of the nidogen family of basement membrane proteins which are cell-adhesion proteins that bind collagens I and IV and laminin and may be involved in maintaining the structure of the basement membrane.

The third gene which was co-identified in both systems is Nfkb2, nuclear factor NF-κB p100 subunit. Nfkb2 was found to be up-regulated in P370L and Q368X expressing cells but not in wild-type suggesting that the mutated myocilin may activate NF-κB signaling pathway.

Overall, quantitative proteomic studies not only corroborated with most of previous identified myocilin phonotypes, but also revealed interesting new findings such as the possible involvement of microtubules, ABC transporters, and pathways such as autophagy, Rac, RhoGDI, aryl hydrocarbon receptor signaling, and superpathway of serine and glycine biosynthesis. These

new data may help direct us to investigate new functions or molecular pathological mechanism(s) caused by myocilin.

Supporting Information

Supplement Table 1. Proteins that were up- or down- regulated for more than 1.5 fold in SILAC quantitative proteomic experiments.

Gene name	Title	Ratio of MYOC/control
Sart3	MOUSE Squamous cell carcinoma antigen recognized by T cells 3	310.44
Vav3	MOUSE Guanine nucleotide exchange factor VAV3	297.10
Pak3	MOUSE Isoform 2 of Serine threonine protein kinase PAK 3	234.59
Arhgap11a	MOUSE Rho GTPase activating protein 11A	198.87
Mtrf1	MOUSE Peptide chain release factor 1 mitochondrial	174.60
Plekhh1	MOUSE Isoform 2 of Pleckstrin homology domain containing family H member 1	166.81
B3gnt9	MOUSE UDP GlcNAc betaGal beta 1 3 N acetylglucosaminyltransferase 9	156.71
Nsrp1	MOUSE Nuclear speckle splicing regulatory protein 1	154.95
Ilf3	MOUSE Interleukin enhancer binding factor 3	134.55
Ikbkb	MOUSE Inhibitor of nuclear factor kappa B kinase subunit beta	128.80
Cog2	MOUSE Conserved oligomeric Golgi complex subunit 2	116.27
Abcc1	MOUSE Multidrug resistance associated protein 1	102.12
Ahctf1	MOUSE Protein ELYS	87.12
Slc27a5	MOUSE Bile acyl CoA synthetase	84.86
Vcpip1	MOUSE Deubiquitinating protein VCIP135	65.75
Zcchc11	MOUSE Terminal uridylyltransferase 4	62.17
Smpd4	MOUSE Isoform 5 of Sphingomyelin phosphodiesterase 4	59.80
Me3	MOUSE NADP dependent malic enzyme mitochondrial	57.04
Nid2	MOUSE Nidogen 2	51.04
Dhx29	MOUSE ATP dependent RNA helicase Dhx29	26.19
Flii	MOUSE Protein flightless 1 homolog	22.37
Myoc	MOUSE GFP fusion protein	12.88

Arrdc1	MOUSE Isoform 2 of Arrestin domain containing protein 1	12.75
Ndufa9	MOUSE NADH dehydrogenase [ubiquinone] 1 alpha subcomplex subunit 9 mitochondrial	12.15
Heatr5a	MOUSE HEAT repeat containing protein 5A	8.94
Plod1	MOUSE Procollagen lysine 2 oxoglutarate 5 dioxygenase 1	8.60
Fam98b	MOUSE Protein FAM98B	8.54
Gfpt2	MOUSE Glucosamine fructose 6 phosphate aminotransferase [isomerizing] 2	4.81
Csk	MOUSE Tyrosine protein kinase CSK	4.29
Ubox5	MOUSE RING finger protein 37	3.46
Strada	MOUSE Isoform 2 of STE20 related kinase adapter protein alpha	2.87
Crlf3	MOUSE Isoform 2 of Cytokine receptor like factor 3	2.73
Prkaca	MOUSE Isoform 2 of cAMP dependent protein kinase catalytic subunit alpha	2.55
Prkacb	MOUSE Isoform 2 of cAMP dependent protein kinase catalytic subunit beta	2.55
Scrn2	MOUSE Secernin 2	2.40
Ipo9	MOUSE Importin 9	2.13
Ercc6l	MOUSE DNA excision repair protein ERCC 6 like	1.88
Gigyf2	MOUSE PERQ amino acid rich with GYF domain containing protein 2	1.83
Txn	MOUSE Thioredoxin	1.80
Aimp2	MOUSE Aminoacyl tRNA synthase complex interacting multifunctional protein 2	1.76
Mtch1	MOUSE Mitochondrial carrier homolog 1	1.69
Eif2b5	MOUSE Translation initiation factor eIF 2B subunit epsilon	1.53
Psmc4	MOUSE 26S protease regulatory subunit 6B	0.67
Crkl	MOUSE Crk like protein	0.67
Nxn	MOUSE Isoform 2 of Nucleoredoxin	0.67
Znf512	MOUSE Zinc finger protein 512	0.67
Cyb5r3	MOUSE Isoform 2 of NADH cytochrome b5 reductase 3	0.67
Anxa3	MOUSE Annexin A3	0.67
Rpl18	MOUSE 60S ribosomal protein L18	0.67
Actn3	MOUSE Alpha actinin 3	0.67
Uba3	MOUSE Isoform 2 of NEDD8 activating enzyme E1 catalytic subunit	0.66
Prdx2	MOUSE Peroxiredoxin 2	0.66
Atp5o	MOUSE ATP synthase subunit O mitochondrial	0.66
Glo1	MOUSE Lactoylglutathione lyase	0.66
Rangap1	MOUSE Ran GTPase activating protein 1	0.66

Ubr5	MOUSE E3 ubiquitin protein ligase UBR5	0.66
Mrc2	MOUSE C type mannose receptor 2	0.66
Gstp1	MOUSE Glutathione S transferase P 1	0.66
Sfxn3	MOUSE Sideroflexin 3	0.66
Samhd1	MOUSE SAM domain and HD domain containing protein 1	0.66
Nudcd3	sp|Q8R1N4 3|NUDC3_MOUSE Isoform 3 of NudC domain containing protein 3	0.66
Dynlt1	MOUSE Dynein light chain Tctex type 1	0.66
Uqcrc1	MOUSE Cytochrome b c1 complex subunit 1 mitochondrial	0.66
Nme2	MOUSE Nucleoside diphosphate kinase B	0.66
Msn	MOUSE Moesin	0.66
Hsd17b12	MOUSE Isoform 2 of Estradiol 17 beta dehydrogenase 12	0.66
Jup	MOUSE Junction plakoglobin	0.66
Brox	MOUSE BRO1 domain containing protein BROX	0.66
Hist1h1a	MOUSE Histone H1.1	0.65
Actn1	MOUSE Alpha actinin 1	0.65
Gdi1	MOUSE Rab GDP dissociation inhibitor alpha	0.65
Comt	MOUSE Isoform Soluble of Catechol O methyltransferase	0.65
Ddt	MOUSE D dopachrome decarboxylase	0.65
Erp44	MOUSE Endoplasmic reticulum resident protein 44	0.65
Acot13	MOUSE Acyl coenzyme A thioesterase 13	0.65
Cnot1	MOUSE Isoform 2 of CCR4 NOT transcription complex subunit 1	0.65
Ywhah	MOUSE 14 3 3 protein eta	0.65
Hspg2	MOUSE Basement membrane specific heparan sulfate proteoglycan core protein	0.65
Hmgcs1	MOUSE Hydroxymethylglutaryl CoA synthase cytoplasmic	0.65
Pigs	MOUSE GPI transamidase component PIG S	0.65
Scfd1	MOUSE Sec1 family domain containing protein 1	0.64
Trove2	MOUSE 60 kDa SS A Ro ribonucleoprotein	0.64
Psma7	MOUSE Proteasome subunit alpha type 7	0.64
Ada	MOUSE Adenosine deaminase	0.64
Gpd2	MOUSE Glycerol 3 phosphate dehydrogenase mitochondrial	0.64
Psmb5	MOUSE Proteasome subunit beta type 5	0.64
Med27	MOUSE Isoform 2 of Mediator of RNA polymerase II transcription subunit 27	0.64
Rars	MOUSE Arginine tRNA ligase cytoplasmic	0.64
Mapk14	MOUSE Isoform 4 of Mitogen activated protein kinase 14	0.64

Eif2b1	MOUSE Translation initiation factor eIF 2B subunit alpha	0.64
Clic1	MOUSE Chloride intracellular channel protein 1	0.63
Psmb1	MOUSE Proteasome subunit beta type 1	0.63
Anxa4	MOUSE Annexin A4	0.63
Capza1	MOUSE F actin capping protein subunit alpha 1	0.63
Plin3	MOUSE Perilipin 3	0.63
Chchd3	MOUSE Coiled coil helix coiled coil helix domain containing protein 3 mitochondrial	0.63
Cct2	MOUSE T complex protein 1 subunit beta	0.63
Psmd5	MOUSE 26S proteasome non ATPase regulatory subunit 5	0.63
Psmb2	MOUSE Proteasome subunit beta type 2	0.63
Atp5o	MOUSE ATP synthase subunit O mitochondrial	0.63
Slc25a11	MOUSE Mitochondrial 2 oxoglutarate malate carrier protein	0.63
Glyr1	MOUSE Putative oxidoreductase GLYR1	0.63
Nes	MOUSE Isoform 2 of Nestin	0.63
Uqcrc2	MOUSE Cytochrome b c1 complex subunit 2 mitochondrial	0.63
Mprip	MOUSE Isoform 3 of Myosin phosphatase Rho interacting protein	0.63
Anxa1	MOUSE Annexin A1	0.62
Prdx4	MOUSE Peroxiredoxin 4	0.62
Spr	MOUSE Sepiapterin reductase	0.62
Ywhaz	MOUSE 14 3 3 protein zeta delta	0.62
Atox1	MOUSE Copper transport protein ATOX1	0.62
Slc25a12	MOUSE Calcium binding mitochondrial carrier protein Aralar1	0.62
Mrc2	MOUSE C type mannose receptor 2	0.62
Anxa2	MOUSE Annexin A2	0.62
Eif2s1	MOUSE Eukaryotic translation initiation factor 2 subunit 1	0.62
Cfl1	MOUSE Cofilin 1	0.61
Ncapd2	MOUSE Condensin complex subunit 1	0.61
Trnt1	MOUSE CCA tRNA nucleotidyltransferase 1 mitochondrial	0.61
Nae1	MOUSE NEDD8 activating enzyme E1 regulatory subunit	0.61
Cfl2	MOUSE Cofilin 2	0.61
Sptbn1	MOUSE Isoform 2 of Spectrin beta chain brain 1	0.61
Samd4a	MOUSE Isoform 2 of Protein Smaug homolog 1	0.61
Eif3h	MOUSE Eukaryotic translation initiation factor 3 subunit H	0.61
Itsn2	MOUSE Intersectin 2	0.61

Bpnt1	MOUSE 3 (2) 5 bisphosphate nucleotidase 1	0.61
Prdx2	MOUSE Peroxiredoxin 2	0.61
Twf1	MOUSE Twinfilin 1	0.61
Eif3m	MOUSE Eukaryotic translation initiation factor 3 subunit M	0.60
Mdh1	MOUSE Malate dehydrogenase cytoplasmic	0.59
Vps35	MOUSE Vacuolar protein sorting associated protein 35	0.59
Fn1	MOUSE Fibronectin	0.59
Fmn1	MOUSE Isoform 5 of Formin 1	0.59
Cope	MOUSE Coatomer subunit epsilon	0.58
Pcyox1	MOUSE Prenylcysteine oxidase	0.58
Eef1b	MOUSE Elongation factor 1 beta	0.58
Atp5h	MOUSE ATP synthase subunit d mitochondrial	0.57
Postn	MOUSE Isoform 5 of Periostin	0.57
Fam114a1	MOUSE Protein Noxp20	0.57
Casp3	MOUSE Caspase 3	0.57
Kank2	MOUSE KN motif and ankyrin repeat domain containing protein 2	0.57
Ap3d1	MOUSE AP 3 complex subunit delta 1	0.57
Ddx6	Probable ATP dependent RNA helicase DDX6	0.56
Plod3	MOUSE Procollagen lysine 2 oxoglutarate 5 dioxygenase 3	0.56
Blmh	MOUSE Bleomycin hydrolase	0.56
Mvk	MOUSE Mevalonate kinase	0.55
Ptgr1	MOUSE Prostaglandin reductase 1	0.55
Anapc5	MOUSE Anaphase promoting complex subunit 5	0.54
Anxa5	MOUSE Annexin A5	0.54
Mtco2	MOUSE Cytochrome c oxidase subunit 2	0.54
Paics	MOUSE Multifunctional protein ADE2	0.54
Serpinb1a	MOUSE Leukocyte elastase inhibitor A	0.53
Erp29	MOUSE Endoplasmic reticulum resident protein 29	0.53
Hprt1	MOUSE Hypoxanthine guanine phosphoribosyltransferase	0.52
Anks6	MOUSE Ankyrin repeat and SAM domain containing protein 6	0.52
Cyp51a1	MOUSE Lanosterol 14 alpha demethylase	0.52
Sirt2	MOUSE Isoform 2 of NAD dependent deacetylase sirtuin 2	0.51
Fdps	MOUSE Farnesyl pyrophosphate synthase	0.51
Nup93	MOUSE Nuclear pore complex protein Nup93	0.51
Acaa1a	MOUSE 3 ketoacyl CoA thiolase A peroxisomal	0.51

Lama5	MOUSE Laminin subunit alpha 5	0.50
Anxa6	MOUSE Annexin A6	0.50
Serpini2	MOUSE Serpin I2	0.49
Top2a	MOUSE DNA topoisomerase 2 alpha	0.49
Tecr	MOUSE Trans 2 3 enoyl CoA reductase	0.48
Tcf20	MOUSE Isoform 2 of Transcription factor 20	0.48
Ufl1	MOUSE E3 UFM1 protein ligase 1	0.48
Psat1	MOUSE Phosphoserine aminotransferase	0.47
Hsd17b4	MOUSE Peroxisomal multifunctional enzyme type 2	0.46
Psmd3	MOUSE 26S proteasome non ATPase regulatory subunit 3	0.46
Isg15	MOUSE Ubiquitin like protein ISG15	0.45
Nup133	MOUSE Nuclear pore complex protein Nup133	0.44
Pgk2	MOUSE Phosphoglycerate kinase 2	0.43
Decr1	MOUSE 2 4 dienoyl CoA reductase mitochondrial	0.43
Cc2d1b	MOUSE Coiled coil and C2 domain containing protein 1B	0.42
Coll2a1	MOUSE Isoform 2 of Collagen alpha 1(XII) chain	0.41
Trap1	MOUSE Heat shock protein 75 kDa mitochondrial	0.39
Sirt2	MOUSE Isoform 2 of NAD dependent deacetylase sirtuin 2	0.39
Sart3	MOUSE Squamous cell carcinoma antigen recognized by T cells 3	0.38
Twf2	MOUSE Twinfilin 2	0.37
Rai14	MOUSE Ankycorbin	0.36
Fam91a1	MOUSE Protein FAM91A1	0.36
Kiaa0564	MOUSE Uncharacterized protein KIAA0564 homolog	0.36
Slc4a7	MOUSE Isoform 2 of Sodium bicarbonate cotransporter 3	0.35
Cox5a	MOUSE Cytochrome c oxidase subunit 5A mitochondrial	0.34
Lig3	MOUSE Isoform Beta of DNA ligase 3	0.34
Vdac2	MOUSE Voltage dependent anion selective channel protein 2	0.34
Myo18a	MOUSE Isoform 5 of Unconventional myosin XVIIIa	0.33
Ostf1	MOUSE Osteoclast stimulating factor 1	0.33
Tk1	MOUSE Thymidine kinase cytosolic	0.29
Anapc4	MOUSE Anaphase promoting complex subunit 4	0.29
Ubr4	MOUSE E3 ubiquitin protein ligase UBR4	0.29
Ifi202	MOUSE Interferon activable protein 202	0.28
Mov10	MOUSE Putative helicase MOV 10	0.27
Ktn1	MOUSE Isoform 6 of Kinectin	0.25

Sarm1	MOUSE Sterile alpha and TIR motif containing protein 1	0.25
Tlk2	MOUSE Isoform 3 of Serine threonine protein kinase tousled like 2	0.25
Dync1li2	MOUSE Cytoplasmic dynein 1 light intermediate chain 2	0.25
Dnm1l	MOUSE Isoform 3 of Dynamin 1 like protein	0.25
Plod1	MOUSE Procollagen lysine 2 oxoglutarate 5 dioxygenase 1	0.25
Mrpl37	MOUSE 39S ribosomal protein L37 mitochondrial	0.24
Plod2	MOUSE Procollagen lysine 2 oxoglutarate 5 dioxygenase 2	0.23
Usp5	MOUSE Ubiquitin carboxyl terminal hydrolase 5	0.23
Gspt1	MOUSE Eukaryotic peptide chain release factor GTP binding subunit ERF3A	0.23
Gigyf1	MOUSE PERQ amino acid rich with GYF domain containing protein 1	0.22
Chaf1b	MOUSE Chromatin assembly factor 1 subunit B	0.22
Scyl1	MOUSE N terminal kinase like protein	0.21
Hk1	MOUSE Isoform HK1 of Hexokinase 1	0.21
Mpp5	MOUSE MAGUK p55 subfamily member 5	0.20
Pitrm1	MOUSE Isoform 3 of Presequence protease mitochondrial	0.19
Upf1	MOUSE Isoform 2 of Regulator of nonsense transcripts 1	0.19
Metap1	MOUSE Methionine aminopeptidase 1	0.19
Sp1	MOUSE Transcription factor Sp1	0.18
Ankfy1	MOUSE Ankyrin repeat and FYVE domain containing protein 1	0.18
Ephb3	MOUSE Ephrin type B receptor 3	0.17
Mdc1	MOUSE Mediator of DNA damage checkpoint protein 1	0.17
Npc1	MOUSE Niemann Pick C1 protein	0.16
Kdelc1	MOUSE Isoform 2 of KDEL motif containing protein 1	0.15
Apaf1	MOUSE Isoform 2 of Apoptotic protease activating factor 1	0.15
Dscr3	MOUSE Down syndrome critical region protein 3 homolog	0.14
Dkc1	MOUSE H ACA ribonucleoprotein complex subunit 4	0.13
Gnai3	MOUSE Guanine nucleotide binding protein G(k) subunit alpha	0.13
Drg2	MOUSE Developmentally regulated GTP binding protein 2	0.12
Eif3a	MOUSE Eukaryotic translation initiation factor 3 subunit A	0.12
Pan2	MOUSE Isoform 4 of PAB dependent poly(A) specific ribonuclease subunit 2	0.11
Tjp1	MOUSE Tight junction protein ZO 1	0.11
Magi2	MOUSE Membrane associated guanylate kinase WW and PDZ domain containing protein 2	0.10
Sun2	MOUSE Isoform 2 of SUN domain containing protein 2	0.10
Lcp1	MOUSE Plastin 2	0.10

Ints5	MOUSE Integrator complex subunit 5	0.09
Neurl4	MOUSE Neuralized like protein 4	0.09
Stard4	MOUSE StAR related lipid transfer protein 4	0.09
Phax	MOUSE Phosphorylated adapter RNA export protein	0.09
Kif11	MOUSE Kinesin like protein KIF11	0.08
Dock7	MOUSE Dedicator of cytokinesis protein 7	0.08
Rabl3	MOUSE Rab like protein 3	0.07
Aqr	MOUSE Intron binding protein aquarius	0.07
Thoc5	MOUSE THO complex subunit 5 homolog	0.07
Cenpi	MOUSE Centromere protein I	0.07
Ppp2r1b	MOUSE Serine threonine protein phosphatase 2A 65 kDa regulatory subunit A beta isoform	0.07
Supt16h	MOUSE FACT complex subunit SPT16	0.07
Sh3gl1	MOUSE Endophilin A2	0.06
Txndc16	MOUSE Thioredoxin domain containing protein 16	0.06
Dctn2	MOUSE Dynactin subunit 2	0.05
Rfc1	MOUSE Replication factor C subunit 1	0.05
Xpot	MOUSE Exportin T	0.05
Tmtc3	MOUSE Isoform 2 of Transmembrane and TPR repeat containing protein 3	0.05
Arid1a	MOUSE Isoform 2 of AT rich interactive domain containing protein 1A	0.05
Itsn1	MOUSE Isoform 2 of Intersectin 1	0.04
Ddx50	MOUSE ATP dependent RNA helicase DDX50	0.04
Utp20	MOUSE Small subunit processome component 20 homolog	0.04
Cul5	MOUSE Cullin 5	0.03
Bcl2l13	MOUSE Bcl 2 like protein 13	0.03
Gba	MOUSE Glucosylceramidase	0.03
Npepps	MOUSE Puromycin sensitive aminopeptidase	0.03
Cog1	MOUSE Conserved oligomeric Golgi complex subunit 1	0.03
Usp15	MOUSE Isoform 2 of Ubiquitin carboxyl terminal hydrolase 15	0.03
Plaa	MOUSE Phospholipase A 2 activating protein	0.03
Heatr5a	MOUSE HEAT repeat containing protein 5A	0.02
Arfgap3	MOUSE ADP ribosylation factor GTPase activating protein 3	0.02
Ltn1	MOUSE E3 ubiquitin protein ligase listerin	0.02
Ddx46	MOUSE Isoform 2 of Probable ATP dependent RNA helicase DDX46	0.02
Ankrd52	Serine threonine protein phosphatase 6 regulatory ankyrin repeat subunit C	0.02

Gemin5	MOUSE Gem associated protein 5	0.02
Clip1	MOUSE Isoform 2 of CAP Gly domain containing linker protein 1	0.02
Pak2	MOUSE Serine threonine protein kinase PAK 2	0.01
Ddx25	MOUSE ATP dependent RNA helicase DDX25	0.01
Lrrk2	MOUSE Leucine rich repeat serine threonine protein kinase 2	0.01
Eppk1	MOUSE Epiplakin	0.01
Adnp	MOUSE Activity dependent neuroprotector homeobox protein	0.01
Plxnb2	MOUSE Plexin B2	0.01
Rpap1	MOUSE Isoform 2 of RNA polymerase II associated protein 1	0.01
Akap12	MOUSE Isoform 2 of A kinase anchor protein 12	0.01
Caprin1	MOUSE Caprin 1	0.01
Krt79	MOUSE Keratin type II cytoskeletal 79	0.01
Pak1	MOUSE Serine threonine protein kinase PAK 1	0.01
Fbxl13	MOUSE F box LRR repeat protein 13	0.00
Stard5	MOUSE StAR related lipid transfer protein 5	0.00
Pold1	MOUSE DNA polymerase delta catalytic subunit	0.00
Rbm12ba	MOUSE RNA binding protein 12B A	0.00
Mphosph8	MOUSE M phase phosphoprotein 8	0.00
EPHA4	HUMAN EPH receptor A4	0.00
Mcu	MOUSE Isoform 2 of Calcium uniporter protein mitochondrial	0.00
Oxr1	MOUSE Isoform 3 of Oxidation resistance protein 1	0.00
Ddx18	MOUSE ATP dependent RNA helicase DDX18	0.00
Sacm1l	MOUSE Phosphatidylinositide phosphatase SAC1	0.00
Egr2	MOUSE E3 SUMO protein ligase EGR2	0.00
Spns1	MOUSE Protein spinster homolog 1	0.00
Ece1	MOUSE Endothelin converting enzyme 1	0.00
Ermap	MOUSE Isoform 3 of Erythroid membrane associated protein	0.00
Nt5c1b	MOUSE Isoform 2 of Cytosolic 5 nucleotidase 1B	0.00
Rif1	MOUSE Isoform 2 of Telomere associated protein RIF1	0.00
Hist1h1c	MOUSE Histone H1.2	0.00
Krt5	MOUSE Keratin type II cytoskeletal 5	0.00
Nfkb2	MOUSE Nuclear factor NF kappa B p100 subunit	0.00

Suplement Table 2. Proteins that were up- or down-regulated for more than 1.5 fold in iTRAQ quantitative proteomic experiments.

Gene Name	Identified Proteins	Control	MYOC-GFP	P370L-GFP	Q368X-GFP
Sec23b	Protein transport protein Sec23B	1	50.55	50.55	50.55
Atxn2l	Ataxin-2-like protein	1	34.73	23.87	23.63
Ddi2	Protein DDI1 homolog 2	1	24.57	1.25	1.15
Snrnp40	U5 small nuclear ribonucleoprotein 40 kDa protein	0.5	19.05	17.85	16.75
Basp1	Brain acid soluble protein 1	1	17.7	15	14.35
Pak4	Serine/threonine-protein kinase PAK 4	0.9	3.8	1.37	1.67
Gatad2a	Transcriptional repressor p66 alpha	1	3.7	2.9	3.8
Myoc	MYOC GFP fusion protein	1	3.7	2.73	4.3
Otud5	OTU domain-containing protein 5	0.83	3.37	2.7	2.63
Mink1	Isoform 3 of Misshapen-like kinase 1	1	3	19.1	14.3
Nup35	Nucleoporin NUP53	1	2.73	1.57	1.43
Ripk3	Receptor-interacting serine/threonine-protein kinase 3	1	2.43	1.33	1.13
Rbbp4	Histone-binding protein RBBP4	1	2.35	2.27	1.5
Caprin1	Caprin-1	1	2.3	1.5	1.5
Ecm1	Extracellular matrix protein 1	1	2.3	2.2	1.2
Lpp	Lipoma-preferred partner homolog	1	2.2	0.8	1.23
Hint2	Histidine triad nucleotide-binding protein 2,	1	2.07	1.03	1.1
Arpc5	Actin-related protein 2/3 complex subunit 5	1	2	0.93	0.9
Dnpep	Aspartyl aminopeptidase	1	2	1.17	1.17
Blvrb	Flavin reductase (NADPH)	1.03	1.97	1.2	1.07
Hbs1l	HBS1-like protein	1.1	1.9	2	1.7
Itgb1	Integrin beta-1	1.03	1.87	1.23	1.17
Lars	Leucine--tRNA ligase, cytoplasmic	1	1.83	1.03	1.4
Capn2	Calpain-2 catalytic subunit	1	1.7	1.8	1.3
Gpc1	Glypican-1	1	1.6	1.15	0.95
Ripk3	Receptor-interacting serine/threonine-protein kinase 3	1.1	1.6	1.5	1.15
Lnp	Protein lunapark	1	1.57	1.17	1.13
Pdia6	Protein disulfide-isomerase A6	1	1.57	1.03	1.23
Thop1	Thimet oligopeptidase	1	1.57	1.2	1.17

Kiaa0564	Uncharacterized protein KIAA0564 homolog	1	1.55	1.2	1.3
Xrn1	5'-3' exoribonuclease 1	1	1.55	1	0.95
HIST1H2AB	Histone H2A type 1-B/E	1	1.53	2	1.33
Lbr	Lamin-B receptor	1	1.53	1.07	0.67
Nfix	Isoform NFIX1 of Nuclear factor 1 X-type	1	1.53	1.07	1.17
Prrc2c	Protein PRRC2C	1	1.53	1.43	1
Slc25a4	ADP/ATP translocase 1	1	1.53	0.97	1.13
ARL3	ADP-ribosylation factor-like protein 3	1	1.5	1.5	1.2
Dbnl	Drebrin-like protein	1	1.5	1.7	1
Lap3	Isoform 2 of Cytosol aminopeptidase	1	1.5	0.9	1.1
Nup93	Nuclear pore complex protein Nup93	1	1.5	1.05	0.85
Map1a	Microtubule-associated protein 1A	1	1.45	1.7	1.23
Aars	Alanine--tRNA ligase, cytoplasmic	1	1.43	1.3	1.57
Ankrd17	Ankyrin repeat domain-containing protein 17	1	1.43	1.6	1.27
Mthfd2	Bifunctional methylenetetrahydrofolate dehydrogenase/cyclohydrolase, mitochondrial	1	1.43	1.43	1.67
Ak2	Adenylate kinase 2, mitochondrial	1	1.4	1.9	1
Ap3b1	AP-3 complex subunit beta-1	0.95	1.4	1	6.43
Gars	Glycine--tRNA ligase	1	1.4	1.45	1.6
Q15149-6-R	Q15149-6-R	1	1.4	2.8	0.7
Slc12a4	Solute carrier family 12 member 4	1	1.4	1.5	0.9
Acot2	Acyl-coenzyme A thioesterase 2, mitochondrial	1	1.37	0.9	1.5
CYB5R3	Cytochrome b5 reductase 3	1	1.35	1.5	1
Hyou1	Hypoxia up-regulated protein 1	1	1.35	1.05	1.6
Hspa5	78 kDa glucose-regulated protein	0.97	1.33	1.17	1.73
Abcb1b	Multidrug resistance protein 1B	1	1.3	1.5	1
Ddx42	ATP-dependent RNA helicase DDX42	1	1.3	1.5	1
Ero1l	ERO1-like protein alpha	1	1.3	1.45	1.55
OTUB1	OTU domain, ubiquitin aldehyde-binding 1	1	1.3	1.65	1.3
Slc3a2	4F2 cell-surface antigen heavy chain	1	1.27	1.23	1.6
Hsp90b1	Endoplasmin	1	1.23	0.9	1.83
Ppa1	Inorganic pyrophosphatase	1	1.23	0.93	0.67
Aldh9a1	4-trimethylaminobutyraldehyde dehydrogenase	1	1.2	0.65	0.75
Asns	Asparagine synthetase [glutamine-hydrolyzing]	1	1.2	1.33	1.53
CDC42	Cell division cycle 42 (GTP-binding protein, 25kDa)	0.95	1.2	28.13	24.27
Nop2	Putative ribosomal RNA methyltransferase NOP2	1	1.2	1	24.7

Umps	Uridine 5'-monophosphate synthase	1	1.2	1.77	0.8
Acadvl	Very long-chain specific acyl-CoA dehydrogenase, mitochondrial	1	1.17	1.67	1.13
Aldh18a1	Delta-1-pyrroline-5-carboxylate synthase	1	1.17	1.53	1.6
Ide	Insulin-degrading enzyme	1	1.17	1.7	1.33
Psat1	Phosphoserine aminotransferase	1	1.17	1.77	1.97
Pafah1b1	Isoform 2 of Platelet-activating factor acetylhydrolase IB subunit alpha	0.95	1.15	1.5	1.15
Calr	Calreticulin	1	1.13	0.93	1.57
Aifm1	Apoptosis-inducing factor 1, mitochondrial	1	1.1	0.93	0.67
Aldh1l2	Mitochondrial 10-formyltetrahydrofolate dehydrogenase	1	1.1	0.8	1.93
Ehd1	EH domain-containing protein 1	1	1.1	1.55	1.6
Gusb	Beta-glucuronidase	1	1.1	1.33	0.63
ISYNA1	Myo-inositol 1-phosphate synthase A1, isoform CRA_d	1	1.1	1.5	1.15
Pdlim1	PDZ and LIM domain protein 1	1	1.1	1.07	1.5
Pola2	DNA polymerase alpha subunit B	1	1.1	1.6	1.45
Rbbp7	Histone-binding protein RBBP7	1	1.1	67.03	67.07
Eef1g	Elongation factor 1-gamma	1	1.07	1.7	1.8
Ankrd52	Serine/threonine-protein phosphatase 6 regulatory ankyrin repeat subunit C	1	1.05	1.5	1
Anxa1	Annexin A1	1	1.03	1.63	1.33
Cspg4	Chondroitin sulfate proteoglycan 4	0.97	1.03	0.67	0.9
Ctsb	Cathepsin B	1	1.03	1.6	0.97
Hist1h1a	Histone H1.1	1	1.03	1.67	1.13
Pc	Pyruvate carboxylase, mitochondrial	1	1.03	1.4	2.03
Cobll1	Cordon-bleu protein-like 1	1	1	1.25	1.55
Gpd2	Glycerol-3-phosphate dehydrogenase, mitochondrial	1	1	0.63	0.87
Hmgn1	Non-histone chromosomal protein HMG-14	0.7	1	1.7	0.8
Nfkb2	Nuclear factor NF-kappa-B p100 subunit	1	1	1.8	1.3
Notch2	Neurogenic locus notch homolog protein 2	1	1	1.5	0.8
Pdcd4	Programmed cell death protein 4	1	1	1.17	1.6
Ralb	Ras-related protein Ral-B	1	1	0.57	1.07
Cfl1	Cofilin-1	1	0.97	1.5	1.27
Msn	Moesin	1	0.97	0.65	0.9
Nid2	Nidogen-2	1	0.97	1.77	1.47
Aak1	AP2-associated protein kinase 1	1	0.95	1.57	0.73
Rpp30	Ribonuclease P protein subunit p30	1	0.95	1.73	1.63

AHNAK	Neuroblast differentiation-associated protein AHNAK	1	0.93	2.1	1.9
Atxn2	Ataxin-2	1	0.93	1.63	1
HMGB1	Uncharacterized protein	1	0.93	0.77	0.67
Ptgfrn	Prostaglandin F2 receptor negative regulator	1	0.93	0.9	0.67
SHMT2	Serine hydroxymethyltransferase	1	0.93	0.93	1.5
Dock7	Dedicator of cytokinesis protein 7	1	0.9	0.6	0.9
Ezr	Ezrin	1	0.9	1.55	1.3
Hmgb2	High mobility group protein B2	1	0.9	0.67	0.8
Lgals3	Galectin-3	1	0.9	1.73	1.4
Myof	Myoferlin	1	0.9	1.67	1.53
Osbp	Oxysterol-binding protein 1	1	0.9	1.5	1.6
Safb	Scaffold attachment factor B1	1	0.9	0.9	50.5
Ganab	Isoform 2 of Neutral alpha-glucosidase AB	1	0.87	1.53	1.5
Prdx5	Isoform Cytoplasmic+peroxisomal of Peroxiredoxin-5, mitochondrial	1	0.87	1.7	1.3
Dak	Bifunctional ATP-dependent dihydroxyacetone kinase/FAD-AMP lyase (cyclizing)	1	0.85	1.7	1.35
Scp2	Non-specific lipid-transfer protein	1	0.83	0.53	0.73
NT5C2	5'-nucleotidase, cytosolic II	1	0.8	2.05	1.75
VPS35	Vacuolar protein sorting 35 homolog (S. cerevisiae)	1	0.77	0.83	0.67
ALB	Albumin	1	0.75	0.8	0.55
Acsl1	Long-chain-fatty-acid--CoA ligase 1	1	0.73	0.6	0.67
EIF3D	Eukaryotic translation initiation factor 3, subunit D	1	0.7	1.1	1
Esyt1	Extended synaptotagmin-1	1	0.7	0.9	0.93
GSR	Glutathion reductase delta8 alternative splicing variant	1	0.67	0.97	0.8
KRT10	Keratin, type I cytoskeletal 10	1	0.67	1	1
Glod4	Isoform 3 of Glyoxalase domain-containing protein 4	1	0.65	1.83	1.47
Cops2	Isoform 2 of COP9 signalosome complex subunit 2	1	0.5	0.97	0.87
EED	Embryonic ectoderm development	1	0.3	1.2	1.07
Eefsec	Selenocysteine-specific elongation factor	1	0.3	0.9	0.8
Foxk1	Forkhead box protein K1	1	0.3	1	1

PART V: IDENTIFICATION OF MIRNAS THAT REGULATE THE EXPRESSION OF MYOCILIN

Despite the intense interest in myocilin, so far there is very little information available regarding its regulation at the posttranscriptional level.

MicroRNAs (miRNA) are short non-coding ribonucleic acid (ncRNA) molecules that are regulators for expression of genes. They bind with the 3' UTR (untranslated region) of mRNA of target genes to result in translational repression or mRNA degradation (preventing genes from translation into proteins).

MiRNA genes are located as clusters in the non-coding or coding region of the genome (Bartel 2004) and are usually transcribed by RNA polymerase II in the nucleus into primary miRNAs (pri-miRNAs) which are cleaved by Drosha, a class 2 RNase III enzyme to generate pre-miRNAs (precursor-miRNAs). Pre-miRNA hairpins are exported from the nucleus and are further cleaved by another RNase III enzyme Dicer into small (~22 nucleotides (nt) long) mature miRNAs. The mature miRNAs are part of an active miRNA ribonucleoprotein complex (miRNP or RISC RNA induced silencing complex) which will prevent mRNA from being translated or will degrade mRNA, leading to silencing of target genes (Lee, Han et al. 2006; Xu 2009).

Our study aimed to identify the miRNAs that regulate the expression of myocilin. This is the first study focused on miRNA regulation of the myocilin gene.

We performed miRNA array using Tet-on inducible RGC5 cell line which was established in part III of this thesis. The miRNA profile in induced cells (when wild-type myocilin was expressed) was compared to non-induced cells (control). The miRNAs that were up- or down-regulated in the induced cells were identified. Computer algorithms were also used to predict miRNAs potentially targeting myocilin. These miRNAs along with those selected from

miRNA array analysis were tested for the inhibition of myocilin expression at RNA and protein levels. Since expression of mutated (Q368X and P370L) myocilin is likely to be under the same miRNA control as the wild-type myocilin, results from the experiments may be applied to silence the mutants. The information obtained will allow not only insights into the myocilin regulation but also development of novel translational strategies to abrogate mutant phenotypes in myocilin glaucoma.

Materials and Methods

MiRNA Profiling

To identify miRNAs that regulate the expression of the human myocilin gene, microarray was carried out for miRNA profiling using Tet-on inducible wild-type myocilin-GFP expressing RGC5 stable cell line. Differences between induced and non-induced cells were analyzed. Total RNAs (including small RNAs) were extracted from RGC5 cells using miRNeasy Mini Kit (Qiagen). Samples were labeled according to FlashTag HSR RNA labeling protocol (Genisphere, Hatfield, PA) and hybridized with Affymetrix V2 miRNA array (three replicates in each group). Each image was analyzed by miRNA QC tool (Affymetrix).

Data Analysis

Data was analyzed with Partek Genomics statistical package from Partek, Inc. (St. Louis, MO). Hybridization signal intensities were normalized and summarized using the Robust Multi-array Average (RMA) (Irizarry, Hobbs et al. 2003).

ANOVA tests were used to calculate significance of the differential expression. Raw p-values were corrected for False Discovery Rate (FDR) according to step-up or Benjamini-

Hochberg (BH) procedure. Differentially expressed transcripts were annotated according to Affymetrix 'NetAffx Analysis Center'.

RT-qPCR

To validate the up- or down-regulation of miRNAs identified, the copy numbers of pre-miRNAs (about 70 nt long) of 5 to 10 most up- and down-regulated miRNAs were quantified by RT-qPCR using total RNA extracted from myocilin-GFP-expressing inducible cells and compared to non-induced control.

To determine the effects of validated miRNAs on the expression levels of myocilin, RGC5 cells were transfected with synthetic miRNA mimic (miRIDIAN microRNA Mimics) or negative control (miRIDIAN microRNA Mimic Transfection Control with Dy547) (Thermo Scientific). Changes in myocilin mRNA levels were determined by RT-qPCR using mouse MYOC Taqman gene expression assay (Life Technologies). The Ct of the gene measured was normalized against housekeeping gene GAPDH. Ratio calculation for target gene expression is the same as in part II of this thesis.

MiRNA Target Identification and Functional Validation of Predicted Targets

MYOC 3' UTR reporter vector which contains the mouse MYOC 3' UTR sequence in mammalian expression vectors (GeneCopoeia, Rockville, MD) (Fig. 32) was used for the miRNA target identification. Mouse MYOC 3' UTR reporter vector was cotransfected with miRNA mimics (or negative control) into RGC5 cells. The medium was changed 24 h post transfection and the supernatant was collected 48 h post transfection. The activities of the secreted Gaussia luciferase (GLuc) and secreted alkaline phosphatase (SEAP) were measured by

Secrete Pair ™ Dual Luminiscence Assay Kit (GeneCopoeia) on a luminometer. The reading of GLuc was normalized with that of the internal control SEAP.

Results

Two methods were used for searching miRNA which may target myocilin: miRNA array and computational algorithm.

MiRNA array

Tet-on inducible RGC5 cells without or with induction were used for the miRNA array. The miRNA profilings were compared between the myocilin$_{WT}$-GFP-expressing and non-expressing control cells. The miRNAs with fold-change (MYOC/control) more than two fold (down-regulated or up-regulated) (Teruel, Corral et al. 2011) are listed in Fig. 28.

A

Probe Set ID	Fold-Change (MYOC vs. Control)
mmu-miR-676_st	-80.8
mmu-miR-206_st	-13.3
mmu-miR-1946a_st	-11.4
mmu-miR-344_st	-5.0
mmu-miR-193-star_st	-4.2
mmu-miR-1946b_st	-4.1
mmu-miR-1941-5p_st	-3.0
mmu-miR-1949_st	-2.9
mmu-miR-714_st	-2.8
mmu-miR-1965_st	-2.8
mmu-miR-330-star_st	-2.7
mmu-miR-1931_st	-2.6
mmu-miR-17_st	-2.2
v11_mmu-miR-685_st	-2.2
mmu-miR-132_st	-2.2
mmu-miR-17-star_st	-2.2
mmu-miR-125b-3p_st	-2.1
v11_mmu-miR-805_st	-2.1
mmu-miR-3473_st	-2.1
mmu-miR-877_st	-2.1
mmu-miR-140_st	-2.1
mmu-miR-29b-star_st	-2.0
mmu-miR-1195_st	-2.0
mmu-miR-500_st	-2.0

B

Probe Set ID	Fold-Change (MYOC vs. Control)
mmu-miR-130b_st	6.3
mmu-miR-145_st	5.0
mmu-miR-574-3p_st	4.3
mmu-miR-143_st	4.0
mmu-miR-1894-3p_st	3.9
mmu-miR-125b-star_st	3.1
mmu-miR-199a-3p_st	2.8
mmu-miR-455_st	2.7
mmu-miR-574-5p_st	2.6
mmu-miR-34b-5p_st	2.5
mmu-miR-146b_st	2.5
mmu-miR-466f-3p_st	2.5
mmu-miR-9-star_st	2.4
mmu-miR-99a_st	2.2
mmu-miR-100_st	2.2
mmu-miR-181c_st	2.2
mmu-miR-181b_st	2.2
mmu-miR-181a-1-star_st	2.2
mmu-miR-322-star_st	2.1
mmu-miR-26a_st	2.0
mmu-miR-2137_st	2.0

Figure 28. MiRNA array results. 24 miRNAs were down-regulated and 21 miRNAs were up-regulated for more than 2 fold when MYOC-GFP was induced to express in RGC5 cells.

An online miRNA prediction algorithm (www.microrna.org) was also used to search for the myocilin-targeting miRNAs. Potential miRNAs that may target the 3' UTR of mouse myocilin is shown in Fig. 29.

Figure 29. MiRNA prediction by computational algorithm (http://www.microrna.org) for the 3' UTR region of mouse MYOC.

Mouse MYOC mRNA Was Knocked Down by MiRNAs

Based on the miRNA array and miRNA prediction algorithm, 4 miRNAs were chosen for further validation: miR676, miR378, miR19b and miR320. miR676 was the most down-regulated one in the miRNA array, miR19b was down-regulated 1.6 fold in the miRNA array and was also predicted by the prediction algorithm. miR378 and miR320 were predicted by the

computer algorithm with high scores. All of them have at least 6 nt seeding region in the 3' UTR region of mouse MYOC (Fig. 30).

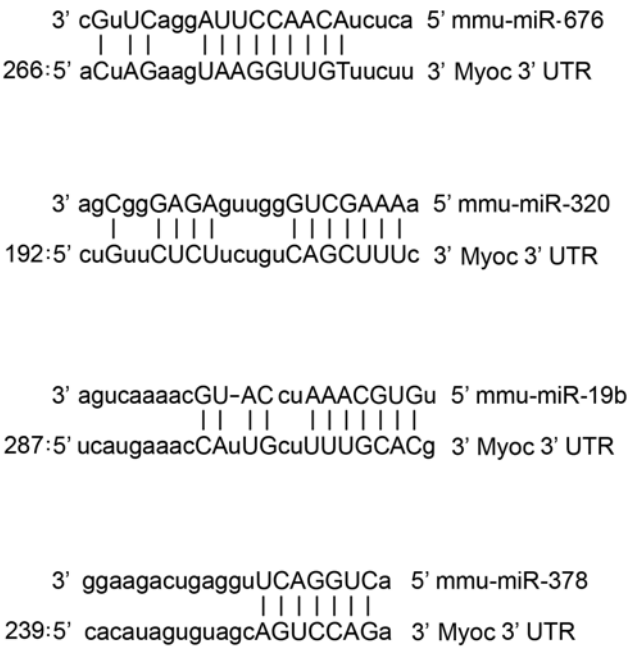

Figure 30. Predicted interactions between the seed region of mmu-miR 676, mmu-miR320, mmu-miR19b and mmu-miR-378 and the 3'UTR from mouse MYOC.

To test whether these miRNAs can knockdown the expression of mouse myocilin, synthetic miRNA mimics were transfected into RGC5 cells. MYOC mRNA level quantified by RT-qPCR using the mouse MYOC Taqman gene expression assay was normalized to that of the mouse GAPDH housekeeping gene. The ratio of miRNA mimics was calculated as MiR19b showed the best knockdown at 100 nM (42% knockdown) and at 50 nM (40% knockdown). Other miRNAs also showed approximately 20-40% effects (Fig. 31) comparing to negative control DY576.

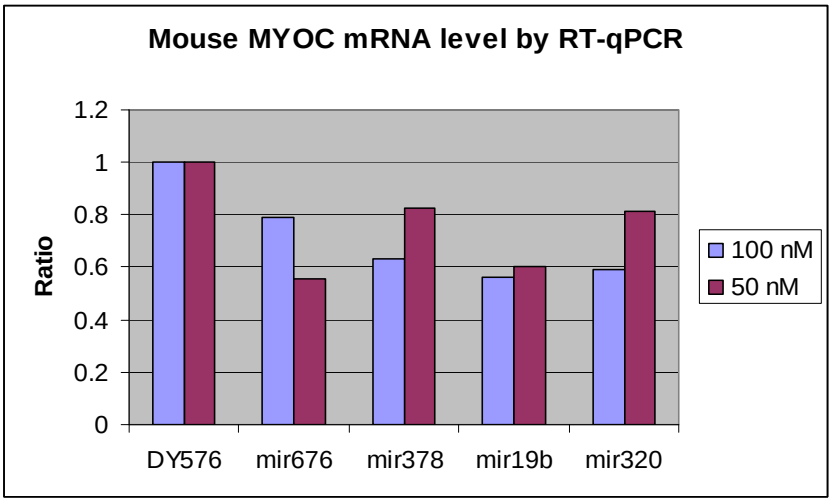

Figure 31. Knockdown of the mouse MYOC mRNA levels by miRNAs. Two miRNA concentrations (100 and 50 nM) of miRNAs were used for transfection. At 100 nM, miR378, miR19b and miR320 showed about 40% knockdown of MYOC mRNA. At 50 nM, miR19b and miR676 showed 40-42% knockdown. DY576 is a negative control.

MiRNA Target Identification and Functional Validation of Predicted Targets

To further test the binding capability of those miRNAs with the 3' UTR region of mouse myocilin, a dual reporter plasmid that contains the mouse myocilin 3' UTR region downstream of GLuc gene in plasmid pEZX-MT05 (Fig. 32) was cotransfected with miRNA mimics or negative control. The GLuc activities were measured as indications of binding efficacies of miRNAs with 3' UTR.

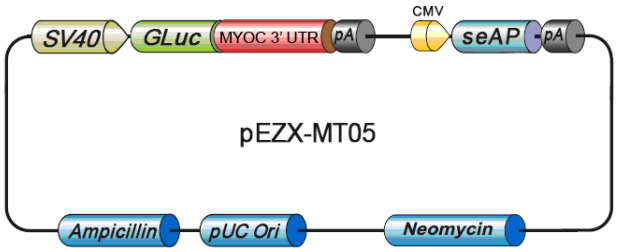

Figure 32. Schematic representation of MYOC 3' UTR reporter vector (modified from GeneCopoeia's plasmid map pEZX-MT05). This vector contains two expression cassettes: GLuc gene with mouse MYOC 3' UTR is driven by SV40 promoter and SEAP gene is driven by CMV promoter. Secreted Gaussia luciferase (GLuc) reporter gene expression is regulated by the downstream MYOC 3' UTR in mammalian cells. SEAP expression that is independent from GLuc expression is used as an internal control.

Besides using GLuc as the miRNA 3' UTR target reporter, a secreted alkaline phosphatase (SEAP) reporter driven by a CMV promoter, was also cloned into the same vector (pEZX-MT05) and served as the internal control.

Different concentrations of miRNA (25, 50, and 100 nM) were cotransfected with mouse MYOC 3' UTR reporter plasmid. The GLuc activity, after normalization with the SEAP activity showed that at 25 nM, only 30% knockdown was observed for all miRNAs tested. At 50 nM, 40-50% of knockdown was observed (miR19b: 50%, miR676: 39%, miR378: 43%, and miR320 40%). Surprisingly, 100 nM did not show efficiently knockdown as other two concentrations (Fig. 33). Higher concentration of synthetic ncRNA (such as siRNA or miRNA) may cause off-target effect or toxicity to the cells (Ishida and Selaru 2013). 100 nM miRNA caused more cell

death after transfection (data not shown) which may be the reason of lower knockdown in the reporter assay.

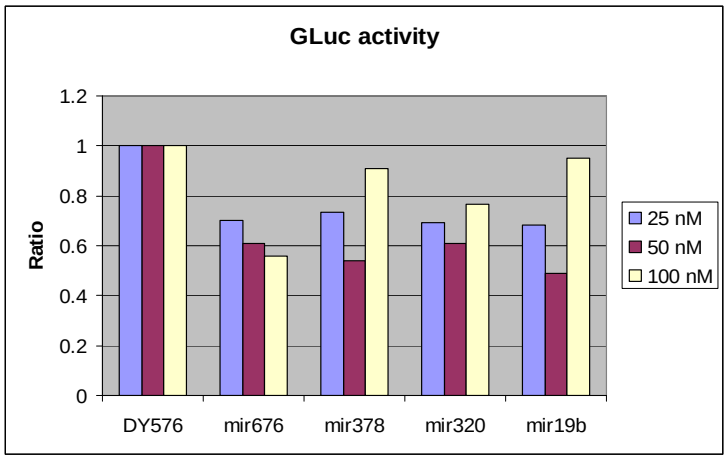

Figure 33. MiRNA target identification by 3' UTR reporter assay. All four miRNAs tested showed various degree of inhibition of GLuc activity after normalized with SEAP activity.

Discussion

MiRNAs are recognized as important regulators of gene expression that participate in numerous normal and pathological biological processes (Stefani and Slack 2008; Holley and Topkara 2011; Amiel, de Pontual et al. 2012). miRNAs have been shown to be involved in various aspects of animal development such as early embryonic development (Stern 2006), neuronal (Kosik 2006), muscle (Chen, Mandel et al. 2006; Yang, Lin et al. 2007), lymphocyte (Fatica, Rosa et al. 2006; Dahlberg and Lund 2007) and germline development (Cook and Blelloch 2013). MiRNAs are extremely conserved, and from early on, their homology has been used as a tool to identify orthologs and paralogs of cloned miRNAs in the genome of other species (Lagos-Quintana, Rauhut et al. 2001; Lau, Lim et al. 2001). Due to the abundance of the

miRNAs in the genome and their roles as key players during development, changes in miRNAs could lead to the congenital malformations (Amiel, de Pontual et al. 2012). Genetic deletions or mutation of miRNAs will generate diverse phenotypes such as increased expression of their target genes. Recent evidence has shown that overexpression, amplification, and deletion of miRNAs and miR-mediated modification of epigenetic silencing can impact oncogenesis (Ventura and Jacks 2009). MicroRNA mutations or mis-expression correlate with various human cancers, suggesting that miRNAs can function as tumour suppressors and oncogenes (Esquela-Kerscher and Slack 2006). More and more miRNAs have been found to associate with diseases. A manually curated, publicly available database, miR2Disease (http://www.mir2disease.org/), documents known relationships between miRNA dysregulation and human diseases (Jiang, Wang et al. 2009). Recently, researchers started to shed light on the regulation of miRNAs on the physiology of the outflow pathway in the eye and on the pathology of glaucoma (Luna, Li et al. 2012). There is however still no information so far about the miRNAs that regulate the expression of myocilin.

Our results showed that mmu-miR 676, one of most down-regulated miRNAs identified by miRNA array, and 3 other miRNAs: mmu-miR-19b, mmu-miR-320 and mmu-miR-378 predicted by computer algorithm all showed inhibition to mouse MYOC at the transcription level (Fig. 31) by RT-qPCR as well as at the protein level by reporter assay (Fig. 33).

Mammalian miRNAs bind with imperfect complementarities to their targets, resulting in a variable degree of miRNA-target mismatches. High complementarities between the seed region (7-nt "seed" sequence found at positions 2 through 8 of the mature miRNA) and the 3' UTR of mRNA decide the binding specificity and direct their posttranscriptional repression. However, these seed matches are not always sufficient for repression, indicating that other characteristics

also help specify targeting. Five other general features of site context that boost site efficacy include AU-rich nucleotide composition near the site, proximity to sites for coexpressed miRNAs (which leads to cooperative action), proximity to residues pairing to miRNA nucleotides 13-16, positioning within the 3'UTR at least 15 nt from the stop codon, and positioning away from the center of long UTRs. A model combining these context determinants quantitatively predicts site performance both for exogenously added miRNAs and for endogenous miRNA-message interactions (Grimson, Farh et al. 2007). From our analysis, mmu-miR-19b, mmu-miR-320 and mmu-miR-378 which have high complementarities of their seed regions with 3' UTR of mouse MYOC (Fig. 30) showed variable inhibition by RT-qPCR and reporter assay. Mmu-miR-676 which has high complementarities in the middle of the sequence with 3'UTR of mouse MYOC also showed inhibition to the expression of mouse MYOC. MicroRNAs that are partially complementary to a target can speed up deadenylation, causing mRNAs to be degraded sooner (Eulalio, Huntzinger et al. 2009). There may exist other miRNAs that can fulfill not only the seed complementarities but also other supplemental requirements and are more potent than the 4 miRNAs we tested. There might also be synergetic effect if we combine two or three miRNAs together.

Mmu-miR-19b is the most effective regulator for mouse MYOC among the 4 miRNAs tested. This miRNA is located in miR-17-92 clusters. The human version of miR-19b (hsa-miR-19b) has been shown to associate with hepatocellular carcinoma (HCC) (Connolly, Melegari et al. 2008), kidney cancer (Chow, Youssef et al. 2010), malignant lymphoma (Tagawa and Seto 2005), medulloblastoma (Northcott, Fernandez et al. 2009), multiple myeloma (MM) (Pichiorri, Suh et al. 2008), and prostate cancer (Porkka, Pfeiffer et al. 2007). Deletion of the miR-17~92 cluster caused skeletal and growth defects (de Pontual, Yao et al. 2011). MYOC might be another target

for this miRNA. Overall, combinatorial regulation is a feature of miRNA regulation. A given miRNA may have multiple different mRNA targets, and a given target might similarly be targeted by multiple miRNAs (Krek, Grun et al. 2005; Rajewsky 2006). Very likely, there is some other miRNAs that may also target on MYOC and the miRNAs that we have tested also have other targets except MYOC.

Identification of miRNAs that target myocilin not only provides fundamental information on how this gene is regulated but also may have clinical applications such as biomarker of glaucoma or a potential therapeutic modality for myocilin glaucoma because myocilin mutants are likely under similar miRNA regulations.

CONCLUSIONS:

New studies have been performed on myocilin, a glaucoma gene. The canonical Wnt signaling pathway was found to be involved in myocilin mediated phenotypes in human TM cells including loss of actin stress fibers and focal adhesions, elevated protein kinase A activity and downregulated RhoA activity. Wnt was also shown to be upstream of cAMP/PKA and RhoA signaling pathways. Blocking Wnt signaling pathway may have therapeutic potential for myocilin-related glaucoma disease.

Two experimental models have been established. The first is a 3 dimensional culture of human TM cells. Among the 3D platforms tested, QGel and Alvetex scaffold showed a more *in vivo* like pattern of gene expression and cell morphology. The Wnt results from 2D TM cultures were validated in Alvetex 3D system. The second model, Tet-on inducible wild-type or mutated (P370L or Q368X) myocilin expressing RGC5 cell lines were created. These cell lines were used to detect alterations in protein expression profile and reveal novel downstream pathways using cutting-edge quantitative proteomics. Bioinformatic analyses suggested that the biological processes associated with the altered proteins may include cytoskeleton reorganization, apoptosis and mitochondria dysfunction that are consistent with previous data. The analyses also revealed interesting new findings such as ABC transporter (multi drug resistant), microtubule, autophagy, and NF-κB signaling pathways. The inducible cell lines along with computational algorithms were also utilized to identify microRNAs (miRNAs) that regulate the expression of mouse myocilin gene. Four miRNAs, miR19b, miR676, miR320 and miR378, were found to be potential regulators.

FUTURE DIRECTIONS:

New information and understanding to myocilin have been obtained through the studies presented in this dissertation. There are nevertheless additional questions that need to be addressed in the future. For instance, upregulation of wild-type and mutated myocilins activate canonical Wnt signaling pathway in TM cells and leads to loss of actin stress fibers and focal adhesion and thus cell softness, does it show similar effects in vivo or in vitro perfusion organ culture? How about the long term effect caused by Wnt activation? Can we establish an aqueous humor resistant tissue (JCT-SC area) -mimic in vitro? How does the wild-type or mutated myocilin affect the health of retinal ganglion cells and their axon in the retina? What may be the other signaling pathways involved in myocilin phenotypes? Can we avert the myocilin phenotypes by inhibiting those signaling pathways? Stresses such as ER stress or oxidative stress have been shown to cause TM cells apoptosis, how to "de-sensitize" TM cells and prevent them from apoptosis? Which miRNAs can regulate the gene expression of **human** myocilin? Can we inhibit the expression of the mutated myocilin by introducing those human myocilin-targeting miRNA into the eye? Can we identify biomarkers (genetic, protein or metabolic) in myocilin glaucoma to facilitate the diagnostics or evaluate the efficacies of the treatment? Addressing these questions will provide further insights into the molecular mechanisms behind myocilin glaucoma and help develop novel therapeutic modalities.

CITED LITERATURE

Amiel, J., L. de Pontual, et al. (2012). "miRNA, development and disease." Adv Genet **80**: 1-36.

Aroca-Aguilar, J. D., F. Sanchez-Sanchez, et al. (2005). "Myocilin mutations causing glaucoma inhibit the intracellular endoproteolytic cleavage of myocilin between amino acids Arg226 and Ile227." J Biol Chem **280**(22): 21043-21051.

Aroca-Aguilar, J. D., F. Sanchez-Sanchez, et al. (2011). "Interaction of recombinant myocilin with the matricellular protein SPARC: functional implications." Invest Ophthalmol Vis Sci **52**(1): 179-189.

Bartel, D. P. (2004). "MicroRNAs: genomics, biogenesis, mechanism, and function." Cell **116**(2): 281-297.

Bill, A. (1975). "Editorial: The drainage of aqueous humor." Invest Ophthalmol **14**(1): 1-3.

Bokhari, M., R. J. Carnachan, et al. (2007). "Culture of HepG2 liver cells on three dimensional polystyrene scaffolds enhances cell structure and function during toxicological challenge." J Anat **211**(4): 567-576.

Bollinger, K. E., J. S. Crabb, et al. (2011). "Quantitative proteomics: TGFbeta(2) signaling in trabecular meshwork cells." Invest Ophthalmol and Vis Sci **52**(11): 8287-8294.

Borras, T. (2003). "Gene expression in the trabecular meshwork and the influence of intraocular pressure." Prog Retin Eye Res **22**(4): 435-463.

Borrás, T. (2008). "What is functional genomics teaching us about intraocular pressure regulation and glaucoma." The Eye's Aqueous Humor **Second Edition**.

Borras, T., W. Xue, et al. (2006). "Mechanisms of AAV transduction in glaucoma-associated human trabecular meshwork cells." J Gene Med **8**(5): 589-602.

Boylan, K. L., J. D. Andersen, et al. (2010). "Quantitative proteomic analysis by iTRAQ(R) for the identification of candidate biomarkers in ovarian cancer serum." Proteome Sci **8**: 31.

Braeuning, A. and A. Buchmann (2009). "The glycogen synthase kinase inhibitor 3-(2,4-dichlorophenyl)-4-(1-methyl-1H-indol-3-yl)-1H-pyrrole-2,5-dione (SB216763) is a partial agonist of the aryl hydrocarbon receptor." Drug Metab Dispos **37**(8): 1576-1580.

Burdon, K. P., S. Macgregor, et al. (2011). "Genome-wide association study identifies susceptibility loci for open angle glaucoma at TMCO1 and CDKN2B-AS1." Nat Genet **43**(6): 574-578.

Caballero, M. and T. Borras (2001). "Inefficient processing of an olfactomedin-deficient myocilin mutant: potential physiological relevance to glaucoma." Biochem Biophys Res Commun **282**(3): 662-670.

Caballero, M., L. L. Rowlette, et al. (2000). "Altered secretion of a TIGR/MYOC mutant lacking the olfactomedin domain." Biochem Biophys Acta **1502**(3): 447-460.

Cadigan, K. M. and M. Peifer (2009). "Wnt signaling from development to disease: insights from model systems." Cold Spring Harb Perspect Biol **1**(2): a002881.

Carbone, M. A., J. F. Ayroles, et al. (2009). "Overexpression of myocilin in the Drosophila eye activates the unfolded protein response: implications for glaucoma." PLoS One **4**(1): e4216.

Chen, A. E., D. D. Ginty, et al. (2005). "Protein kinase A signalling via CREB controls myogenesis induced by Wnt proteins." Nature **433**(7023): 317-322.

Chen, J., S. A. Runyan, et al. (2011). "Novel ocular antihypertensive compounds in clinical trials." Clin Ophthalmol **5**: 667-677.

Chen, J. F., E. M. Mandel, et al. (2006). "The role of microRNA-1 and microRNA-133 in skeletal muscle proliferation and differentiation." Nat Genet **38**(2): 228-233.

Chen, L. J., T. K. Ng, et al. (2012). "Evaluation of NTF4 as a causative gene for primary open-angle glaucoma." Mol Vis **18**: 1763-1772.

Choi, J., A. M. Miller, et al. (2005). "Soluble CD44 is cytotoxic to trabecular meshwork and retinal ganglion cells in vitro." Invest Ophthalmol Vis Sci **46**(1): 214-222.

Chow, T. F., Y. M. Youssef, et al. (2010). "Differential expression profiling of microRNAs and their potential involvement in renal cell carcinoma pathogenesis." Clin Biochem **43**(1-2): 150-158.

Clark, A. F., K. Kawase, et al. (2001). "Expression of the glaucoma gene myocilin (MYOC) in the human optic nerve head." FASEB J **15**(7): 1251-1253.

Clark, A. F., H. T. Steely, et al. (2001). "Glucocorticoid induction of the glaucoma gene MYOC in human and monkey trabecular meshwork cells and tissues." Invest Ophthalmol Vis Sci **42**(8): 1769-1780.

Comes, N., L. K. Buie, et al. (2011). "Evidence for a role of angiopoietin-like 7 (ANGPTL7) in extracellular matrix formation of the human trabecular meshwork: implications for glaucoma." Genes Cells **16**(2): 243-259.

Connolly, E., M. Melegari, et al. (2008). "Elevated expression of the miR-17-92 polycistron and miR-21 in hepadnavirus-associated hepatocellular carcinoma contributes to the malignant phenotype." Am J Pathol **173**(3): 856-864.

Cook, M. S. and R. Blelloch (2013). "Small RNAs in germline development." Curr Top Dev Biol **102**: 159-205.

Cox, J. and M. Mann (2011). "Quantitative, high-resolution proteomics for data-driven systems biology." Annu Rev Biochem **80**: 273-299.

Dahlberg, J. E. and E. Lund (2007). "Micromanagement during the innate immune response." Sci STKE **2007**(387): pe25.

de Iongh, R. U., H. E. Abud, et al. (2006). "WNT/Frizzled signaling in eye development and disease." Front in Biosci **11**: 2442-2464.

de Pontual, L., E. Yao, et al. (2011). "Germline deletion of the miR-17 approximately 92 cluster causes skeletal and growth defects in humans." Nat Genet **43**(10): 1026-1030.

Dejana, E. (2010). "The role of wnt signaling in physiological and pathological angiogenesis." Circ Res **107**(8): 943-952.

Esquela-Kerscher, A. and F. J. Slack (2006). "Oncomirs - microRNAs with a role in cancer." Nat Rev Cancer **6**(4): 259-269.

Eulalio, A., E. Huntzinger, et al. (2009). "Deadenylation is a widespread effect of miRNA regulation." RNA **15**(1): 21-32.

Ezzat, M. K., K. G. Howell, et al. (2008). "Characterization of monoclonal antibodies against the glaucoma-associated protein myocilin." Exp Eye Res **87**(4): 376-384.

Fan, B. J. and J. L. Wiggs (2010). "Glaucoma: genes, phenotypes, and new directions for therapy." J Clin Invest **120**(9): 3064-3072.

Fang, X., S. X. Yu, et al. (2000). "Phosphorylation and inactivation of glycogen synthase kinase 3 by protein kinase A." Proc Natl Acad Sci U S A **97**(22): 11960-11965.

Fatica, A., A. Rosa, et al. (2006). "MicroRNAs and hematopoietic differentiation." Cold Spring Harb Symp Quant Biol **71**: 205-210.

Fautsch, M. P., K. G. Howell, et al. (2005). "Primary trabecular meshwork cells incubated in human aqueous humor differ from cells incubated in serum supplements." Invest Ophthalmol Vis Sci **46**(8): 2848-2856.

Fautsch, M. P., A. M. Vrabel, et al. (2006). "The identification of myocilin-associated proteins in the human trabecular meshwork." Exp Eye Res **82**(6): 1046-1052.

Filiou, M. D., D. Martins-de-Souza, et al. (2012). "To label or not to label: applications of quantitative proteomics in neuroscience research." Proteomics **12**(4-5): 736-747.

Filla, M. S., X. Liu, et al. (2002). "In vitro localization of TIGR/MYOC in trabecular meshwork extracellular matrix and binding to fibronectin." Invest Ophthalmol Vis Sci **43**(1): 151-161.

Fingert, J. H. (2011). "Primary open-angle glaucoma genes." Eye (Lond) **25**(5): 587-595.

Fingert, J. H., E. M. Stone, et al. (2002). "Myocilin glaucoma." Surv Ophthalmol **47**(6): 547-561.

Fingert, J. H., L. Ying, et al. (1998). "Characterization and comparison of the human and mouse GLC1A glaucoma genes." Genome Res **8**(4): 377-384.

Frassetto, L. J., C. R. Schlieve, et al. (2006). "Kinase-dependent differentiation of a retinal ganglion cell precursor." Invest Ophthalmol Vis Sci **47**(1): 427-438.

Gardiner, P. A. (1978). "ABC of ophthalmology. Glaucoma." Br Med J **2**(6153): 1689-1692.

Gasiorowski, J. Z. and P. Russell (2009). "Biological properties of trabecular meshwork cells." Exp Eye Res **88**(4): 671-675.

Gimelbrant, A. A., A. W. Ensminger, et al. (2005). "Monoallelic expression and asynchronous replication of p120 catenin in mouse and human cells." J Biol Chem **280**(2): 1354-1359.

Gobeil, S., L. Letartre, et al. (2006). "Functional analysis of the glaucoma-causing TIGR/myocilin protein: integrity of amino-terminal coiled-coil regions and olfactomedin homology domain is essential for extracellular adhesion and secretion." Exp Eye Res **82**(6): 1017-1029.

Goldwich, A., M. Scholz, et al. (2009). "Myocilin promotes substrate adhesion, spreading and formation of focal contacts in podocytes and mesangial cells." Histochem Cell Biol **131**(2): 167-180.

Gong, G., O. Kosoko-Lasaki, et al. (2004). "Genetic dissection of myocilin glaucoma." Hum Mol Genet **13 Spec No 1**: R91-102.

Gonzalez, P., D. L. Epstein, et al. (2000). "Characterization of gene expression in human trabecular meshwork using single-pass sequencing of 1060 clones." Invest Ophthalmol Vis Sci **41**(12): 3678-3693.

Gottfredsdottir, M. S., T. Sverrisson, et al. (1999). "Chronic open-angle glaucoma and associated ophthalmic findings in monozygotic twins and their spouses in Iceland." J Glaucoma **8**(2): 134-139.

Gould, D. B., L. Miceli-Libby, et al. (2004). "Genetically increasing Myoc expression supports a necessary pathologic role of abnormal proteins in glaucoma." Mol Cell Biol **24**(20): 9019-9025.

Grierson I, H. P. (1995). "The proliferative and migratory activities of trabecular meshwork cells." Prog Retin Eye Res **15**: 33-67.

Griffith, L. G. and M. A. Swartz (2006). "Capturing complex 3D tissue physiology in vitro." Nat Rev Mol Cell Biol **7**(3): 211-224.

Grimson, A., K. K. Farh, et al. (2007). "MicroRNA targeting specificity in mammals: determinants beyond seed pairing." Mol Cell **27**(1): 91-105.

Harvey, R. and S. K. Chintala (2007). "Inhibition of plasminogen activators attenuates the death of differentiated retinal ganglion cells and stabilizes their neurite network in vitro." Invest Ophthalmol Vis Sci **48**(4): 1884-1891.

Hayman, M. W., K. H. Smith, et al. (2004). "Enhanced neurite outgrowth by human neurons grown on solid three-dimensional scaffolds." Biochem Biophys Res Commun **314**(2): 483-488.

He, Y., K. W. Leung, et al. (2009). "Pro370Leu mutant myocilin impairs mitochondrial functions in human trabecular meshwork cells." Mol Vis **15**: 815-825.

Holley, C. L. and V. K. Topkara (2011). "An introduction to small non-coding RNAs: miRNA and snoRNA." Cardiovasc Drugs Ther **25**(2): 151-159.

Honjo, M., H. Tanihara, et al. (2001). "Effects of rho-associated protein kinase inhibitor Y-27632 on intraocular pressure and outflow facility." Invest Ophthalmol Vis Sci **42**(1): 137-144.

Irizarry, R. A., B. Hobbs, et al. (2003). "Exploration, normalization, and summaries of high density oligonucleotide array probe level data." Biostatistics **4**(2): 249-264.

Ishida, M. and F. M. Selaru (2013). "miRNA-Based Therapeutic Strategies." Curr Anesthesiol Rep **1**(1): 63-70.

Jacobson, N., M. Andrews, et al. (2001). "Non-secretion of mutant proteins of the glaucoma gene myocilin in cultured trabecular meshwork cells and in aqueous humor." Hum Mol Genet **10**(2): 117-125.

Jampel, H. D. (2011). "Glaucoma surgery: as easy as ABC?" Ophthalmology **118**(3): 433-434.

Jiang, Q., Y. Wang, et al. (2009). "miR2Disease: a manually curated database for microRNA deregulation in human disease." Nucleic Acids Res **37**(Database issue): D98-104.

Jin, T., I. George Fantus, et al. (2008). "Wnt and beyond Wnt: multiple mechanisms control the transcriptional property of beta-catenin." Cell Signal **20**(10): 1697-1704.

Joe, M. K., S. Sohn, et al. (2005). "Identification of flotillin-1 as a protein interacting with myocilin: implications for the pathogenesis of primary open-angle glaucoma." Biochem Biophys Res Commun **336**(4): 1201-1206.

Joe, M. K., S. Sohn, et al. (2003). "Accumulation of mutant myocilins in ER leads to ER stress and potential cytotoxicity in human trabecular meshwork cells." Biochem Biophys Res Commun **312**(3): 592-600.

Joe, M. K. and S. I. Tomarev (2010). "Expression of myocilin mutants sensitizes cells to oxidative stress-induced apoptosis: implication for glaucoma pathogenesis." Am J Pathol **176**(6): 2880-2890.

Jurynec, M. J., C. P. Riley, et al. (2003). "TIGR is upregulated in the chronic glial scar in response to central nervous system injury and inhibits neurite outgrowth." Mol Cell Neurosci **23**(1): 69-80.

Kang, J. H., W. C. Willett, et al. (2007). "Prospective study of alcohol consumption and the risk of primary open-angle glaucoma." Ophthalmic Epidemiol **14**(3): 141-147.

Karali, A., P. Russell, et al. (2000). "Localization of myocilin/trabecular meshwork--inducible glucocorticoid response protein in the human eye." Invest Ophthalmol Vis Sci **41**(3): 729-740.

Keller, A., A. I. Nesvizhskii, et al. (2002). "Empirical statistical model to estimate the accuracy of peptide identifications made by MS/MS and database search." Anal Chem **74**(20): 5383-5392.

Keller, K. E., M. Aga, et al. (2009). "Extracellular matrix turnover and outflow resistance." Exp Eye Res **88**(4): 676-682.

Kikuchi, A., H. Yamamoto, et al. (2011). "New insights into the mechanism of Wnt signaling pathway activation." Int Rev Cell Mol Biol **291**: 21-71.

Kim, B. S., O. V. Savinova, et al. (2001). "Targeted Disruption of the Myocilin Gene (Myoc) Suggests that Human Glaucoma-Causing Mutations Are Gain of Function." Mol Cell Biol **21**(22): 7707-7713.

Kim, J. B. (2005). "Three-dimensional tissue culture models in cancer biology." Semin Cancer Biol **15**(5): 365-377.

Koga, T., X. Shen, et al. (2010). "Differential effects of myocilin and optineurin, two glaucoma genes, on neurite outgrowth." Am J Pathol **176**(1): 343-352.

Kopczynski, C., G. D. Novack, et al. (2013). "Ocular hypotensive efficacy, safety and systemic absorption of AR-12286 ophthalmic solution in normal volunteers." Br J Ophthalmol **97**(5): 567-572.

Kosik, K. S. (2006). "The neuronal microRNA system." Nat Rev Neurosci **7**(12): 911-920.

Krek, A., D. Grun, et al. (2005). "Combinatorial microRNA target predictions." Nat Genet **37**(5): 495-500.

Krishnamoorthy, R. R., P. Agarwal, et al. (2001). "Characterization of a transformed rat retinal ganglion cell line." Brain Res Mol Brain Res **86**(1-2): 1-12.

Kuhl, M., L. C. Sheldahl, et al. (2000). "The Wnt/Ca2+ pathway: a new vertebrate Wnt signaling pathway takes shape." Trends Genet **16**(7): 279-283.

Kuroda, T., S. D. Rabkin, et al. (2006). "Effective treatment of tumors with strong beta-catenin/T-cell factor activity by transcriptionally targeted oncolytic herpes simplex virus vector." Cancer Res **66**(20): 10127-10135.

Kwak, M. K. and T. W. Kensler (2006). "Induction of 26S proteasome subunit PSMB5 by the bifunctional inducer 3-methylcholanthrene through the Nrf2-ARE, but not the AhR/Arnt-XRE, pathway." Biochem Biophys Res Commun **345**(4): 1350-1357.

Kwon, H. S., H. S. Lee, et al. (2009). "Myocilin is a modulator of Wnt signaling." Mol Cell Biol **29**(8): 2139-2154.

Kwon, Y. H., J. H. Fingert, et al. (2009). "Primary open-angle glaucoma." N Engl J Med **360**(11): 1113-1124.

Lagos-Quintana, M., R. Rauhut, et al. (2001). "Identification of novel genes coding for small expressed RNAs." Science **294**(5543): 853-858.

Last, J. A., T. Pan, et al. (2011). "Elastic modulus determination of normal and glaucomatous human trabecular meshwork." Invest Ophthalmol Vis Sci **52**(5): 2147-2152.

Lau, N. C., L. P. Lim, et al. (2001). "An abundant class of tiny RNAs with probable regulatory roles in Caenorhabditis elegans." Science **294**(5543): 858-862.

Lee, J. G. and E. P. Kay (2009). "Common and distinct pathways for cellular activities in FGF-2 signaling induced by IL-1beta in corneal endothelial cells." Invest Ophthalmol Vis Sci **50**(5): 2067-2076.

Lee, Y., J. Han, et al. (2006). "Drosha in primary microRNA processing." Cold Spring Harb Symp Quant Biol **71**: 51-57.

Li, Y., J. D. Aroca-Aguilar, et al. (2006). "Interaction of myocilin with the C-terminal region of hevin." Biochem Biophys Res Commun **339**(3): 797-804.

Liton, P. B., C. Luna, et al. (2006). "Genome-wide expression profile of human trabecular meshwork cultured cells, nonglaucomatous and primary open angle glaucoma tissue." Mol Vis **12**: 774-790.

Liu, X., Y. Hu, et al. (2005). "The effect of C3 transgene expression on actin and cellular adhesions in cultured human trabecular meshwork cells and on outflow facility in organ cultured monkey eyes." Mol Vis **11**: 1112-1121.

Liu, Y., D. Munro, et al. (2011) "Serial analysis of gene expression (SAGE) in normal human trabecular meshwork." Mol Vis **17**: 885-893.

Liu, Y. and D. Vollrath (2004). "Reversal of mutant myocilin non-secretion and cell killing: implications for glaucoma." Hum Mol Genet **13**(11): 1193-1204.

Logan, C. Y. and R. Nusse (2004). "The Wnt signaling pathway in development and disease." Annu Rev Cell Dev Biol **20**: 781-810.

Luna, C., G. Li, et al. (2012). "Regulation of trabecular meshwork cell contraction and intraocular pressure by miR-200c." PLoS One **7**(12): e51688.

Luo, G., P. Ducy, et al. (1997). "Spontaneous calcification of arteries and cartilage in mice lacking matrix GLA protein." Nature **386**(6620): 78-81.

Luo, J., J. Chen, et al. (2007). "Wnt signaling and human diseases: what are the therapeutic implications?" Lab Invest **87**(2): 97-103.

Maaike Schutte, B. F., Marc-Olivier Baradez, Alison Devonshire, Jesus Minguez, Maria Bokhari, Stefan Przyborski, and Damian Marshall. (October 2011). "Rat Primary Hepatocytes Show Enhanced Performance and Sensitivity to Acetaminophen During Three-Dimensional Culture on a Polystyrene Scaffold Designed for Routine Use " Assay Drug Dev Technol **9**(5).

Mao, W., T. Tovar-Vidales, et al. (2011). "Perfusion-cultured bovine anterior segments as an ex vivo model for studying glucocorticoid-induced ocular hypertension and glaucoma." Invest Ophthalmol Vis Sci **52**(11): 8068-8075.

Matsuda, Y., Y. Kawamoto, et al. (1253). "Morphological and cytoskeletal alterations of nervous system tumor cells with different culturing methods." Int J Oncol **38**(5): 1253-1258.

McKee, C. T., J. A. Wood, et al. (2011). "The effect of biophysical attributes of the ocular trabecular meshwork associated with glaucoma on the cell response to therapeutic agents." Biomaterials **32**(9): 2417-2423.

Meguro, A., H. Inoko, et al. (2010). "Genome-wide association study of normal tension glaucoma: common variants in SRBD1 and ELOVL5 contribute to disease susceptibility." Ophthalmology **117**(7): 1331-1338 e1335.

Mii, Y. and M. Taira (2011). "Secreted Wnt "inhibitors" are not just inhibitors: regulation of extracellular Wnt by secreted Frizzled-related proteins." Dev Growth Differ **53**(8): 911-923.

Monemi, S., G. Spaeth, et al. (2005). "Identification of a novel adult-onset primary open-angle glaucoma (POAG) gene on 5q22.1." Hum Mol Genet **14**(6): 725-733.

Moon, R. T., A. D. Kohn, et al. (2004). "WNT and beta-catenin signalling: diseases and therapies." Nat Rev Genet **5**(9): 691-701.

Munday, D. C., R. Surtees, et al. (2012). "Using SILAC and quantitative proteomics to investigate the interactions between viral and host proteomes." Proteomics **12**(4-5): 666-672.

Neofytou, E. A., E. Chang, et al. (2011). "Adipose tissue-derived stem cells display a proangiogenic phenotype on 3D scaffolds." J Biomed Mater Res A **98**(3): 383-393.

Nesvizhskii, A. I., A. Keller, et al. (2003). "A statistical model for identifying proteins by tandem mass spectrometry." Anal Chem **75**(17): 4646-4658.

Nguyen, T. D., P. Chen, et al. (1998). "Gene structure and properties of TIGR, an olfactomedin-related glycoprotein cloned from glucocorticoid-induced trabecular meshwork cells." J Biol Chem **273**(11): 6341-6350.

Northcott, P. A., L. A. Fernandez, et al. (2009). "The miR-17/92 polycistron is up-regulated in sonic hedgehog-driven medulloblastomas and induced by N-myc in sonic hedgehog-treated cerebellar neural precursors." Cancer Res **69**(8): 3249-3255.

Osada, T., M. Chen, et al. (2011). "Antihelminth compound niclosamide downregulates Wnt signaling and elicits antitumor responses in tumors with activating APC mutations." Cancer Res **71**(12): 4172-4182.

Pagan, J., T. Seto, et al. (2013). "Role of the ubiquitin proteasome system in the heart." Circ Res **112**(7): 1046-1058.

Park, B. C., M. Tibudan, et al. (2007). "Interaction between two glaucoma genes, optineurin and myocilin." Genes Cells **12**(8): 969-979.

Pasutto, F., T. Matsumoto, et al. (2009). "Heterozygous NTF4 mutations impairing neurotrophin-4 signaling in patients with primary open-angle glaucoma." Am J Hum Genet **85**(4): 447-456.

Payen, L., M. Gao, et al. (2005). "Functional interactions between nucleotide binding domains and leukotriene C4 binding sites of multidrug resistance protein 1 (ABCC1)." Mol Pharmacol **67**(6): 1944-1953.

Peters, D. M., K. Herbert, et al. (2005). "Myocilin binding to Hep II domain of fibronectin inhibits cell spreading and incorporation of paxillin into focal adhesions." Exp Cell Res **303**(2): 218-228.

Pichiorri, F., S. S. Suh, et al. (2008). "MicroRNAs regulate critical genes associated with multiple myeloma pathogenesis." Proc Natl Acad Sci U S A **105**(35): 12885-12890.

Polansky, J. R., D. J. Fauss, et al. (1997). "Cellular pharmacology and molecular biology of the trabecular meshwork inducible glucocorticoid response gene product." Ophthalmologica **211**(3): 126-139.

Polansky, J. R., R. M. Kurtz, et al. (1989). "Eicosanoid production and glucocorticoid regulatory mechanisms in cultured human trabecular meshwork cells." Prog Clin Biol Res **312**: 113-138.

Polansky, J. R., R. N. Weinreb, et al. (1979). "Human trabecular cells. I. Establishment in tissue culture and growth characteristics." Invest Ophthalmol Vis Sci **18**(10): 1043-1049.

Porkka, K. P., M. J. Pfeiffer, et al. (2007). "MicroRNA expression profiling in prostate cancer." Cancer Res **67**(13): 6130-6135.

Qi, P. X., E. D. Wickham, et al. (2004). "Thermal and alkaline denaturation of bovine beta-casein." Protein J **23**(6): 389-402.

Quigley, H. A. (2011). "Glaucoma." Lancet **377**(9774): 1367-1377.

Quigley, H. A. and A. T. Broman (2006). "The number of people with glaucoma worldwide in 2010 and 2020." Br J Ophthalmol **90**(3): 262-267.

Rajewsky, N. (2006). "microRNA target predictions in animals." Nat Genet **38 Suppl**: S8-13.

Rao, P. V., R. R. Allingham, et al. (2000). "TIGR/myocilin in human aqueous humor." Exp Eye Res **71**(6): 637-641.

Rao, T. P. and M. Kuhl (2010). "An updated overview on Wnt signaling pathways: a prelude for more." Circ Res **106**(12): 1798-1806.

Rezaie, T., A. Child, et al. (2002). "Adult-onset primary open-angle glaucoma caused by mutations in optineurin." Science **295**(5557): 1077-1079.

Russell, P., J. Z. Gasiorowski, et al. (2008). "Response of human trabecular meshwork cells to topographic cues on the nanoscale level." Invest Ophthalmol Vis Sci **49**(2): 629-635.

Sacharidou, A., A. N. Stratman, et al. (2012). "Molecular mechanisms controlling vascular lumen formation in three-dimensional extracellular matrices." Cells Tissues Organs **195**(1-2): 122-143.

Sakai, H., B. C. Park, et al. (2006). "Transduction of TAT fusion proteins into the human and bovine trabecular meshwork." Invest Ophthalmol Vis Sci **47**(10): 4427-4434.

Sakai, H., X. Shen, et al. (2007). "Mitochondrial association of myocilin, product of a glaucoma gene, in human trabecular meshwork cells." J Cell Physiol **213**(3): 775-784.

Sanchez-Sanchez, F., F. Martinez-Redondo, et al. (2007). "Characterization of the intracellular proteolytic cleavage of myocilin and identification of calpain II as a myocilin-processing protease." J Biol Chem **282**(38): 27810-27824.

Sarfarazi, M., A. Child, et al. (1998). "Localization of the fourth locus (GLC1E) for adult-onset primary open-angle glaucoma to the 10p15-p14 region." Am J Hum Genet **62**(3): 641-652.

Schwechter, B. R., L. E. Millet, et al. (2007). "Histone deacetylase inhibition-mediated differentiation of RGC-5 cells and interaction with survival." Invest Ophthalmol Vis Sci **48**(6): 2845-2857.

Senatorov, V., I. Malyukova, et al. (2006). "Expression of mutated mouse myocilin induces open-angle glaucoma in transgenic mice." J Neurosci **26**(46): 11903-11914.

Shadforth, I. P., T. P. Dunkley, et al. (2005). "i-Tracker: for quantitative proteomics using iTRAQ." BMC Genomics **6**: 145.

Shen, X., T. Koga, et al. (2008). "Rho GTPase and cAMP/protein kinase A signaling mediates myocilin-induced alterations in cultured human trabecular meshwork cells." J Biol Chem **283**(1): 603-612.

Shepard, A. R., N. Jacobson, et al. (2003). "Characterization of rabbit myocilin: Implications for human myocilin glycosylation and signal peptide usage." BMC Genet **4**: 5.

Sivils, J. C., I. Gonzalez, et al. (2010). "Mice lacking Mrp1 have reduced testicular steroid hormone levels and alterations in steroid biosynthetic enzymes." Gen Comp Endocrinol **167**(1): 51-59.

Sohn, S., W. Hur, et al. (2002). "Expression of wild-type and truncated myocilins in trabecular meshwork cells: their subcellular localizations and cytotoxicities." Invest Ophthalmol Vis Sci **43**(12): 3680-3685.

Stamer, W. D. and T. S. Acott (2012). "Current understanding of conventional outflow dysfunction in glaucoma." Curr Opin Ophthalmol **23**(2): 135-143.

Stamer, W. D., K. Peppel, et al. (2001). "Expression of aquaporin-1 in human trabecular meshwork cells: role in resting cell volume." Invest Ophthalmol Vis Sci **42**(8): 1803-1811.

Stefani, G. and F. J. Slack (2008). "Small non-coding RNAs in animal development." Nat Rev Mol Cell Biol **9**(3): 219-230.

Stern, C. D. (2006). "Evolution of the mechanisms that establish the embryonic axes." Curr Opin Genet Dev **16**(4): 413-418.

Stone, E. M., J. H. Fingert, et al. (1997). "Identification of a gene that causes primary open angle glaucoma." Science **275**(5300): 668-670.

Stumpff, F. and M. Wiederholt (2000). "Regulation of trabecular meshwork contractility." Ophthalmologica **214**(1): 33-53.

Swiderski, R. E., J. L. Ross, et al. (2000). "Localization of MYOC transcripts in human eye and optic nerve by in situ hybridization." Invest Ophthalmol Vis Sci **41**(11): 3420-3428.

Tagawa, H. and M. Seto (2005). "A microRNA cluster as a target of genomic amplification in malignant lymphoma." Leukemia **19**(11): 2013-2016.

Takahashi, H., S. Noda, et al. (1998). "Mouse myocilin (Myoc) gene expression in ocular tissues." Biochem Biophys Res Commun **248**(1): 104-109.

Tamm, E. R. (2002). "Myocilin and glaucoma: facts and ideas." Prog Retin Eye Res **21**(4): 395-428.

Taurin, S., N. Sandbo, et al. (2006). "Phosphorylation of beta-catenin by cyclic AMP-dependent protein kinase." J Biol Chem **281**(15): 9971-9976.

Teikari, J. M. (1990). "Genetic influences in open-angle glaucoma." Int Ophthalmol Clin **30**(3): 161-168.

Teruel, R., J. Corral, et al. (2011). "Potential role of miRNAs in developmental haemostasis." PLoS One **6**(3): e17648.

Thorleifsson, G., G. B. Walters, et al. (2010). "Common variants near CAV1 and CAV2 are associated with primary open-angle glaucoma." Nat Genet **42**(10): 906-909.

Tian, B., B. T. Gabelt, et al. (2009). "The role of the actomyosin system in regulating trabecular fluid outflow." Exp Eye Res **88**(4): 713-717.

Tibbitt, M. W. and K. S. Anseth (2009). "Hydrogels as extracellular matrix mimics for 3D cell culture." Biotechnol Bioeng **103**(4): 655-663.

Tielsch, J. M., J. Katz, et al. (1994). "Family history and risk of primary open angle glaucoma. The Baltimore Eye Survey." Arch Ophthalmol **112**(1): 69-73.

Tomarev, S. I., E. R. Tamm, et al. (1998). "Characterization of the mouse Myoc/Tigr gene." Biochem Biophys Res Commun **245**(3): 887-893.

Tomarev, S. I., G. Wistow, et al. (2003). "Gene expression profile of the human trabecular meshwork: NEIBank sequence tag analysis." Invest Ophthalmol Vis Sci **44**(6): 2588-2596.

Torrado, M., R. Trivedi, et al. (2002). "Optimedin: a novel olfactomedin-related protein that interacts with myocilin." Hum Mol Genet **11**(11): 1291-1301.

Ueda, J., K. Wentz-Hunter, et al. (2002). "Distribution of myocilin and extracellular matrix components in the juxtacanalicular tissue of human eyes." Invest Ophthalmol Vis Sci **43**(4): 1068-1076.

Van Bergen, N. J., J. P. Wood, et al. (2009). "Re-characterization of the RGC-5 retinal ganglion cell line." Invest Ophthalmol Vis Sci. 50(9):4267-72.

Veeman, M. T., J. D. Axelrod, et al. (2003). "A second canon. Functions and mechanisms of beta-catenin-independent Wnt signaling." Dev Cell **5**(3): 367-377.

Ventura, A. and T. Jacks (2009). "MicroRNAs and cancer: short RNAs go a long way." Cell **136**(4): 586-591.

Vithana, E. N., M. E. Nongpiur, et al. (2010). "Identification of a novel mutation in the NTF4 gene that causes primary open-angle glaucoma in a Chinese population." Mol Vis **16**: 1640-1645.

Vittal, V., A. Rose, et al. (2005). "Changes in gene expression by trabecular meshwork cells in response to mechanical stretching." Invest Ophthalmol Vis Sci **46**(8): 2857-2868.

Vittitow, J. and T. Borras (2004). "Genes expressed in the human trabecular meshwork during pressure-induced homeostatic response." J Cell Physiol **201**(1): 126-137.

Vittitow, J. L., R. Garg, et al. (2002). "Gene transfer of dominant-negative RhoA increases outflow facility in perfused human anterior segment cultures." Mol Vis **8**: 32-44.

Wang, W., H. Liu, et al. (2011). "A diterpenoid derivative 15-oxospiramilactone inhibits Wnt/beta-catenin signaling and colon cancer cell tumorigenesis." Cell Res **21**(5): 730-740.

Wang, W. H., L. G. McNatt, et al. (2008). "Increased expression of the WNT antagonist sFRP-1 in glaucoma elevates intraocular pressure." J Clin Invest **118**(3): 1056-1064.

Wang, X., J. Harmon, et al. (2010). "Using the Utah Population Database to assess familial risk of primary open angle glaucoma." Vision Res **50**(23): 2391-2395.

Wentz-Hunter, K., X. Shen, et al. (2004). "Overexpression of myocilin in cultured human trabecular meshwork cells." Exp Cell Res **297**(1): 39-48.

Wiggs, J. L. (2007). "Genetic etiologies of glaucoma." Arch Ophthalmol **125**(1): 30-37.

Wiggs, J. L. (2012). "The cell and molecular biology of complex forms of glaucoma: updates on genetic, environmental, and epigenetic risk factors." Invest Ophthalmol Vis Sci **53**(5): 2467-2469.

Wiggs, J. L., J. H. Kang, et al. (2011). "Common variants near CAV1 and CAV2 are associated with primary open-angle glaucoma in Caucasians from the USA." Hum Mol Genet **20**(23): 4707-4713.

Wood, J. A., C. T. McKee, et al. (2011). "Substratum Compliance Regulates Human Trabecular Meshwork Cell Behaviors and Response to Latrunculin B." Invest Ophthalmol Vis Sci 52(13):9298-303.

Xu, S. (2009). "microRNA expression in the eyes and their significance in relation to functions." Prog Retin Eye Res **28**(2): 87-116.

Xue, W., R. Wallin, et al. (2006). "Matrix GLA protein function in human trabecular meshwork cells: inhibition of BMP2-induced calcification process." Invest Ophthalmol Vis Sci **47**(3): 997-1007.

Yagami, K., J. Y. Suh, et al. (1999). "Matrix GLA protein is a developmental regulator of chondrocyte mineralization and, when constitutively expressed, blocks endochondral and intramembranous ossification in the limb." J Cell Biol **147**(5): 1097-1108.

Yam, G. H., K. Gaplovska-Kysela, et al. (2007). "Aggregated myocilin induces russell bodies and causes apoptosis: implications for the pathogenesis of myocilin-caused primary open-angle glaucoma." Am J Pathol **170**(1): 100-109.

Yang, B., D. J. Cao, et al. (2004). "Different roles of ERK and p38 MAP kinases during tube formation from endothelial cells cultured in 3-dimensional collagen matrices." J Cell Physiol **200**(3): 360-369.

Yang, B., H. Lin, et al. (2007). "The muscle-specific microRNA miR-1 regulates cardiac arrhythmogenic potential by targeting GJA1 and KCNJ2." Nat Med **13**(4): 486-491.

Yang, C., J. Lafleur, et al. (2009). "The role of lysophosphatidic acid receptor (LPA1) in the oxygen-induced retinal ganglion cell degeneration." Invest Ophthalmol Vis Sci **50**(3): 1290-1298.

Yang, Z. Q., G. Liu, et al. (2009). "Methylation-associated silencing of SFRP1 with an 8p11-12 amplification inhibits canonical and non-canonical WNT pathways in breast cancers." Int J Cancer **125**(7): 1613-1621.

Yeghiazaryan, K., J. Flammer, et al. (2005). "An enhanced expression of ABC 1 transporter in circulating leukocytes as a potential molecular marker for the diagnostics of glaucoma." Amino Acids **28**(2): 207-211.

Ying, H., X. Shen, et al. (2010). "Posttranslational modifications, localization, and protein interactions of optineurin, the product of a glaucoma gene." PLoS One **5**(2): e9168.

Yue, B. (2007). "Cellular mechanisms in the trabecular meshwork affecting aqueous humoroutflow pathway." Principles and Practice of Ophthalmology (book) **3rd edition**(Chapter 192).

Yue, B. Y. (1996). "The extracellular matrix and its modulation in the trabecular meshwork." Surv Ophthalmol **40**(5): 379-390.

Zhang, M., R. Maddala, et al. (2008). "Novel molecular insights into RhoA GTPase-induced resistance to aqueous humor outflow through the trabecular meshwork." Am J Physiol Cell Physiol **295**(5): C1057-1070.

Zhao, X., K. E. Ramsey, et al. (2004). "Gene and protein expression changes in human trabecular meshwork cells treated with transforming growth factor-beta." Invest Ophthalmol Vis Sci **45**(11): 4023-4034.

Zhou, L., T. Fukuchi, et al. (1995). "Loss of cell-matrix cohesiveness after phagocytosis by trabecular meshwork cells." Invest Ophthalmol Vis Sci **36**(5): 787-795.

Zhou, L., S. R. Zhang, et al. (1996). "Adhesion of human trabecular meshwork cells to extracellular matrix proteins. Roles and distribution of integrin receptors." Invest Ophthalmol Vis Sci **37**(1): 104-113.

Zhou, Y., O. Grinchuk, et al. (2008). "Transgenic mice expressing the Tyr437His mutant of human myocilin protein develop glaucoma." Invest Ophthalmol Vis Sci **49**(5): 1932-1939.

Zhou, Z. and D. Vollrath (1999). "A cellular assay distinguishes normal and mutant TIGR/myocilin protein." Hum Mol Genet **8**(12): 2221-2228.

Zode, G. S., M. H. Kuehn, et al. (2011). "Reduction of ER stress via a chemical chaperone prevents disease phenotypes in a mouse model of primary open angle glaucoma." J Clin Invest **121**(9): 3542-3553.

VITA

HONGYU YING

EDUCATION

PhD candidate in Bioengineering, Dept. of Bioengineering, Univ. of Illinois at Chicago, Chicago, IL, USA (2011-present)

MEng in Bioinformatics, Department of Bioengineering, Univ. of Illinois at Chicago, Chicago, IL, USA (2009-2011)

MS in Immunology, Department of Immunology/Microbiology, Rush University, Chicago, IL, USA (1999-2002)

BS in Biology, Department of Biology, Zhejiang University, Hangzhou, Zhejiang, P.R.China (1987-1991)

PROFESSIONAL EXPERIENCE:

September 2006- present: **Senior research technologist.** Cellular and Molecular Biology Core Module, Dept. of Ophthalmology, Univ. of Illinois at Chicago.

March 2002-August 2006: **Senior research technologist II**, Department of Neurobiology, Pharmacology & Physiology, The University of Chicago.

AWARDS AND GRANTS

2012 The Association for Research in Vision and Ophthalmology (ARVO) travel grant ($750). Poster titled: **Alterations in the Barrier Function and Cell Migration Induced by Expression of Wild Type and Mutated Myocilinin stable RGC5 Cell Lines.**

2012 Illinois Society for the Prevention of Blindness (ISPB) grant ($4,000): **Identification of miRNAs that Regulate the Expression of Myocilin, a Glaucoma Gene.**

PUBLICATIONS:

1. Turturro S, Sunoqrot S, **Ying H**, Hong S, Yue BY. Sustained Release of Matrix Metalloproteinase-3 to Trabecular Meshwork Cells using Biodegradable PLGA Microparticles. Molecular Pharmaceuticals (under revision).

2. McAnany JJ, Alexander KR, Kumar NM, **Ying H**, Anastasakis A, Fishman GA. Electroretinographic Findings in a Patient with Congenital Stationary Night Blindness Due to a Novel NYX Mutation. Ophthalmic Genet. 2013 Jan 4.

3. **Ying H**, Shen X, Yue BY. Establishment of Inducible Wild Type and Mutant Myocilin-GFP-expressing RGC5 Cell Lines. PLoS One. 2012;7(10):e47307.

4. Shen X, **Ying H**, Yue BY. Wnt Activation by Wild-type and Mutant Myocilin in Cultured Human Trabecular Meshwork Cells. PLoS One. 2012;7(9):e44902.

5. Movahedan A, Majdi M, Afsharkhamseh N, Sagha HM, Saadat NS, Shalileh K, Milani BY, **Ying H**, Djalilian AR. Notch Inhibition during Corneal Epithelial Wound Healing Promotes Migration. Invest Ophthalmol Vis Sci. 2012 Nov 1;53(12):7476-83.

6. **Ying H,** Yue BY. Cellular and Molecular Biology of Optineurin (review). Int Rev Cell Mol Biol. 2012;294:223-58.

7. Shen X, **Ying H**, Qiu Y, Park JS, Shyam R, Chi ZL, Iwata T, Yue BY. Processing of Optineurin in Neuronal Cells. J Biol Chem. 2011 Feb 4;286(5):3618-29.

8. Beyer J, Zhao XC, Yee R, Khaliq S, McMahon TT, **Ying H**, Yue BY, Malicki JJ. The Role of Crumbs Genes in the Vertebrate Cornea. Invest Ophthalmol Vis Sci. 2010 Sep;51(9):4549-56.

9. Park B, **Ying H**, Shen X, Park JS, Qiu Y, Shyam R, Yue BY. Impairment of Protein Trafficking upon Overexpression and Mutation of Optineurin. PLoS One. 2010 Jul 12;5(7):e11547.

10. **Ying H,** Shen X, Park B, Yue BY. Posttranslational Modifications, Localization, and Protein Interactions of Optineurin, the Product of a Glaucoma Gene. PLoS One. 2010 Feb 11;5(2):e9168.

11. **Ying H**, Ji X, Hart ML, Gupta K, Saifuddin M, Zariffard MR, Spear GT. Interaction of Mannose-binding Lectin with HIV type 1 is Sufficient for Virus Opsonization but not Neutralization. AIDS Res Hum Retroviruses. 2004 Mar;20(3):327-35